

2016

# Active sites engineering of metal-organic frameworks for heterogeneous catalysis

Xinle Li

*Iowa State University*

Follow this and additional works at: <https://lib.dr.iastate.edu/etd>

 Part of the [Chemistry Commons](#)

## Recommended Citation

Li, Xinle, "Active sites engineering of metal-organic frameworks for heterogeneous catalysis" (2016). *Graduate Theses and Dissertations*. 15961.

<https://lib.dr.iastate.edu/etd/15961>

This Dissertation is brought to you for free and open access by the Iowa State University Capstones, Theses and Dissertations at Iowa State University Digital Repository. It has been accepted for inclusion in Graduate Theses and Dissertations by an authorized administrator of Iowa State University Digital Repository. For more information, please contact [digirep@iastate.edu](mailto:digirep@iastate.edu).

**Active sites engineering of metal-organic frameworks for heterogeneous catalysis**

by

**Xinle Li**

A dissertation submitted to the graduate faculty  
in partial fulfillment of the requirements for the degree of

**DOCTOR OF PHILOSOPHY**

Major: Chemistry

Program of Study Committee:

Wenyu Huang, Major adviser  
Yan Zhao  
Levi Stanley  
Igor Slowing  
George Kraus

Iowa State University

Ames, Iowa

2016

Copyright © Xinle Li, 2016. All rights reserved.

## TABLE OF CONTENTS

## CHAPTER 1. GENERAL INTRODUCTION

Dissertation Organization .....	1
Literature Review .....	3
References.....	7

CHAPTER 2. SYNTHESIS AND CATALYSIS OF MONODISPERSE  
PALLADIUM NANOCCLUSERS USING METAL-ORGANIC FRAMEWORKS  
AS SACRIFICIAL TEMPLATE

Abstract .....	13
Introduction .....	14
Results and Discussion .....	17
Conclusions .....	29
Experimental Section .....	30
Acknowledgment .....	32
References .....	32

CHAPTER 3. TANDEM CATALYSIS BY PALLADIUM NANOCCLUSERS  
ENCAPSULATED IN METAL ORGANIC FRAMEWORKS

Abstract .....	36
Introduction .....	37
Results and Discussion .....	40
Conclusion .....	54
Experimental Section .....	55
Acknowledgment .....	58
References .....	59

CHAPTER 4. CONTROLLING CATALYTIC PROPERTIES OF PALLADIUM  
NANOCCLUSERS THROUGH THEIR CHEMICAL ENVIRONMENT AT THE  
ATOMIC LEVEL USING ISORETICULAR METAL-ORGANIC FRAMEWORKS

Abstract .....	64
Introduction .....	65
Results and Discussion .....	67
Conclusions.....	86
Experimental Section .....	87
Acknowledgment .....	90
References .....	91

CHAPTER 5. IMPACT OF LINKER ENGINEERING ON THE CATALYTIC ACTIVITY OF METAL–ORGANIC FRAMEWORKS CONTAINING PD(II)-BIPYRIDINE COMPLEXES

Abstract .....	96
Introduction .....	97
Results and Discussion .....	100
Conclusions .....	111
Experimental Section .....	112
Acknowledgment .....	124
References .....	124

CHAPTER 6. PLATINUM NANOCLUSTERS IN AMINE-FUNCTIONALIZED METAL–ORGANIC FRAMEWORKS: COOPERATIVE MULTIFUNCTIONAL CATALYSTS FOR NITRONE SYNTHESIS

Abstract .....	128
Introduction .....	129
Results and Discussion .....	131
Conclusions .....	138
Experimental Section .....	139
Acknowledgment .....	141
References .....	141

CHAPTER 7. METAL-ORGANIC FRAMEWORK DERIVED CARBONS AS SOLID BASE CATALYSTS AND THEIR POTENTIAL APPLICATION IN TANDEM CATALYSIS

Abstract .....	143
Introduction .....	144
Results and Discussion .....	149
Conclusions .....	155
Experimental Section .....	156
Acknowledgment .....	158
References .....	158

## ACKNOWLEDGEMENTS

First and foremost, I would like to show my deepest gratitude and appreciation to my adviser, Professor Wenyu Huang, for your invaluable patience, guidance and support during my doctoral studies since 2011. Thank you for teaching me to be a professional researcher, offering me the freedom and opportunity to explore the research areas I am interested in and encouraging me to stay positive in the advent of setbacks and difficulties. Besides my advisor, I would also like to thank the rest of my committee: Professor Yan Zhao, Professor Levi Stanley, Professor Gordon Miller, Professor George Kraus, and Professor Jason Chen, for your insightful comments, suggestions and helpful advice throughout my POS meeting, preliminary examination and Ph.D. defense.

In addition, I would like to thank my colleagues in Dr. Huang's group, for the stimulating discussions, and for the late nights we worked in the lab together in the last five years. Special thanks go to Raghu V. Maligal-Ganesh and Yuchen Pei, for your comfort, entertainment, advice and help whenever I had hard time in research and life. Thank you for making my time in Huang's group a wonderful experience.

I must acknowledge Dr. Ryan Van Zeeland, for our wonderful and successful collaboration together in 2014-2016. I could not have had two more publications without you.

Last but certainly not least, my sincere appreciation goes to my family members: my parents, parents-in-law, my wife and sister, for supporting me spiritually throughout my life in general. Words cannot express how grateful I am to my beloved wife, Fei Wang, for your constant love and giving birth to our lovely baby daughter, Olivia (Jiayi) Li, I could not have finished this without my family.

## CHAPTER 1

### GENERAL INTRODUCTION

#### Dissertation Organization

This dissertation is composed of 7 chapters. The first chapter is a general review of the active sites engineering of metal-organic frameworks (MOFs) in heterogeneous catalysis. The second chapter was published in *ChemNanoMat* as VIP paper and highlighted in <http://www.chemistryviews.org> in 2016. We developed an interfacial etching approach for the synthesis of monodisperse and ultra-small thiolated palladium (Pd) nanoclusters (NCs) using Zr-UiO-66-NH<sub>2</sub> MOFs as sacrificial templates. The released thiolated Pd NCs have an unprecedented small size and narrow distribution ( $1.1 \pm 0.1$  nm in diameter). More importantly, the size of Pd NCs can be tuned by changing the cavity diameter of the MOFs template. The released Pd NCs displayed good activity in Suzuki-Miyaura coupling reaction. The third chapter was published in *ACS Catalysis* in 2014. A bifunctional Zr-MOF catalyst containing Pd NCs has been developed. Combining the oxidation activity of Pd NCs and the acetalization activity of the Lewis acid sites in UiO-66-NH<sub>2</sub>, this heterogeneous multifunctional catalyst (Pd@UiO-66-NH<sub>2</sub>) exhibited excellent catalytic activity and selectivity in a one-pot tandem oxidation-acetalization reaction. The fourth chapter was published in *ACS Catalysis* in 2016. We synthesized Pd NCs in different atomically tunable chemical environment using isorecticular MOFs as the support (Pd@UiO-66-X, X = H, NH<sub>2</sub>, and OMe). In an aerobic reaction between benzaldehyde and ethylene glycol, these heterogeneous catalysts Pd@UiO-66-X

showed product distributions that are completely altered from the acetal to the ester when we changed the functional groups on the MOF linkers from  $-\text{NH}_2$  to  $-\text{H}/-\text{OMe}$ . The fifth chapter was published in *ACS Catalysis* in 2016 as well. For the first time, a new series of mixed-linker bipyridyl MOF-supported palladium (II) catalysts were used to elucidate the electronic and steric effects of linker substitution on the activity of these catalysts in the context of Suzuki–Miyaura cross-coupling reactions. This work demonstrates the first example of systematic linker engineering of metalated units in bipyridyl MOFs and highlights the importance of linker design for immobilization of homogeneous catalysts in MOFs. The sixth chapter is to be submitted and demonstrates the first attempt for a one-pot synthesis of nitrene using heterogeneous multifunctional MOFs catalyst. We developed ultrasmall platinum NCs encapsulated in UiO-66- $\text{NH}_2$  ( $\text{Pt}@$ UiO-66- $\text{NH}_2$ ) and used it as a multifunctional catalyst in the one-pot tandem nitrene synthesis.  $\text{Pt}@$ UiO-66- $\text{NH}_2$  exhibited high activity and enhanced selectivity in the tandem nitrene synthesis, in comparison to Pt/carbon, Pt@UiO-66, Pt/UiO-66- $\text{NH}_2$  and Pd@UiO-66- $\text{NH}_2$ . The last chapter was submitted and represents the first example of using MOFs-derived carbons as solid base catalysts and their potential applications in tandem catalysis. We have developed a novel solid base catalyst, MOF-253 derived porous carbons (Cz-MOF-253) by facile pyrolysis of bipyridyl MOF-253 and subsequent acid treatment to remove alumina. Cz-MOF-253 is highly porous and exhibited high efficiency in Knoevenagel condensation reaction. More importantly, the high basicity and porous nature enable the design of bifunctional catalyst and facilitated tandem Knoevenagel condensation-hydrogenation reactions.

## Literature Review

The past two decades have witnessed explosive interest in the preparation, characterization, and application of metal-organic frameworks (MOFs) since the first use of the term 'MOF' in the literature.<sup>1</sup> MOFs are porous coordination networks by self-assembly of metal ions/clusters and rigid organic linkers. As a result of intriguing structural/chemical flexibilities, numerous metal ions and organic linkers have been used in the synthesis of MOFs and more than 20,000 structures have been reported so far.<sup>2,3</sup> Currently, MOFs are eliciting noteworthy attention in scientific community and industries,<sup>4</sup> not only due to notable advantages such as ultrahigh surface area/porosity and structural/chemical tunabilities, but also their vast potential in a wide spectrum of applications, such as gas storage,<sup>5</sup> separation,<sup>6</sup> chemical sensing,<sup>7</sup> drug delivery,<sup>8</sup> biomedical imaging,<sup>9</sup> photoluminescence,<sup>10</sup> proton conductivity,<sup>11</sup> and catalysis, etc.<sup>12</sup>

With the depletion of fossil fuels and global energy crisis confronting us, there is a pressing need for developing economically, environmentally benign and efficient processes in catalytic reactions for chemical synthesis. In comparison to homogeneous catalysis, which is hurdled by metal contamination and limited recyclability, heterogeneous catalysis, which holds multiple advantages of facile separation, recyclability and potential in continuous flow reaction systems, is promptly developing field in chemical manufacturing nowadays. Since the first catalytic applications of MOFs reported by Fujita and coworkers in 1994,<sup>13</sup> the use of MOFs in heterogeneous catalysis is under intense investigation.<sup>14,15</sup> From viewpoint of catalysis, the high design versatility of MOFs renders unparalleled advantages for their applications in catalysis, since it is feasible to rationally engineer not only the



active sites but also its chemical environment at the atomic level.<sup>16</sup> Furthermore, the ultrahigh surface area/porosity and periodical structures of MOFs is beneficial to the transportation of reactants/products and guarantee the accessibility of active sites, leading to high activity in catalysis. In principle, the catalytic sites in MOFs can be divided by several categories. 1) The organic linker and the inorganic nodes, which can be induced by direct synthesis or post-synthetic modification.<sup>17,18</sup> 2) The inner pores of the MOFs can serve as scaffold in which the catalytic species (e.g., metal or metal oxide nanoparticle, metal complex, etc.) is encapsulated.<sup>19,20</sup> 3) The pyrolysis of MOFs to porous carbon or metal/carbon hybrid composites is prone to preserve the merits of MOFs and demonstrate huge potential in heterogeneous and electrochemical catalysis.<sup>21,22</sup>

### **Organic functional linker as active site**

MOFs with catalytic active and accessible functional organic linkers have been well studied. Acidic sites such as sulfonic acid groups,<sup>23</sup> dicarboxylic acid groups,<sup>24</sup> and basic sites like amino,<sup>25</sup> pyridyl,<sup>26</sup> pyrrolidine,<sup>27</sup> N-Heterocyclic carbene,<sup>28</sup> and amide groups<sup>29</sup> can be incorporated in the linker either by using pre-designed linker or post-synthetic modification of as-formed MOFs.<sup>30,31</sup> These incorporated acid/basic functional groups serve as an intrinsic part of the organic linker in the MOFs and show excellent catalytic performance in a variety of catalytic organic transformations like esterification,<sup>32</sup> acetalization,<sup>33</sup> alcoholysis of epoxides,<sup>34</sup> aldol condensation,<sup>35</sup> Knoevenagel condensation,<sup>36</sup> and Michael addition,<sup>37</sup> etc. Remarkably, as a result of high tunability and flexibility endowed by MOFs, it is feasible to insert multiple functional linkers within MOFs via careful design. Recently,

incorporation of mixed acid/base functional linkers into MOF has been reported, and the obtained bifunctional catalyst displayed high integrated catalytic activity in tandem catalysis.<sup>38</sup>

### **Inorganic metal nodes as active site**

Heterogeneous catalysts have been developed based on MOFs where the metal atoms/clusters are located at the nodes and utilized in chemical transformation, especially in Lewis-acid catalyzed reactions.<sup>39</sup> Upon solvent removing, the metal atoms become unsaturated and more accessible, rendering great potential in heterogeneous catalysis. A broad range of metal nodes in MOFs such as Ag(I), Al(III), Cr(III), Co(II), Cu(II), Fe(III), Mn(II), Mg(II), Ni(II), Pd(II), Ti(III), Zr(IV) and Zn(II), etc. have been shown as active sites in heterogeneous catalysis such as cyanosilylation reaction,<sup>40</sup> cyclopropanation,<sup>41</sup> acetalization,<sup>42</sup> cycloaddition of CO<sub>2</sub> and epoxides,<sup>43</sup> esterification,<sup>44</sup> Friedel–Crafts acylation,<sup>45</sup> oxidation of alcohol/hydrocarbons,<sup>46,47</sup> Henry reaction,<sup>48</sup> 1,3-dipolar cycloaddition,<sup>49</sup> isomerization,<sup>50</sup> Aza-Michael reaction<sup>51</sup>, etc.

### **MOFs as scaffold for the catalytic species**

Owing to exceptional high chemical flexibility and highly porous nature, MOFs have been ideal scaffold for immobilization of catalytic species and heterogenization of homogeneous complex. For example, transition metal complexes can be immobilized in bipyridyl and porphyrin-based MOFs and afford single-site catalysts with enhanced activity in comparison to homogeneous counterparts.<sup>25,52-54</sup> Metal nanoparticles have also been widely embedded in MOFs (designated as NPs@MOF).<sup>55</sup> NPs@MOFs systems are of particular interest in catalysis because of

their rationally designed structures, ease to modify the pore environment, and possible electronic interaction between the NPs and frameworks,<sup>56</sup> which is of significant importance for controlling the growth of NPs and leading to enhanced activities and selectivities.<sup>57</sup> Until now, quite a few metals NPs (e.g., Pt,<sup>58</sup> Pd,<sup>59</sup> Ru,<sup>60</sup> Au,<sup>61</sup> Cu,<sup>62</sup> PdAg,<sup>63</sup> etc.) have been finely encapsulated in the MOF cavities and exhibited great potential as heterogeneous catalysts for reactions such as selective hydrogenation,<sup>64</sup> oxidation,<sup>65</sup> C-H activation<sup>66</sup>, ammonia borane hydrolysis,<sup>67</sup> dehalogenation of aryl chlorides,<sup>68</sup> etc. In addition, other catalytic active sites such as metal-organic polyhedral,<sup>69</sup> polyoxometalates,<sup>70</sup> and enzymes<sup>71</sup> have also been incorporated into MOFs for advanced catalysis.

#### **MOFs as sacrificial precursor for new active sites**

Since the first report of MOFs as template for carbon synthesis in 2008,<sup>72</sup> MOFs have been exploited as promising templates/precursors for preparation of porous carbons and nanostructured functional composites, due to their high surface areas, tailorable structures, abundant metal/organic varieties and heteroatom doping. The direct pyrolysis of MOFs in inert atmosphere (N<sub>2</sub>, Ar) usually generates binary metal/metal oxide-carbon hybrids, such as Co-CoO/carbon, Fe<sub>3</sub>C/carbon, Co-P/carbon, which showed great potential in catalysis such as alcohol and CO oxidation,<sup>73</sup> hydrogenation,<sup>74</sup> Fisher-Tropsch synthesis,<sup>75</sup> and electro-catalysis,<sup>76,77</sup> etc. The metal-free porous carbon after acid treatment emerges as promising catalyst in oxygen reduction reaction<sup>78</sup> and metal-free oxidation.<sup>79</sup> If the carbonization is performed in air/oxygen atmosphere, metal oxides will be the main products. For example, Co<sub>3</sub>O<sub>4</sub> nanowires synthesized by carbonization of Co-

naphthalenedicarboxylate MOF in air have been demonstrated as good catalysts in heterogenous catalysis.<sup>80</sup>

In this dissertation, I present several design of heterogeneous catalysts for desired/model catalytic reactions via active sites engineering in MOFs, that is, using MOFs as scaffold for noble metal NPs and heterogenization of organometallic species and explore its application in catalytic organic transformations; using MOFs as sacrificial templates to prepare monodisperse thiolated Pd NCs or to afford porous carbons with Lewis base sites and investigate its catalytic performance in heterogeneous catalysis. By virtue of MOFs' tunability, versatility, and flexibility, the rationally-designed MOF catalysts exhibited excellent catalytic performance in tandem catalysis and established a clear structure-activity relationship in the heterogeneous catalysis. Future work on exploring novel and efficient tandem catalysis and elucidate the underlying mechanism of linker engineering in heterogeneous MOFs catalysis is currently undergoing.

## References

- (1) Yaghi, O. M.; Li, G.; Li, H. *Nature* **1995**, *378*, 703-706.
- (2) Furukawa, H.; Cordova, K. E.; O'Keeffe, M.; Yaghi, O. M. *Science* **2013**, *341*, 1230444.

- (3) Stock, N.; Biswas, S. *Chem. Rev.* **2011**, *112*, 933-969.
- (4) Li, B.; Leng, K.; Zhang, Y.; Dynes, J. J.; Wang, J.; Hu, Y.; Ma, D.; Shi, Z.; Zhu, L.; Zhang, D. *J. Am. Chem. Soc.* **2015**, *137*, 4243-4248.
- (5) Mason, J. A.; Veenstra, M.; Long, J. R. *Chem. Sci.* **2014**, *5*, 32-51.
- (6) Li, J.-R.; Kuppler, R. J.; Zhou, H.-C. *Chem. Soc. Rev.* **2009**, *38*, 1477-1504.
- (7) Kreno, L. E.; Leong, K.; Farha, O. K.; Allendorf, M.; Van Duyne, R. P.; Hupp, J. T. *Chem. Rev.* **2011**, *112*, 1105-1125.
- (8) Huxford, R. C.; Della Rocca, J.; Lin, W. *Curr. Opin. Chem. Biol.* **2010**, *14*, 262-268.
- (9) Della Rocca, J.; Liu, D.; Lin, W. *Acc. Chem. Res.* **2011**, *44*, 957-968.
- (10) Cui, Y.; Yue, Y.; Qian, G.; Chen, B. *Chem. Rev.* **2011**, *112*, 1126-1162.
- (11) Sen, S.; Nair, N. N.; Yamada, T.; Kitagawa, H.; Bharadwaj, P. K. *J. Am. Chem. Soc.* **2012**, *134*, 19432-19437.
- (12) Liu, J.; Chen, L.; Cui, H.; Zhang, J.; Zhang, L.; Su, C.-Y. *Chem. Soc. Rev.* **2014**, *43*, 6011-6061.
- (13) Fujita, M.; Kwon, Y. J.; Washizu, S.; Ogura, K. *J. Am. Chem. Soc.* **1994**, *116*, 1151-1152.
- (14) Chughtai, A. H.; Ahmad, N.; Younus, H. A.; Laypkov, A.; Verpoort, F. *Chem. Soc. Rev.* **2015**, *44*, 6804-6849.
- (15) Dhakshinamoorthy, A.; Garcia, H. *ChemSusChem* **2014**, *7*, 2392-2410.
- (16) Allendorf, M. D.; Stavila, V. *CrystEngComm* **2015**, *17*, 229-246.
- (17) Tanabe, K. K.; Cohen, S. M. *Chem. Soc. Rev.* **2011**, *40*, 498-519.
- (18) Deria, P.; Mondloch, J. E.; Karagiari, O.; Bury, W.; Hupp, J. T.; Farha, O. K. *Chem. Soc. Rev.* **2014**, *43*, 5896-5912.
- (19) Rösler, C.; Fischer, R. A. *CrystEngComm* **2015**, *17*, 199-217.
- (20) Zhu, Q.-L.; Xu, Q. *Chem. Soc. Rev.* **2014**, *43*, 5468-5512.
- (21) Song, Y.; Li, X.; Sun, L.; Wang, L. *RSC Adv.* **2015**, *5*, 7267-7279.

- (22) Sun, J.-K.; Xu, Q. *Energy Environ. Sci.* **2014**, *7*, 2071-2100.
- (23) Chen, J.; Li, K.; Chen, L.; Liu, R.; Huang, X.; Ye, D. *Green Chem.* **2014**, *16*, 2490-2499.
- (24) Ragon, F.; Campo, B.; Yang, Q.; Martineau, C.; Wiersum, A. D.; Lago, A.; Guillerm, V.; Horcajada, P.; Vimont, A.; Llewellyn, P. L.; Daturi, M.; Devautour-Vinot, S.; Maurin, G.; Serre, C.; Devic, T.; Clet, G. *J. Mater. Chem. A* **2015**, *3*, 3294-3309.
- (25) Hajek, J.; Vandichel, M.; Van de Voorde, B.; Bueken, B.; De Vos, D.; Waroquier, M.; Van Speybroeck, V. *J. Catal.* **2015**, *331*, 1-12.
- (26) Bloch, E. D.; Britt, D.; Lee, C.; Doonan, C. J.; Uribe-Romo, F. J.; Furukawa, H.; Long, J. R.; Yaghi, O. M. *J. Am. Chem. Soc.* **2010**, *132*, 14382-14384.
- (27) Banerjee, M.; Das, S.; Yoon, M.; Choi, H. J.; Hyun, M. H.; Park, S. M.; Seo, G.; Kim, K. *J. Am. Chem. Soc.* **2009**, *131*, 7524-7525.
- (28) Kong, G.-Q.; Ou, S.; Zou, C.; Wu, C.-D. *J. Am. Chem. Soc.* **2012**, *134*, 19851-19857.
- (29) Xi, F.-G.; Liu, H.; Yang, N.-N.; Gao, E.-Q. *Inorg. Chem.* **2016**, *55*, 4701-4703.
- (30) Garibay, S. J.; Cohen, S. M. *Chem. Commun.* **2010**, *46*, 7700-7702.
- (31) Jiang, J.; Yaghi, O. M. *Chem. Rev.* **2015**, *115*, 6966-6997.
- (32) Jiang, J.; Gándara, F.; Zhang, Y.-B.; Na, K.; Yaghi, O. M.; Klemperer, W. G. *J. Am. Chem. Soc.* **2014**, *136*, 12844-12847.
- (33) Jin, Y.; Shi, J.; Zhang, F.; Zhong, Y.; Zhu, W. *J. Mol. Catal. A: Chem.* **2014**, *383*, 167-171.
- (34) Zhou, Y. X.; Chen, Y. Z.; Hu, Y.; Huang, G.; Yu, S. H.; Jiang, H. L. *Chem. – Eur. J.* **2014**, *20*, 14976-14980.
- (35) Lun, D. J.; Waterhouse, G. I. N.; Telfer, S. G. *J. Am. Chem. Soc.* **2011**, *133*, 5806-5809.
- (36) Burgoyne, A. R.; Meijboom, R. *Catal. Lett.* **2013**, *143*, 563-571.
- (37) Beheshti, S.; Morsali, A. *RSC Adv.* **2014**, *4*, 37036-37040.
- (38) Liu, H.; Xi, F.-G.; Sun, W.; Yang, N.-N.; Gao, E.-Q. *Inorg. Chem.* **2016**.

- (39) Vermoortele, F.; Vandichel, M.; Van de Voorde, B.; Ameloot, R.; Waroquier, M.; Van Speybroeck, V.; De Vos, D. E. *Angew. Chem. Int. Ed.* **2012**, *51*, 4887-4890.
- (40) Neogi, S.; Sharma, M. K.; Bharadwaj, P. K. *J. Mol. Catal. A: Chem.* **2009**, *299*, 1-4.
- (41) Falkowski, J. M.; Wang, C.; Liu, S.; Lin, W. *Angew. Chem.* **2011**, *123*, 8833-8837.
- (42) Dhakshinamoorthy, A.; Alvaro, M.; Garcia, H. *Adv. Synth. Catal.* **2010**, *352*, 3022-3030.
- (43) Cho, H.-Y.; Yang, D.-A.; Kim, J.; Jeong, S.-Y.; Ahn, W.-S. *Cata. Today* **2012**, *185*, 35-40.
- (44) de la Iglesia, Ó.; Sorribas, S.; Almendro, E.; Zornoza, B.; Téllez, C.; Coronas, J. *Renew. Energy* **2016**, *88*, 12-19.
- (45) Phan, N. T.; Le, K. K.; Phan, T. D. *Appl. Catal., A* **2010**, *382*, 246-253.
- (46) Xie, M. H.; Yang, X. L.; Wu, C. D. *Chem. – Eur. J.* **2011**, *17*, 11424-11427.
- (47) Tonigold, M.; Lu, Y.; Bredenkötter, B.; Rieger, B.; Bahn Müller, S.; Hitzbleck, J.; Langstein, G.; Volkmer, D. *Angew. Chem. Int. Ed.* **2009**, *48*, 7546-7550.
- (48) Shi, L.-X.; Wu, C.-D. *Chem. Commun.* **2011**, *47*, 2928-2930.
- (49) Jing, X.; He, C.; Dong, D.; Yang, L.; Duan, C. *Angew. Chem. Int. Ed.* **2012**, *51*, 10127-10131.
- (50) Dhakshinamoorthy, A.; Alvaro, M.; Chevreau, H.; Horcajada, P.; Devic, T.; Serre, C.; Garcia, H. *Catal. Sci. Tech.* **2012**, *2*, 324-330.
- (51) Nguyen, L. T.; Nguyen, T. T.; Nguyen, K. D.; Phan, N. T. *Appl. Catal., A* **2012**, *425*, 44-52.
- (52) Guo, Z.; Chen, B. *Dalton Trans.* **2015**, *44*, 14574-14583.
- (53) Manna, K.; Zhang, T.; Lin, W. *J. Am. Chem. Soc.* **2014**, *136*, 6566-6569.
- (54) Manna, K.; Zhang, T.; Greene, F. X.; Lin, W. *J. Am. Chem. Soc.* **2015**, *137*, 2665-2673.
- (55) Aijaz, A.; Xu, Q. *J. Phys. Chem. Lett* **2014**, *5*, 1400-1411.

- (56) Chen, L.; Chen, H.; Luque, R.; Li, Y. *Chem. Sci.* **2014**, *5*, 3708-3714.
- (57) Yang, Q.; Xu, Q.; Yu, S. H.; Jiang, H. L. *Angew. Chem.* **2016**, *128*, 3749-3753.
- (58) Aijaz, A.; Karkamkar, A.; Choi, Y. J.; Tsumori, N.; Rönnebro, E.; Autrey, T.; Shioyama, H.; Xu, Q. *J. Am. Chem. Soc.* **2012**, *134*, 13926-13929.
- (59) Li, X.; Guo, Z.; Xiao, C.; Goh, T. W.; Tesfagaber, D.; Huang, W. *ACS Catal.* **2014**, *4*, 3490-3497.
- (60) Schröder, F.; Esken, D.; Cokoja, M.; van den Berg, M. W.; Lebedev, O. I.; Van Tendeloo, G.; Walaszek, B.; Buntkowsky, G.; Limbach, H.-H.; Chaudret, B. *J. Am. Chem. Soc.* **2008**, *130*, 6119-6130.
- (61) Liu, H.; Liu, Y.; Li, Y.; Tang, Z.; Jiang, H. *The Journal of Physical Chemistry C* **2010**, *114*, 13362-13369.
- (62) Müller, M.; Hermes, S.; Kähler, K.; van den Berg, M. W.; Muhler, M.; Fischer, R. A. *Chem. Mater.* **2008**, *20*, 4576-4587.
- (63) Chen, L.; Huang, B.; Qiu, X.; Wang, X.; Luque, R.; Li, Y. *Chem. Sci.* **2016**, *7*, 228-233.
- (64) Guo, Z.; Xiao, C.; Maligal-Ganesh, R. V.; Zhou, L.; Goh, T. W.; Li, X.; Tesfagaber, D.; Thiel, A.; Huang, W. *ACS Catal.* **2014**, *4*, 1340-1348.
- (65) Chen, G.; Wu, S.; Liu, H.; Jiang, H.; Li, Y. *Green Chem.* **2013**, *15*, 230-235.
- (66) Pascanu, V.; Carson, F.; Solano, M. V.; Su, J.; Zou, X.; Johansson, M. J.; Martín - Matute, B. *Chem. - Eur. J.* **2015**.
- (67) Aijaz, A.; Karkamkar, A.; Choi, Y. J.; Tsumori, N.; Rönnebro, E.; Autrey, T.; Shioyama, H.; Xu, Q. *J. Am. Chem. Soc.* **2012**, *134*, 13926-13929.
- (68) Huang, Y.; Liu, S.; Lin, Z.; Li, W.; Li, X.; Cao, R. *J. Catal.* **2012**, *292*, 111-117.
- (69) Qiu, X.; Zhong, W.; Bai, C.; Li, Y. *J. Am. Chem. Soc.* **2016**, *138*, 1138-1141.
- (70) Sun, J.-W.; Yan, P.-F.; An, G.-H.; Sha, J.-Q.; Li, G.-M.; Yang, G.-Y. *Sci. Rep.* **2016**, *6*.
- (71) Mehta, J.; Bhardwaj, N.; Bhardwaj, S. K.; Kim, K.-H.; Deep, A. *Coord. Chem. Rev.* **2016**, *322*, 30-40.



- (72) Liu, B.; Shioyama, H.; Akita, T.; Xu, Q. *J. Am. Chem. Soc.* **2008**, *130*, 5390-5391.
- (73) Zhong, W.; Liu, H.; Bai, C.; Liao, S.; Li, Y. *ACS Catal.* **2015**, *5*, 1850-1856.
- (74) Ma, X.; Zhou, Y.-X.; Liu, H.; Li, Y.; Jiang, H.-L. *Chem. Commun.* **2016**, *52*, 7719-7722.
- (75) Wezendonk, T. A.; Santos, V. P.; Nasalevich, M. A.; Warringa, Q. S. E.; Dugulan, A. I.; Chojecki, A.; Koeken, A. C. J.; Ruitenbeek, M.; Meima, G.; Islam, H.-U.; Sankar, G.; Makkee, M.; Kapteijn, F.; Gascon, J. *ACS Catal.* **2016**, *6*, 3236-3247.
- (76) You, B.; Jiang, N.; Sheng, M.; Gul, S.; Yano, J.; Sun, Y. *Chem. Mater.* **2015**, *27*, 7636-7642.
- (77) Xia, W.; Mahmood, A.; Zou, R.; Xu, Q. *Energy Environ. Sci.* **2015**, *8*, 1837-1866.
- (78) Chen, Y. Z.; Wang, C.; Wu, Z. Y.; Xiong, Y.; Xu, Q.; Yu, S. H.; Jiang, H. L. *Adv. Mater.* **2015**, *27*, 5010-5016.
- (79) Wang, X.; Li, Y. *J. Mater. Chem. A* **2016**, *4*, 5247-5257.
- (80) Ma, T. Y.; Dai, S.; Jaroniec, M.; Qiao, S. Z. *J. Am. Chem. Soc.* **2014**, *136*, 13925-13931.

**CHAPTER 2**  
**SYNTHESIS AND CATALYSIS OF MONODISPERSE PALLADIUM**  
**NANOCLUSTERS USING METAL-ORGANIC FRAMEWORKS AS**  
**SACRIFICIAL TEMPLATE**

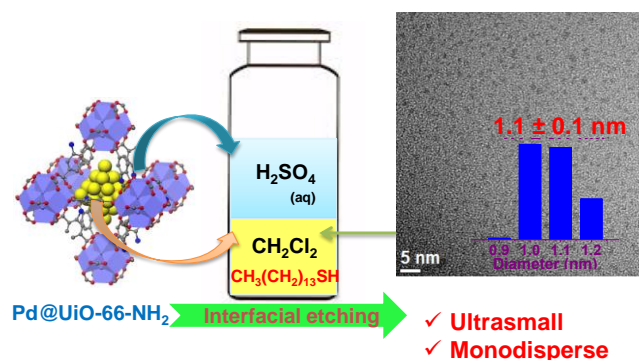
A VIP paper published in *ChemNanoMat*, **2016**, 2, 810-815

Highlighted in *ChemistryViews*

Xinle Li, Chaoxian Xiao, Prashant K. Jain and Wenyu Huang

**Abstract**

An interfacial etching approach was developed for the synthesis of monodisperse and ultrasmall thiolated palladium NCs using Zr-UiO-66-NH<sub>2</sub> MOFs as sacrificial templates. The Pd NCs were originally synthesized inside the cavities of the MOFs (Pd@UiO-66-NH<sub>2</sub>). The Pd NCs released from the MOFs have a strikingly small size with narrow distribution ( $1.1 \pm 0.1$  nm), amounting to a cluster size of ca. 40 Pd atoms. The <sup>1</sup>H NMR spectrum indicates that thiol is the only capping agent for these Pd NCs. We derived the composition of the thiolated Pd NCs using thermogravimetric analysis (TGA) and inductively coupled plasma mass spectrometry (ICP-MS) analysis. Moreover, the Pd NCs size can be tuned by using MOF templates with different cavity sizes. The thiolated Pd NCs are catalytically active in a model Suzuki–Miyaura coupling reaction.



## Introduction

Downsizing nanoparticles (NPs) to the ultra-small size ( $< 2$  nm) offers dramatically high surface-to-volume fraction of atoms and thereby an increased number of active/reactive under-coordinated surface sites. As a result, ultra-small metal nanocrystals often exhibit enhanced or novel catalytic activities.<sup>1</sup> Other molecule-like properties resulting from quantum confinement<sup>2</sup> like discrete, narrow luminescent emission can also result at this size.<sup>3</sup> In addition to ultra-small size of nanocrystals, the narrow size dispersion, often termed as monodispersity, is also critical because it can allow an ensemble of NCs to exhibit high homogeneity with respect to catalytic, electrical, and optical properties, that are often size-dependent.<sup>4</sup> The capability to synthesize monodisperse NCs enables a more systematic investigation of these size-dependent properties.<sup>5</sup> Significant progress has been realized in the synthesis of monodisperse metal NCs in solutions.<sup>6-8</sup> Current solution-phase methods for synthesizing metal NCs can be divided into two major categories, thermodynamic- and template-controlled syntheses. Using appropriate capping ligands (e.g., thiols or phosphines), thermodynamic-controlled synthesis usually yields NCs, freely dispersed in solution, possessing the most stable structures.<sup>9-11</sup>

Compared to thiolated Au NCs synthesis, which has been well established, Pd NCs have received relatively less attention and the preparation of monodisperse Pd NCs still poses a grand challenge. Most of previously synthesized Pd particles have a large diameter ( $> 2.5$  nm) and/or a broad size distribution.<sup>12-15</sup> There has been limited success in the synthesis of Pd NCs smaller than 2 nm. For example, the Nishihara group developed a one-pot method for the preparation of alkanethiol-protected Pd NCs with a broader size distribution ( $1.3 \pm 0.3$  nm).<sup>16</sup> The Fornasiero group synthesized amphiphilic thiol-protected Pd NPs in water-acetone solution with a narrow size distribution ( $1.9 \pm 0.2$  nm).<sup>17</sup> However, these aforementioned approaches need further purification steps.

Template-controlled synthesis uses small cavities within the templating materials (e.g., dendrimers and micelles) to limit the growth of NCs, and form small particles stabilized inside those cavities.<sup>18-21</sup> Template-controlled synthesis exhibits several advantages, including simplicity, high stability, and partially non-blocked surface active sites. However, the monodispersity of metal NCs, made by template-controlled synthesis, depends highly on the quality of templating materials used. For example, micelles formed in solution usually have a significant size distribution (4 - 13 nm) and aggregate in certain solvents, which makes it difficult to synthesize monodisperse metal NCs.<sup>22,23</sup>

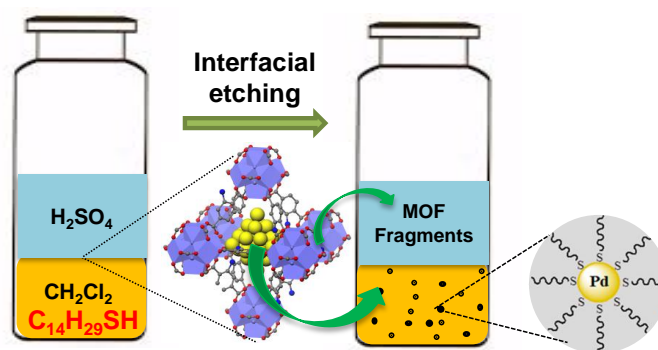
A removable and well-defined template is critical to the synthesis of monodisperse NCs using the templating strategy. We envisioned that MOFs could serve as the template for the preparation of ultra-small thiolated NCs of narrow size distribution. Recently, MOFs have emerged as a promising class of sacrificial

templates for nanomaterials synthesis,<sup>24,25</sup> e.g., silver nanowires/nanoparticles,<sup>26</sup> CdS nanotubes,<sup>27</sup> nanoporous carbon,<sup>28</sup> and metal/metal oxide nanostructures.<sup>29</sup> Compared to the conventional templates, MOFs possess highly uniform and identical cavities, which ensure the monodispersity of the templated Pd NCs. Moreover, the nanometric sized cavities in MOFs can be precisely tunable, which further improves the versatility of our synthesis protocol for Pd NCs.

Here we report a facile interfacial etching approach for the preparation of monodisperse and ultra-small thiolated Pd NCs, using amine-functionalized Zr-MOFs as sacrificial templates (Scheme 1). Compared to the previous template methodologies, this approach holds multiple advantages, including simplicity (ease of operation), and precise size control of the Pd NCs through rational selection of isorecticular Zr-MOFs. We demonstrated the synthesis of thiolated Pd NCs unprecedented in terms of their ultra-small size and their monodispersity. To the best of our knowledge, this is the first example of using MOFs as sacrificial templates for the synthesis of monodisperse and ultra-small Pd NCs. The as-prepared thiolated Pd NCs is catalytically active in the Suzuki-Miyaura coupling reaction.

With the aim of preparing monodisperse metal NCs, the selection of MOFs is critical. Firstly, the metal precursor must be able to diffuse into the cages of the MOFs and be entrapped there. Secondly, the cage size is desired to be sub-2 nm, in order to obtain ultra-small NCs. Taking both aforementioned principles, we selected UiO-66-NH<sub>2</sub> (UiO = University of Oslo) as the template. UiO-66-NH<sub>2</sub> is assembled from [Zr<sub>6</sub>O<sub>4</sub>(OH)<sub>4</sub>(CO<sub>2</sub>)<sub>12</sub>] clusters bridged by 2-aminoterephthalic acid and it is comprised of octahedral and tetrahedral cages having free diameters of ~1.1 nm and ~

0.8 nm, respectively.<sup>30</sup> Furthermore, Zr-MOFs possess inherent thermal and chemical stability, necessary for prevention of a rapid collapse of MOFs during the etching process, thereby diminishing the agglomeration of Pd NCs. Lastly, the amino groups on the linkers serve to stabilize Pd NPs/NCs and prevent agglomeration, as demonstrated in previous work.<sup>31</sup>



**Scheme 1.** Schematic illustration of the preparation of thiolated Pd NCs using UiO-66-NH<sub>2</sub> as the sacrificial template via an interfacial etching approach.

## Results and Discussion

The preparation procedure of thiolated Pd NCs is schematically depicted in Scheme 1. First, UiO-66-NH<sub>2</sub> was prepared via a reported protocol,<sup>32</sup> and it showed identical powder X-ray diffraction (PXRD) patterns to the simulated patterns (Figure 1). Pd NCs inside UiO-66-NH<sub>2</sub> (Pd@UiO-66-NH<sub>2</sub>) were synthesized following a solution impregnation method reported in recent work by our group.<sup>33</sup> The unchanged PXRD of Pd@UiO-66-NH<sub>2</sub> confirmed the crystalline structure was retained after incorporation of Pd and reduction. The transmission electron microscopy images

(TEM) of Pd@UiO-66-NH<sub>2</sub> revealed that Pd NCs are well dispersed within the pores of UiO-66-NH<sub>2</sub> without aggregation on the external surface (Figure 2a).

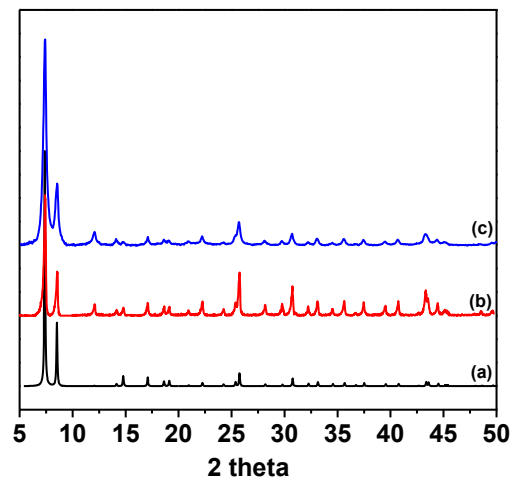


**Figure 1.** PXRD patterns of (a) simulated UiO-66, (b) UiO-66-NH<sub>2</sub>, (c) 4.0 wt.% Pd@UiO-66-NH<sub>2</sub>.

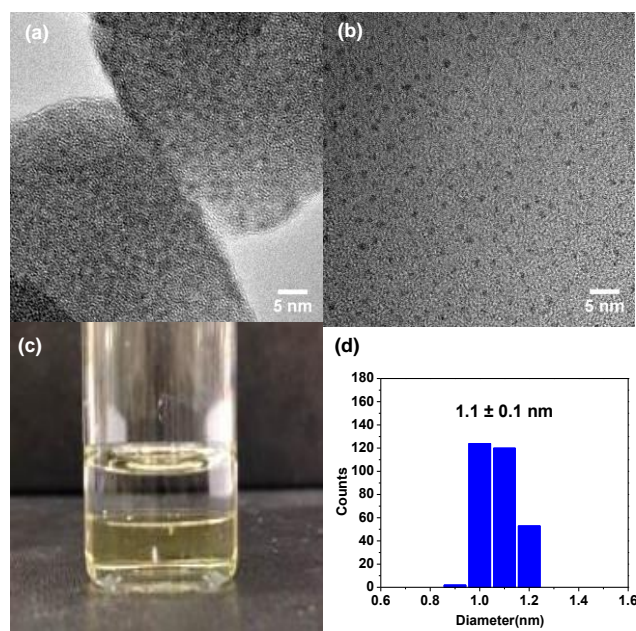


**Figure 2.** (a) TEM image of Pd@UiO-66-NH<sub>2</sub>; (b) TEM image of thiolated Pd NCs prepared using UiO-66-NH<sub>2</sub> as the sacrificial template; (c) Photograph of the process of interfacial etching of Pd@UiO-66-NH<sub>2</sub> in 6 hours. Top layer: aqueous solution,

bottom layer:  $\text{CH}_2\text{Cl}_2$  solution; (d) Size distribution histogram for synthesized thiolated Pd NCs. The diameter of NCs is 1.1 nm in average and the standard deviation ( $\pm 0.1$  nm) is based on a measurement of 300 particles from three independent experiments.

After obtaining Pd@UiO-66-NH<sub>2</sub>, in which Pd NCs are well embedded and restricted by the cages of UiO-66-NH<sub>2</sub>, we sought to remove the MOFs and release the encapsulated Pd NCs. A screening experiment using different acid and base etchants confirmed that H<sub>2</sub>SO<sub>4</sub> was superior to HCl, HF, trifluoroacetic acid (TFA), ammonia, or NaOH in removing MOFs (Table 1). To circumvent the agglomeration of Pd NCs upon removal of the MOF, we used thiols to stabilize the released Pd NCs, since thiol ligands are widely recognized as stabilizers in noble metal NC synthesis. We found that the method we used to remove UiO-66-NH<sub>2</sub> was critical to the formation of monodisperse Pd NCs.

**Table 1.** Screening acid/base for etching of UiO-66-NH<sub>2</sub> (2 mg) in 0.5 mL of H<sub>2</sub>O under stirring.

Acid/base	NH <sub>3</sub> H <sub>2</sub> O (6M)	NaOH (5M)	HF (0.03 M)	TFA (99.5%)	HCl (5M)	H <sub>2</sub> SO <sub>4</sub> (5M)
Amount	100 $\mu\text{L}$	100 $\mu\text{L}$	8 $\mu\text{L}$	500 $\mu\text{L}$	500 $\mu\text{L}$	500 $\mu\text{L}$
Appearance after 1 h	Emulsion	Precipitate	Mostly dissolved	Emulsion	Emulsion	Completely dissolved



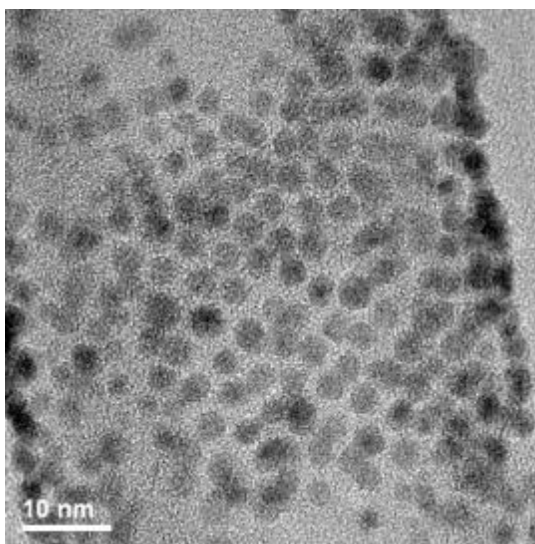


**Figure 3.** TEM images of thiolated Pd NPs using one-phase synthesis.

In our initial attempts, we first mixed Pd@UiO-66-NH<sub>2</sub> with n-tetradecanethiol in H<sub>2</sub>O-MeOH (v:v =5:1) and subsequently added an aqueous solution of 1.25 M H<sub>2</sub>SO<sub>4</sub>. We observed a black precipitate in the bottom of solution. However, we only observed large Pd NPs with an average diameter of 3 nm in TEM images (Figure 3). We speculated that the direct addition of aqueous H<sub>2</sub>SO<sub>4</sub> into Pd@UiO-66-NH<sub>2</sub> caused the rapid collapse of the MOF. The Pd NCs were released rapidly, leading to their agglomeration in solution. Therefore, we turned to an interfacial etching approach to achieve a slower breakdown of the MOFs. Following this method, we dispersed the Pd@UiO-66-NH<sub>2</sub> and n-tetradecanethiol in methylene chloride first, to which the aqueous H<sub>2</sub>SO<sub>4</sub> was added drop-wise under vigorous stirring, leading to a biphasic CH<sub>2</sub>Cl<sub>2</sub>-H<sub>2</sub>O system. Since the Pd@UiO-66-NH<sub>2</sub> was suspended in methylene chloride, the acid etching of the MOF only happened at the interface of the two solvents, which slowed down the etching of MOFs. Additionally, this method also allowed the MOFs fragments (e.g., Zr clusters and 2-

aminoterephthalic acid) to preferentially remain in H<sub>2</sub>O, leading to a spontaneous phase separation of thiolated Pd NCs from the MOF fragments. After the etching process, the MOF solid disappeared and methylene chloride phase turned yellowish (Figure 2c), indicating the collapse of the MOF and the formation of Pd NCs.

To our delight, we found that the synthesized Pd NCs are ultra-small and highly monodisperse, as revealed by TEM in Figure 2b. The average particle diameter of 1.1 nm matches well with the size of the larger octahedral cage in UiO-66-NH<sub>2</sub> (~1.1 nm), demonstrating the templating effect exerted by the MOFs. Compared to previous studies on the synthesis of thiolated Pd NCs/NPs (Table 2), the thiolated NCs in our study are among the smallest and most monodisperse Pd NCs/NPs reported to date.

**Table 2.** Size and distribution comparison between our Pd NCs and previously reported ultra-small (< 2 nm) thiolated Pd NCs.

Method	Pd/thiol ratio	Size and distribution	Reference
Interfacial etching	1/1	1.1 ± 0.1 nm	Our work
Amphiphilic thiol	1/0.5	1.9 ± 0.2 nm	48
Extraction	1/0.5	1.5 ± 0.3 nm	49
Phase-transfer agents	1/40	1.3 ± 0.3 nm	50
Phase-transfer agents	1/2	1.6 nm	51
Phase-transfer agents	1/1	1.2 nm	52

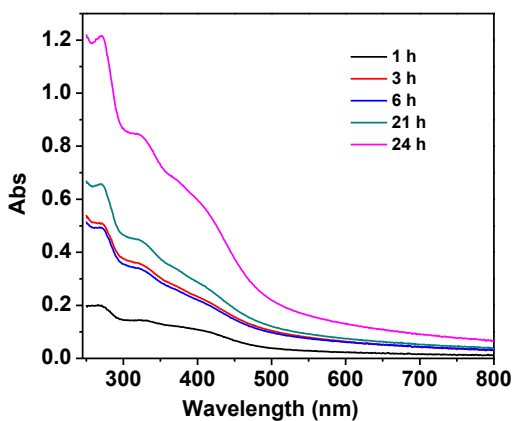


**Figure 4.** UV-vis absorption spectra of thiolated Pd NCs in methylene chloride for different times.

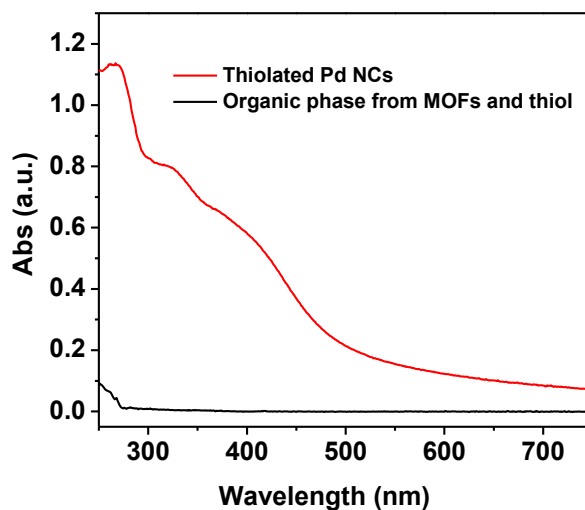


**Figure 5.** UV-Vis absorption spectra of thiolated Pd NCs and control sample prepared by etching of UiO-66-NH<sub>2</sub> and thiol in CH<sub>2</sub>Cl<sub>2</sub>.

UV-Vis absorption spectra of the methylene chloride solution at different etching times are illustrated in Figure 4. These absorbance wavelengths are in good agreement with those of Pd NCs reported previously.<sup>34,35</sup> We also performed a control

experiment by etching the bare MOF (UiO-66-NH<sub>2</sub>) in the presence of n-tetradecanethiol. The methylene chloride phase did not show any absorbance in UV-Vis absorption spectra (Figure 5), implying that the strong absorbance was due to Pd species.

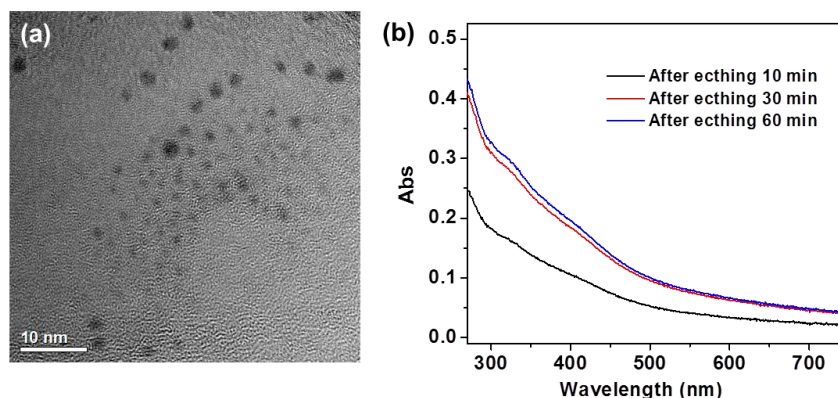


**Figure 6.** (a) TEM images of thiolated Pd NCs using 5 M H<sub>2</sub>SO<sub>4</sub> using interfacial etching and (b) UV-vis absorption spectra of thiolated Pd NCs from UiO-66-NH<sub>2</sub>.

We evaluated the impact of the H<sub>2</sub>SO<sub>4</sub> concentration on the preparation of monodisperse Pd NCs. We observed that when more concentrated H<sub>2</sub>SO<sub>4</sub>, i.e., 5 M, was used to break the MOFs, the obtained Pd NPs were not as monodisperse as those using 1.25 M H<sub>2</sub>SO<sub>4</sub>, as seen from their broader features in UV-Vis absorption spectra (Figure 6).<sup>36</sup> Hence, higher concentrations of the acid are not optimal for monodispersity even when used with the biphasic system. We also tested the feasibility of using other hydrophobic solvent (i.e., n-hexane) in the interfacial etching approach. Under the identical conditions, the as-obtained thiolated Pd NCs by

etching Pd@UiO-66-NH<sub>2</sub> feature a similar size although with a slightly broader size distribution ( $1.1 \pm 0.2$  nm, Figure 7), demonstrating the generality of the solvent.

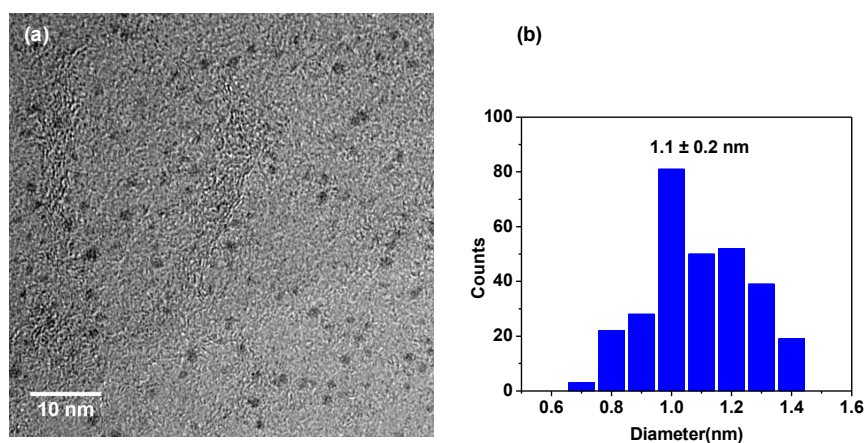


**Figure 7.** (a) TEM image of thiolated Pd NCs synthesized by using UiO-66-NH<sub>2</sub> as sacrificial template and n-hexane as the etching solvent. (b) Size distribution of thiolated Pd NCs (statistics are based on 300 particles counts).

Since amines can serve as capping agents in Pd NPs synthesis,<sup>37</sup> it is possible that the Pd NCs are capped with a mixed ligand shell consisting of tetradecanethiolate and 2-aminoterephthalic acid. But given that the Pd NCs are only soluble in the organic phase (CH<sub>2</sub>Cl<sub>2</sub>) and 2-aminoterephthalic acid (or its ammonium form in acidic condition) preferentially remains in H<sub>2</sub>O, tetradecanethiolate should be the main capping ligand on the as-prepared Pd NCs. To determine the exact composition of the capping agent, we used <sup>1</sup>H NMR to explore the organic content of the Pd NCs. In the <sup>1</sup>H NMR spectra of Pd NCs (Figure 8), we did not observe any peaks from 2-aminoterephthalic acid, which indicates n-tetradecanethiol may be the sole ligand of the Pd NCs. We also isolated and dried the thiolated Pd NCs to obtain a powder sample. The thermal stability of Pd NCs and the Pd/thiol ratio were assessed by

thermogravimetric analysis (TGA) (Figure 9). The Pd NCs start to lose thiols at 200 °C and the thiol layer decomposes completely at ~ 650 °C. Thus, the organic mass fraction is determined to be 73% and the remaining 27% is likely the Pd sulphide species (e.g., Pd<sub>4</sub>S,<sup>38</sup> PdS<sup>39</sup>). The two-stage weight loss in TGA suggested a mixed Pd-S and thiolated layers in the as-synthesized Pd NCs, which is proposed by Murayama et al.<sup>14</sup> Using ICP-MS analysis, we found the Pd content in this powder is 24 wt.%, which agrees with the TGA analysis assuming PdS is the final product. From both TGA and ICP-MS results, the molar ratio of Pd and tetradecanethiol capping is calculated to be 1:1.5 in average, implying a molecular formula of Pd<sub>m</sub>(C<sub>14</sub>H<sub>29</sub>S)<sub>1.5m</sub> for the NCs. Based on the size (ca.1.1 nm) in TEM, we estimate the Pd NCs contains approximately 40 Pd atoms.<sup>40</sup>

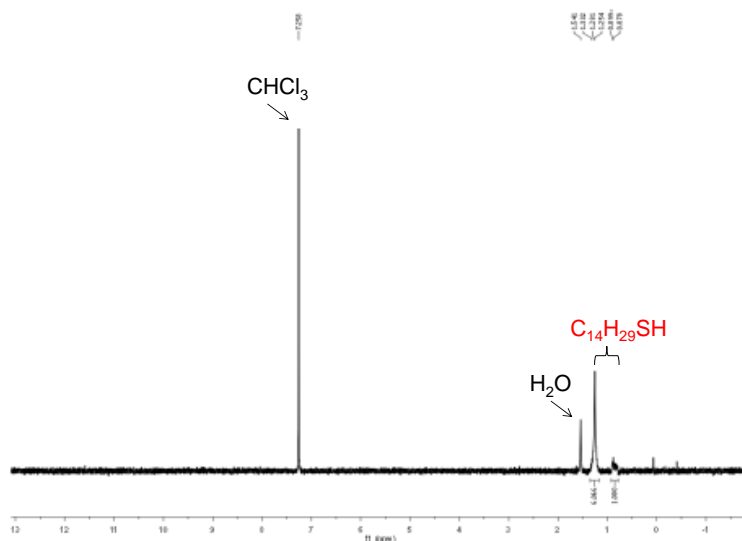


**Figure 8.** <sup>1</sup>H NMR spectra of thiolated Pd NCs synthesized by using UiO-66-NH<sub>2</sub> as sacrificial template (CDCl<sub>3</sub> as solvent).

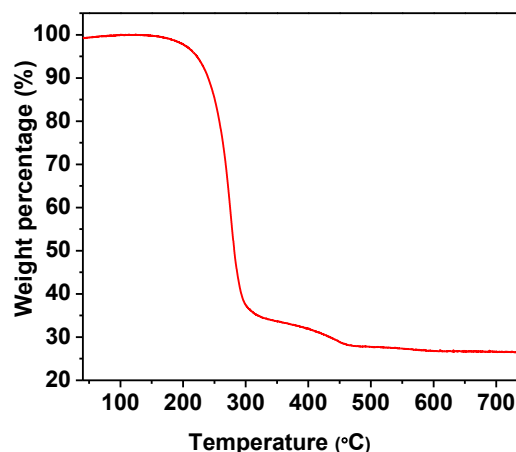


**Figure 9.** Thermogravimetric analysis of thiolated Pd NCs from UiO-66-NH<sub>2</sub>.

It has been reported that monodisperse Au NCs can be synthesized by thiol etching of polydisperse Au particles due to the strong Au-S interaction.<sup>41,42</sup> In order to exclude the role of such thiol etching in the formation of monodisperse Pd NCs synthesized in this work, we deliberately synthesized Pd NCs on UiO-66-NH<sub>2</sub> (denoted as Pd/UiO-66-NH<sub>2</sub>) using a less controlled method. This method allowed us to grow Pd NCs both on the external surface and in the internal cavities of the MOF, which leads to large Pd NCs of a broad size distribution ( $1.5 \pm 0.5$  nm) as shown in Figure 10a and c. After etching the Pd/UiO-66-NH<sub>2</sub> under the same conditions as for the Pd@UiO-66-NH<sub>2</sub>, the released Pd NPs still have a broad size distribution ( $1.6 \pm 0.4$  nm) as shown in Figure 10b and d, implying the thiol etching did not occur under the employed conditions that could lead to monodisperse Pd NCs. Moreover, the thiol concentration (1 equiv. of Pd) used in our method was far less than that in those typical ligand-induced etching methods.<sup>43,44</sup> All these aforementioned observations

strongly support the hypothesis that the uniform cavity of MOFs is the major factor in regulating the size of the released Pd NCs.

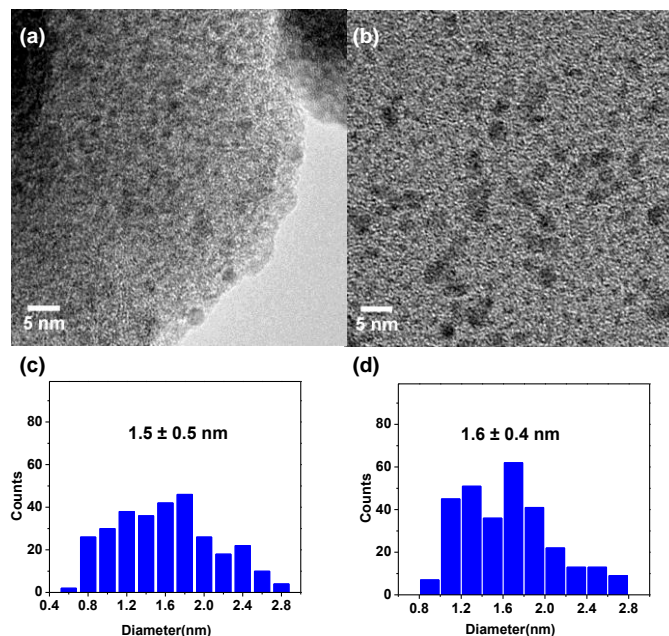
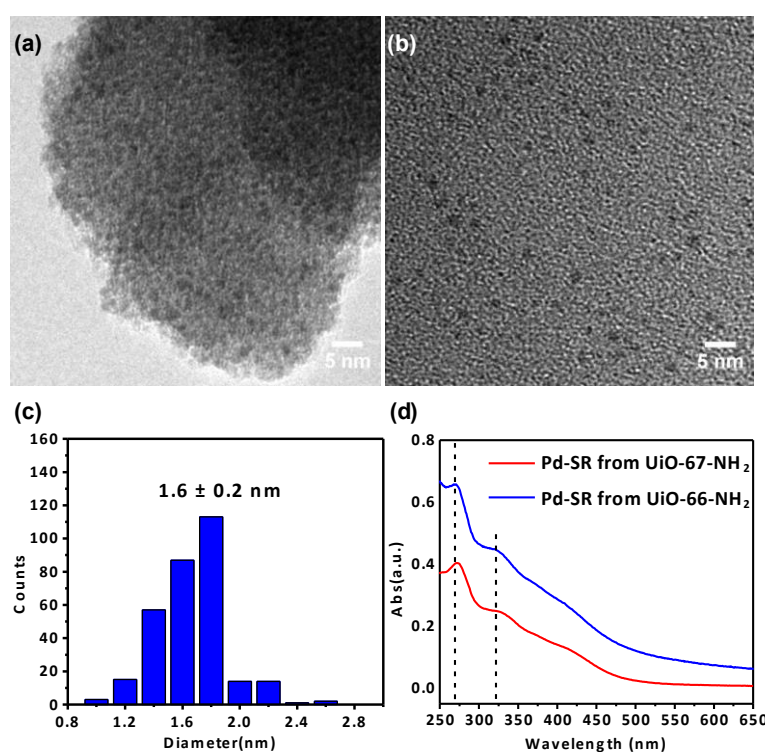


**Figure 10.** (a) TEM image of Pd/Uio-66-NH<sub>2</sub> before etching; (b) TEM image of thiolated Pd NCs after etching Pd/Uio-66-NH<sub>2</sub>; (c) Size distributions of Pd NCs in Pd/Uio-66-NH<sub>2</sub>; (d) Size distributions of thiolated Pd NCs.

Encouraged by the forgoing results, we considered enlarging the diameter of the MOF cavity to tune the resultant Pd NCs size, due to the cavity size tunability that MOFs can offer. Using the extended aminated linker, 1,1'-biphenyl-3-amino-4,4'-dicarboxylic acid, we constructed the isostructural analogue of Uio-66-NH<sub>2</sub>, i.e., Uio-67-NH<sub>2</sub>, which has enlarged octahedral cavities ( $\sim 1.6$  nm) and tetrahedral cavities ( $\sim 1.1$  nm) compared to Uio-66-NH<sub>2</sub> MOFs. PXRD confirmed the formation of Uio-67-NH<sub>2</sub>.<sup>45</sup> We used Uio-67-NH<sub>2</sub> as sacrificial templates for the synthesis of Pd NCs. The TEM images of Pd@Uio-67-NH<sub>2</sub> (Figure 12a) exhibited a uniform

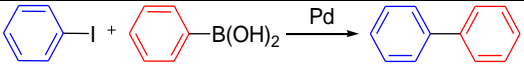


dispersion of Pd NCs. After interfacial etching, the Pd NCs exhibited an enlarged diameter of  $1.6 \pm 0.2$  nm (Figure 11b and c) compared to those synthesized using UiO-66-NH<sub>2</sub> as the template ( $1.1 \pm 0.1$  nm). This experiment demonstrates the diameter of Pd NCs can be readily controlled by the manipulation of the cavity diameter of the MOF templates. Moreover, the UV-Vis absorption peaks of the larger Pd NCs exhibited red-shift ( $\sim 5$  nm) compared to those of the smaller Pd NCs synthesized from UiO-66-NH<sub>2</sub> (Figure 11d).



**Figure 11.** TEM images of (a) Pd@UiO-67-NH<sub>2</sub> and (b) thiolated Pd NCs using UiO-67-NH<sub>2</sub> as a sacrificial template. (c) Size distributions of thiolated Pd NCs (based on 300 particles counts). (d) Comparison of UV-Vis absorption spectra of thiolated Pd NCs prepared by etching Pd@UiO-66-NH<sub>2</sub> and those from etching Pd@UiO-67-NH<sub>2</sub> in CH<sub>2</sub>Cl<sub>2</sub>.

**Table 3.** Suzuki-Miyaura coupling reaction by thiolated Pd NCs.

				
Entry	Catalyst	Time	Conv. <sup>a</sup>	Sel.
1	Blank	10 h	/	/
2	Pd-SR from UiO-66-NH <sub>2</sub>	10 h	97%	99%
3	Pd-SR from UiO-67-NH <sub>2</sub>	10 h	93%	99%

Conditions: 1 equiv. of iodobenzene, 1.5 equiv. of arylboronic acid, 3 equiv. of K<sub>2</sub>CO<sub>3</sub>, 2.5 mol% Pd, 2 mL of EtOH, 75 °C.  
<sup>a</sup> Conversion was determined by GC.

The catalytic activity of thiolated Pd NCs was evaluated with a model Suzuki-Miyaura coupling reaction, which has been extensively used for C-C bond formation in organic synthesis.<sup>46</sup> As illustrated in Table 3, a blank experiment in the absence of catalysts show negligible conversion, confirming that Pd is the active site for the reaction. The coupling reaction proceeded using these thiolated Pd NCs derived from the MOF templates as the catalysts and the corresponding products were obtained with high yields, implying the thiolated Pd NCs are catalytically active for the Suzuki-Miyaura coupling reaction. Future work on applying this methodology for the preparation of other noble metal NCs (e.g., Au, Ag, Pt) and optimizing the methodology via using non-thiol capping agents are currently underway.

## Conclusions

In summary, we have developed a novel and facile methodology for the preparation of thiolated Pd NCs with UiO MOFs (UiO-66-NH<sub>2</sub> and UiO-67-NH<sub>2</sub>) as sacrificial templates. Highly monodisperse and ultra-small thiolated Pd NCs were formed and characterized by TEM, UV-Vis absorption spectroscopy, TGA, and <sup>1</sup>H NMR to

understand their structure properties. We also demonstrated that the size of Pd NCs could be tuned by controlling the cavity diameter of the MOF template. These thiolated Pd NCs were shown to be efficient catalysts for a model Suzuki-Miyaura coupling reaction. Owing to its simplicity, and the precise control over the NCs size and uniformity, which are of key importance for the catalytic and optical properties of NCs, this novel methodology opens up fascinating avenues towards the synthesis of ultra-small and monodisperse metal NCs using MOFs as sacrificial templates. These ultra-small and monodisperse metal NCs will allow us to develop more active catalysts and study their size-dependent properties in a systematic manner.

### **Experimental section**

**General Method.** All reagents and solvents were of ACS certified grade or higher, and were used as received from commercial suppliers. UV-vis spectra of the Pd NCs were acquired using a Cary 100 Bio UV-visible spectrophotometer at ambient temperature. Samples were dissolved in  $\text{CH}_2\text{Cl}_2$  at 0.2 mg/mL to see strong peaks.  $^1\text{H}$  NMR spectra were acquired on a Bruker DRX400 spectrometer at 400 MHz. The actual loading of palladium in UiO MOFs was determined using a perkin 2100 plasma atomic emission spectrometer. Exact amount of Pd@MOFs was dissolved in aqua regia solution in autoclave under high pressure for ICP-MS analysis. Thermogravimetric analysis was conducted using TGA Q50 (TA Instruments, Inc.). Heating rate is  $20^\circ\text{C}/\text{min}$ ,  $\text{N}_2$  flow rate is 60 mL/min, balance gas (nitrogen) flow rate 40 mL/min. The size and morphology of Pd@MOFs and thiolate-Pd NCs were investigated by using TEM and high angle annular dark field scanning transmission

electron microscopy (HAADF-STEM) images recorded on a Tecnai G2 F20 electron microscope with EDX analysis (Oxford INCA EDS) operated at 200 kV. Methylene chloride solution of Pd NCs was drop-cast onto lacey formvar with carbon film grid followed by drying in open air.

### **Synthesis of Pd NCs**

The preparation process consists of two steps: (1) Synthesis of Pd@UiO-66-NH<sub>2</sub> and (2) Preparation of thiolate-Pd NCs via etching Pd@UiO-66-NH<sub>2</sub>. For synthesis of Pd@UiO-66-NH<sub>2</sub>, 100 mg of activated UiO-66-NH<sub>2</sub> were dispersed in methylene chloride solution of Pd(OAc)<sub>2</sub> for 24 hours. The as-prepared Pd-infiltrated MOFs were washed thrice for 12 hours each time with fresh methylene chloride to completely remove the remaining palladium salts. The reduction process of the Pd(OAc)<sub>2</sub>@UiO-66-NH<sub>2</sub> was performed under a 50 mL/min flow of 10% H<sub>2</sub>/Ar at 200 °C for 2 hours to yield Pd NCs@UiO-66-NH<sub>2</sub>. 2 mg of the resulting Pd NC@UiO-66-NH<sub>2</sub> was dispersed in 2 mL of methylene chloride and *n*-tetradecanethiol in methylene chloride (HSC<sub>14</sub>H<sub>29</sub>:Pd = 1:1) was added subsequently. After stirring for 1 hour, 2 mL of H<sub>2</sub>SO<sub>4</sub> (1.25M) was added into the solution dropwise under vigorous stirring at 800 rpm and this process lasts 10 min. The lower phase turned yellow and the UiO-66-NH<sub>2</sub> solid disappeared with time proceeding, indicating the breakdown of the MOFs and formation of Pd NCs. After 6 h, the reaction was stopped and the organic phase was collected for further characterization.

### **Preparation of Pd NPs deposited on the surface of UiO-66-NH<sub>2</sub> (Pd/UiO-66-NH<sub>2</sub>)**

100 mg of UiO-66-NH<sub>2</sub> was in a mortar and 8.6 mg of Pd(OAc)<sub>2</sub> in 0.5 mL of methylene chloride ( volume exceeds the pore volume of UiO-66-NH<sub>2</sub>) was added

onto the MOFs. The mixture was grinded and air-dried. The sample was reduced under a 50 mL/min flow of 10% H<sub>2</sub>/Ar at 200 °C for 2 hours.

#### **General experimental procedure for Suzuki cross-coupling reaction.**

Under aerobic conditions, thiolated Pd NCs (2.5 mol% Pd) was dissolved in EtOH (2 mL), followed by the addition of iodobenzene (1.2 μL, 1 equiv.), arylboronic acid (1.9 mg, 1.5 equiv.), potassium carbonate (4.5 mg, 3 equiv.) and n-decane (3 μL, internal standard). The reaction mixture was stirred at 75 °C in a 20 mL glass vial. Upon completion of the reaction, the products were analyzed using a HP 5890 gas chromatograph (GC) equipped with a HP-5 capillary column (30 m × 0.32 mm × 0.25 μm) with a flame ionization detector and Agilent 6890N/5975 gas chromatograph mass spectroscopy (GC-MS) equipped with a HP-5ms capillary column (30 m × 0.32 mm × 0.25 μm).

#### **Acknowledgements**

We gratefully acknowledge the financial support from the Ames Laboratory (Royalty Account) and Iowa State University. The Ames Laboratory is operated for the U.S. Department of Energy by Iowa State University under Contract No. DE-AC02-07CH11358. P.K.J acknowledges support through a Sloan Fellowship. We thank Robert J. Angelici for his advice in the writing of this manuscript. We thank Gordon J. Miller for the use of XRD instrument and Yan Zhao for the use of UV-Vis instrument.

#### **References**

- (1) Li, G.; Jin, R. *Acc. Chem. Res.* **2013**, *46*, 1749-1758.

- (2) Qian, H.; Zhu, M.; Wu, Z.; Jin, R. *Acc. Chem. Res.* **2012**, *45*, 1470-1479.
- (3) Tian, D.; Qian, Z.; Xia, Y.; Zhu, C. *Langmuir* **2012**, *28*, 3945-3951.
- (4) Park, J.; An, K.; Hwang, Y.; Park, J.-G.; Noh, H.-J.; Kim, J.-Y.; Park, J.-H.; Hwang, N.-M.; Hyeon, T. *Nat. Mater.* **2004**, *3*, 891-895.
- (5) Li, G.; Jiang, D.-e.; Kumar, S.; Chen, Y.; Jin, R. *ACS Catal.* **2014**, *4*, 2463-2469.
- (6) Parker, J. F.; Fields-Zinna, C. A.; Murray, R. W. *Acc. Chem. Res.* **2010**, *43*, 1289-1296.
- (7) Jin, R. *C. Nanoscale* **2015**, *7*, 1549-1565.
- (8) Lang, H. F.; May, R. A.; Iversen, B. L.; Chandler, B. D. *J. Am. Chem. Soc.* **2003**, *125*, 14832-14836.
- (9) Lu, Y.; Chen, W. *Chem. Soc. Rev.* **2012**, *41*, 3594-3623.
- (10) Goulet, P. J.; Lennox, R. B. *J. Am. Chem. Soc.* **2010**, *132*, 9582-9584.
- (11) Yu, Y.; Yao, Q.; Luo, Z.; Yuan, X.; Lee, J. Y.; Xie, J. *Nanoscale* **2013**, *5*, 4606-4620.
- (12) Yonezawa, T.; Imamura, K.; Kimizuka, N. *Langmuir* **2001**, *17*, 4701-4703.
- (13) Zamborini, F. P.; Gross, S. M.; Murray, R. W. *Langmuir* **2001**, *17*, 481-488.
- (14) Murayama, H.; Ichikuni, N.; Negishi, Y.; Nagata, T.; Tsukuda, T. *Chem. Phys. Lett.* **2003**, *376*, 26-32.
- (15) Chen, S.; Huang, K.; Stearns, J. A. *Chem. Mater.* **2000**, *12*, 540-547.
- (16) Quiros, I.; Yamada, M.; Kubo, K.; Mizutani, J.; Kurihara, M.; Nishihara, H. *Langmuir* **2002**, *18*, 1413-1418.
- (17) Cargnello, M.; Wieder, N. L.; Canton, P.; Montini, T.; Giambastiani, G.; Benedetti, A.; Gorte, R. J.; Fornasiero, P. *Chem. Mater.* **2011**, *23*, 3961-3969.
- (18) Croy, J. R.; Mostafa, S.; Liu, J.; Sohn, Y.-H.; Cuenya, B. R. *Catal. Lett.* **2007**, *118*, 1-7.
- (19) Huang, W.; Kuhn, J. N.; Tsung, C.-K.; Zhang, Y.; Habas, S. E.; Yang, P.; Somorjai, G. A. *Nano Lett.* **2008**, *8*, 2027-2034.
- (20) de Jesus, D. M.; Spiro, M. *Langmuir* **2000**, *16*, 4896-4900.

- (21) Voloskiy, B.; Niwa, K.; Chen, Y.; Zhao, Z.; Weiss, N. O.; Zhong, X.; Ding, M.; Lee, C.; Huang, Y.; Duan, X. *ACS Nano* **2015**, *9*, 3044-3049.
- (22) Zhang, S.; Zhao, Y. *Chem. Commun.* **2012**, *48*, 9998-10000.
- (23) Zhang, S.; Zhao, Y. *ACS Nano* **2011**, *5*, 2637-2646.
- (24) Sun, J.-K.; Xu, Q. *Energy Environ. Sci.* **2014**, *7*, 2071-2100.
- (25) Lux, L.; Williams, K.; Ma, S. *CrystEngComm* **2015**, *17*, 10-22.
- (26) Jacobs, B. W.; Houk, R. J. T.; Anstey, M. R.; House, S. D.; Robertson, I. M.; Talin, A. A.; Allendorf, M. D. *Chem. Sci.* **2011**, *2*, 411-416.
- (27) Kuang, X.; Ma, Y.; Zhang, C.; Su, H.; Zhang, J.; Tang, B. *Chem. Commun.* **2015**, *51*, 5955-5958.
- (28) Liu, B.; Shioyama, H.; Akita, T.; Xu, Q. *J. Am. Chem. Soc.* **2008**, *130*, 5390-5391.
- (29) Song, Y.; Li, X.; Sun, L.; Wang, L. *RSC Adv.* **2015**, *5*, 7267-7279.
- (30) Yang, Q.; Wiersum, A. D.; Llewellyn, P. L.; Guillerm, V.; Serre, C.; Maurin, G. *Chem. Commun.* **2011**, *47*, 9603-9605.
- (31) Li, X.; Guo, Z.; Xiao, C.; Goh, T. W.; Tesfagaber, D.; Huang, W. *ACS Catal.* **2014**, *4*, 3490-3497.
- (32) Guo, Z.; Xiao, C.; Maligal-Ganesh, R. V.; Zhou, L.; Goh, T. W.; Li, X.; Tesfagaber, D.; Thiel, A.; Huang, W. *ACS Catal.* **2014**, *4*, 1340-1348.
- (33) Li, X.; Goh, T. W.; Li, L.; Xiao, C.; Guo, Z.; Zeng, X. C.; Huang, W. *ACS catal.* **2016**, 3461-3468.
- (34) Negishi, Y.; Murayama, H.; Tsukuda, T. *Chem. Phys. Lett.* **2002**, *366*, 561-566.
- (35) Yang, Z.; Smetana, A. B.; Sorensen, C. M.; Klabunde, K. J. *Inorg. Chem.* **2007**, *46*, 2427-2431.
- (36) AlanáCreighton, J. *J. Chem. Soc., Faraday Trans.* **1991**, *87*, 3881-3891.
- (37) Moreno, M.; Ibanez, F. J.; Jasinski, J. B.; Zamborini, F. P. *J. Am. Chem. Soc.* **2011**, *133*, 4389-4397.

- (38) Grønvold, F.; Røst, E. *Acta Crystallogr.* **1962**, *15*, 11-13.
- (39) Brese, N. E.; Squattrito, P. J.; Ibers, J. A. *Acta Crystallographica Section C: Crystal Structure Communications* **1985**, *41*, 1829-1830.
- (40) Zhao, M.; Crooks, R. M. *Angew. Chem. Int. Ed.* **1999**, *38*, 364-366.
- (41) Nimmala, P. R.; Dass, A. *J. Am. Chem. Soc.* **2014**, *136*, 17016-17023.
- (42) Qian, H.; Zhu, M.; Andersen, U. N.; Jin, R. *J. Phys. Chem. A* **2009**, *113*, 4281-4284.
- (43) Schaaff, T. G.; Whetten, R. L. *J. Phys. Chem. B* **1999**, *103*, 9394-9396.
- (44) Shichibu, Y.; Negishi, Y.; Tsukuda, T.; Teranishi, T. *J. Am. Chem. Soc.* **2005**, *127*, 13464-13465.
- (45) Schaate, A.; Roy, P.; Godt, A.; Lippke, J.; Waltz, F.; Wiebcke, M.; Behrens, P. *Chem. Eur. J.* **2011**, *17*, 6643-6651.
- (46) Miyaura, N.; Suzuki, A. *Chem. Rev.* **1995**, *95*, 2457-2483.
- (47) Cavka, J. H.; Jakobsen, S.; Olsbye, U.; Guillou, N.; Lamberti, C.; Bordiga, S.; Lillerud, K. P. *J. Am. Chem. Soc.* **2008**, *130*, 13850-13851.
- (48) Cargnello, M.; Wieder, N. L.; Canton, P.; Montini, T.; Giambastiani, G.; Benedetti, A.; Gorte, R. J.; Fornasiero, P. A. *Chem. Mater.* **2011**, *23*, 3961-3969.
- (49) Garcia-Martinez, J. C.; Scott, R. W.; Crooks, R. M. *J. Am. Chem. Soc.* **2003**, *125*, 11190-11191.
- (50) Quiros, I.; Yamada, M.; Kubo, K.; Mizutani, J.; Kurihara, M.; Nishihara, H. *Langmuir* **2002**, *18*, 1413-1418.
- (51) Zamborini, F. P.; Gross, S. M.; Murray, R. W. *Langmuir* **2001**, *17*, 481-488.
- (52) Litrán, R.; Sampedro, B.; Rojas, T. C.; Multigner, M.; Sánchez-López, J. C.; Crespo, P.; López-Cartes, C.; García, M.; Hernando, A.; Fernández, A. *Phys. Rev. B* **2006**, *73*, 054404.



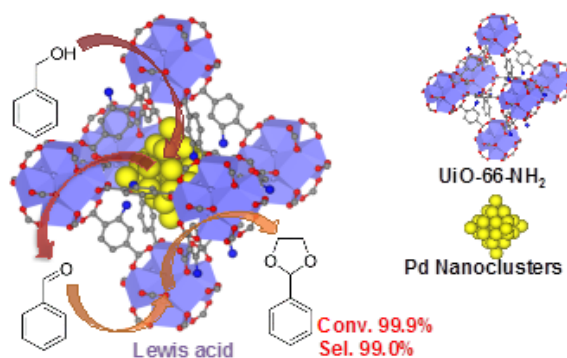
**CHAPTER 3**  
**TANDEM CATALYSIS BY PALLADIUM NANOCCLUSERS**  
**ENCAPSULATED IN METAL ORGANIC FRAMEWORKS**

A paper published in *ACS Catal.* **2014**, 4, 3490–34971

Xinle Li, Zhiyong Guo, Chaoxian Xiao, Wenyu Huang

**Abstract**

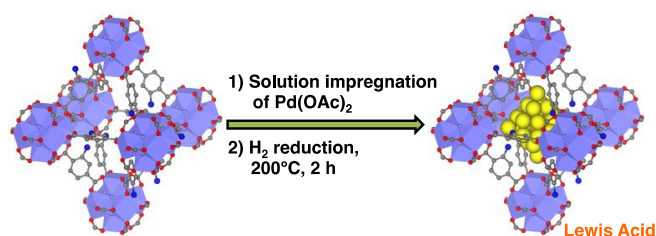
A bifunctional Zr-MOF catalyst containing palladium NCs has been developed. Combining the oxidation activity of Pd NCs and the acetalization activity of the Lewis acid sites in UiO-66-NH<sub>2</sub>, this catalyst (Pd@UiO-66-NH<sub>2</sub>) exhibits excellent catalytic activity and selectivity in a one-pot tandem oxidation-acetalization reaction. This catalyst shows 99.0% selectivity to benzaldehyde ethylene acetal in the tandem reaction of benzyl alcohol and ethylene glycol at 99.9% conversion of benzyl alcohol. We investigated Pd@UiO-66 in the same system and proved the superiority of using Pd@UiO-66-NH<sub>2</sub>. We also examined various substituted benzyl alcohols and found that alcohols with electron-donating groups showed better conversion and selectivity compared to those with electron-withdrawing groups. We further proved that there was no leaching of active catalytic species during the reaction and the catalyst can be recycled at least five times without significant deactivation.



## Introduction

With the pressing need for catalysis technologies that could address the energy crisis and environmental pollution confronting our societies, a great deal of research effort has been devoted to finding novel and efficient multifunctional catalysts for one-pot tandem reactions.<sup>1-8</sup> Tandem catalysis, in which multi-step chemical transformations are catalysed with a multifunctional catalyst, has attracted increasing research attention because selective multifunctional catalysts will make a multi-step reaction go to the desired products in one reactor without the need for separation, purification, and transfer of intermediates produced in each step. The development of multi-step catalytic processes using multifunctional catalysts can also minimize the amount of by-products/waste produced during multi-step chemical reactions and achieve atomic efficiency, one of the focuses of green chemistry. Conversely, traditional multi-step catalytic processes involve a series of conversions in different reactors with intermediate purification steps to achieve a desired product. Therefore, traditional multi-step catalytic processes usually require a high-energy input for the separation of intermediates and cause a low yield of the final products due to the losses of intermediates within individual steps of the processes.

In recent years, MOFs have demonstrated their potential application as heterogeneous catalysts, especially those using MOFs as a supporting matrix for metal nanoparticles (known as metal@MOFs).<sup>9-18</sup> Despite the many investigations of the MOFs' role in catalysis, there are only a limited number of studies of bifunctional metal@MOFs systems for tandem catalysis. Fischer et al. and Haruta et al. reported Au@ZIF-8 and Au@MOF-5 as catalyst in the synthesis of methyl benzoate from the aerobic oxidation of benzyl alcohol, respectively;<sup>19,20</sup> Corma et al. developed Pd@MIL-101 as a catalyst for one-pot synthesis of menthol from citronellal.<sup>21</sup> Li's group prepared Pd@MIL-101 for the one-pot synthesis of methyl isobutyl (MIBK) ketone from acetone.<sup>22</sup> Recently, Li's group also prepared a bimetallic MOF catalyst (Au-Pd@MIL-101) and used it for the one-pot synthesis of aromatic esters from alkyl aromatics.<sup>23,24</sup> Tang et al. designed a core-shell Pd@IRMOF-3 and used it as a multifunctional catalyst for a cascade condensation-hydrogenation reaction.<sup>25</sup>



**Scheme 1.** Synthesis of the heterogeneous tandem catalyst by encapsulating Pd NCs inside the cavities of UiO-66-NH<sub>2</sub>.

As pointed out by recent reviews, the field of developing tandem catalysis using MOFs remains relatively unexplored and will have a large impact on current industrial processes.<sup>26</sup> Herein, we have developed a bifunctional tandem heterogeneous catalyst by encapsulating Pd NCs in the cavities of UiO-66-NH<sub>2</sub>

(Scheme 1), which could catalyse the oxidation of benzyl alcohol and the subsequent acetalization of benzaldehyde with ethylene glycol. One-pot tandem reaction through oxidation of alcohols followed by acetalization of the carbonyl compounds using heterogeneous catalysts in liquid phase has rarely been studied so far. Considerable research aiming at one-step gas phase conversion of methanol to 1,1-dimethoxymethane (DMM) over a variety of heterogeneous catalytic systems can be found in the literature, i.e. molybdenum-based catalysts,<sup>27</sup> heteropolyacids (HPAs),<sup>28</sup> oxides of ruthenium and rhenium,<sup>29-32</sup> as well as vanadium-based catalysts,<sup>33-35</sup> typically at temperatures above 400 K. With regard to one-pot higher acetals synthesis, we have found limited work related to direct synthesis from ethanol via photocatalytic oxidation or H<sub>2</sub>O<sub>2</sub> oxidation catalysed by Fe (III) complexes.<sup>36-38</sup> Moreover, Gusevskaya et al. reported the use of a chloride-free Pd(OAc)<sub>2</sub>/Cu(OAc)<sub>2</sub>/p-toluenesulfonic acid catalytic combination for the selective aerobic oxidation of primary alcohols to the corresponding acetals.<sup>39</sup> Graham et al. performed the one-pot tandem oxidation/ acetalization reaction of benzyl alcohol with manganese dioxide, trialkyl orthoformate and catalytic quantities of indium triflate.<sup>40</sup> To the best of our knowledge, this is the first example of applying MOF-based heterogeneous catalysts in tandem oxidation-acetalization liquid phase reaction.

UiO-66-NH<sub>2</sub> is built up from [Zr<sub>6</sub>O<sub>4</sub>(OH)<sub>4</sub>(CO<sub>2</sub>)<sub>12</sub>] clusters linked with 2-aminoterephthalic acid.<sup>41</sup> UiO-66-NH<sub>2</sub> possesses uncoordinated zirconium sites, which could serve as Lewis acid sites for catalysis. These Lewis acid sites have been used to catalyse the cross-aldol condensation, cyclization of citronellal and acetalization.<sup>42-44</sup> By combining the oxidation activity of Pd NCs and the acetalization

activity of the Lewis acid sites on UiO-66-NH<sub>2</sub>, we developed this tandem Pd@UiO-66-NH<sub>2</sub> catalyst, which showed 99.9% conversion of benzyl alcohol in the one-pot tandem reaction of benzyl alcohol and ethylene glycol with 99.0% acetal selectivity. Acetals are a class of chemicals that can be used for the protection of carbonyl compounds. They are also widely utilized as organic solvents, fuel additives, steroids, besides being important in the pharmaceutical and fragrance industries.<sup>45,46</sup> Generally, acetal syntheses are carried out by the condensation of glycols with aldehydes using mineral acid catalysts.<sup>47</sup> However, these catalysts are toxic, corrosive, and difficult to remove after the reaction.

## Results and Discussion

The Pd@UiO-66-NH<sub>2</sub> catalyst was synthesized by loading Pd precursor, palladium (II) acetate, into UiO-66-NH<sub>2</sub> in methylene chloride. After separating the MOF powder by centrifugation, we dried the powder under vacuum at 80 °C and then reduced the Pd (II) loaded MOF under 50 mL/min flow of 10% H<sub>2</sub>/Ar at 200 °C to form Pd NCs (Scheme 1). The successful loading of Pd in UiO-66-NH<sub>2</sub> was confirmed by EDX spectroscopy. As shown in Figure 1, a clear Pd peak was resolved when we probed selected area 1 on the Pd loaded MOF. We also observed a similar EDX spectrum when we probed area 2. The loading of Pd in UiO-66-NH<sub>2</sub> is 2.0 wt.%, as measured by ICP-AES.

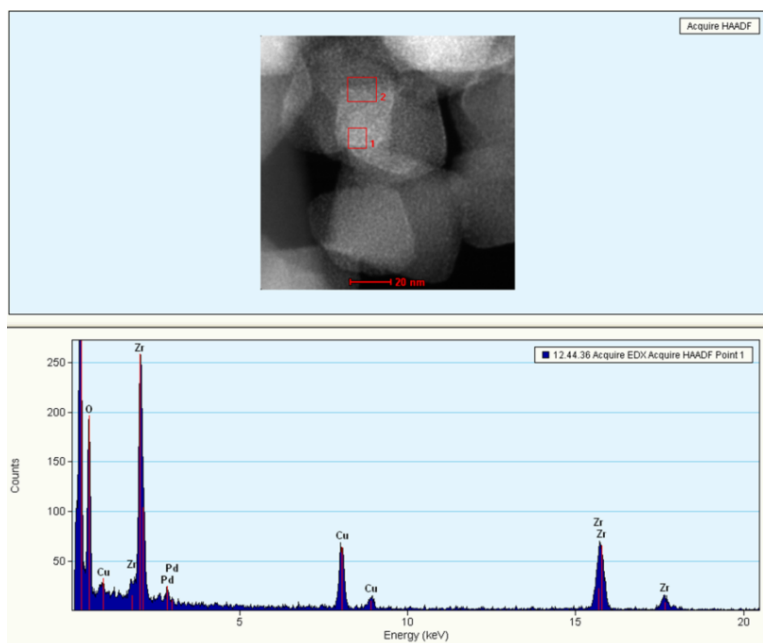


**Figure 1.** EDX spectrum of 2.0 wt.% Pd@UiO-66-NH<sub>2</sub> collected from area 1 as shown in the HAADF-STEM measurement.

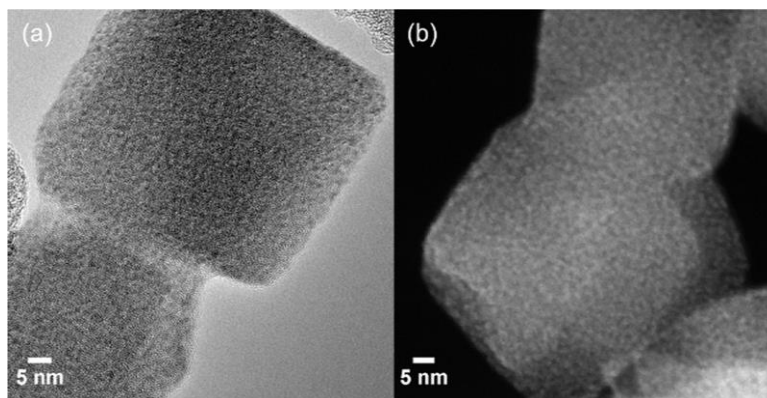


**Figure 2.** (a) TEM and (b) HAADF-STEM images of 2.0 wt.% Pd@UiO-66-NH<sub>2</sub>. The Pd@UiO-66-NH<sub>2</sub> was synthesized by loading palladium (II) acetate, into UiO-66-NH<sub>2</sub> in CH<sub>2</sub>Cl<sub>2</sub>. After separating and drying the powder, we reduced it under 50 mL/min flow of 10% H<sub>2</sub>/Ar at 200 °C to form Pd NCs.

The TEM image of Pd@UiO-66-NH<sub>2</sub> is shown in Figure 2a, in which Pd NCs are well dispersed with a mean diameter less than 1.2 nm (the diameter of the large octahedral cages in UiO-66-NH<sub>2</sub>). To increase the contrast of the Pd NCs against the

MOF support, we also measured high angle annular dark field scanning transmission electron microscopy (HAADF-STEM) images of Pd@UiO-66-NH<sub>2</sub> as shown in Figure 2b. We could not find any particle that has a diameter larger than 1.2 nm, which indicates that the formed Pd NCs are well dispersed inside the cavities of the MOF.

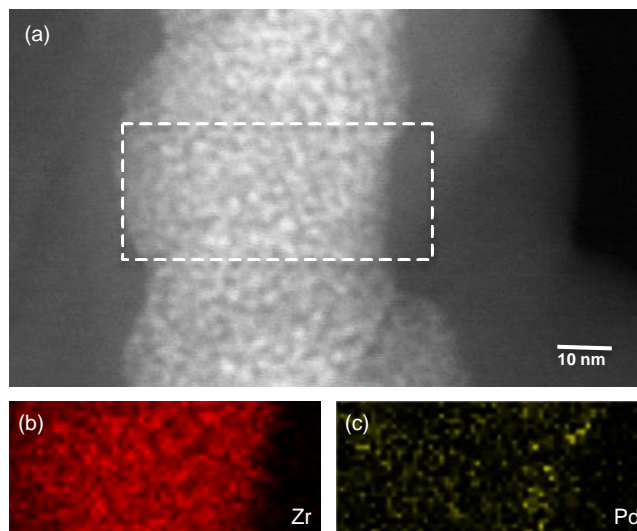


**Figure 3.** (a) HAADF-STEM image of 2.0 wt.% Pd@UiO-66-NH<sub>2</sub> after reduction. EDX elemental mapping of the selected area (rectangle indicated by the dash line in a) for (b) Zr and (c) Pd. Pd element (green) was shown to uniformly disperse with Zr (red) in UiO-66-NH<sub>2</sub>

From the EDX mapping of selected area on the Pd@UiO-66-NH<sub>2</sub> (the rectangle indicated by the dashed line in Figure 3), Pd was found to exist along with Zr as shown in Figure 3b and 3c, indicating Pd was effectively trapped by the MOF. The dispersion was uniform, and no sign of aggregation was observed. We are aware that the 2D TEM images cannot exclusively determine whether the Pd NCs are located inside or on the surface of the MOF. Therefore, we tried to rotate the TEM sample and tracked the same Pd NCs to confirm that these NCs are located inside the

MOF. Using this method, we were able to confirm that Pt NCs are encapsulated in UiO-66-NH<sub>2</sub> in our previous work.<sup>54</sup> However, to follow the same Pd NC is extremely hard during the TEM measurement because of the small difference in electron beam contrast for Pd NCs and [Zr<sub>6</sub>O<sub>4</sub>(OH)<sub>4</sub>(CO<sub>2</sub>)<sub>12</sub>] clusters in the MOF.

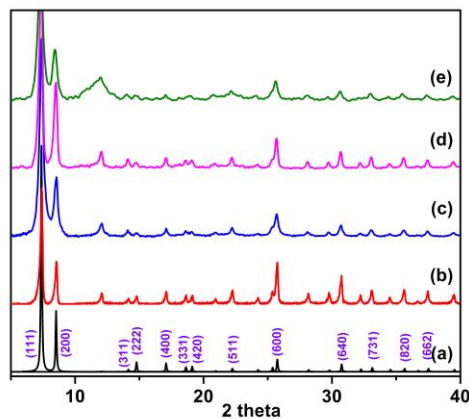


**Figure 4.** Indexed PXRD patterns of (a) simulated UiO-66, (b) as-synthesized UiO-66-NH<sub>2</sub>, (c) 2.0 wt.% Pd@UiO-66-NH<sub>2</sub> after reduction, (d) 2.0 wt.% Pd@UiO-66-NH<sub>2</sub> after reaction, (e) 2.0 wt.% Pd@UiO-66-NH<sub>2</sub> after recycle test.

The PXRD pattern of as-synthesized UiO-66-NH<sub>2</sub> matches well with the reported patterns of the MOF (pattern b in Figure 4).<sup>48,55</sup> UiO-66-NH<sub>2</sub> is very stable during the loading of Pd precursor and the reduction treatment under 10 % H<sub>2</sub>/Ar at 200 °C. We do not observe any obvious changes in the XRD patterns of Pd@UiO-66-NH<sub>2</sub> that indicates the loss of the MOF's crystalline structure (pattern c in Figure 4). Furthermore, we do not find any X-ray diffraction peaks from Pd nanocrystal, which suggests that the encapsulated Pd particles are very small. TGA indicates that Pd@UiO-66-NH<sub>2</sub> is thermally stable below ~280 °C (Figure 5).



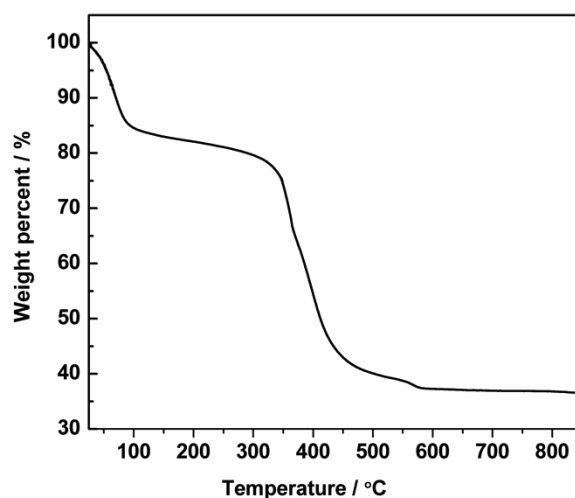


**Figure 5.** TGA of 2.0 wt.%Pd@UiO-66-NH<sub>2</sub> in N<sub>2</sub>. The initial weight loss below 100 °C is due to the removal of water.

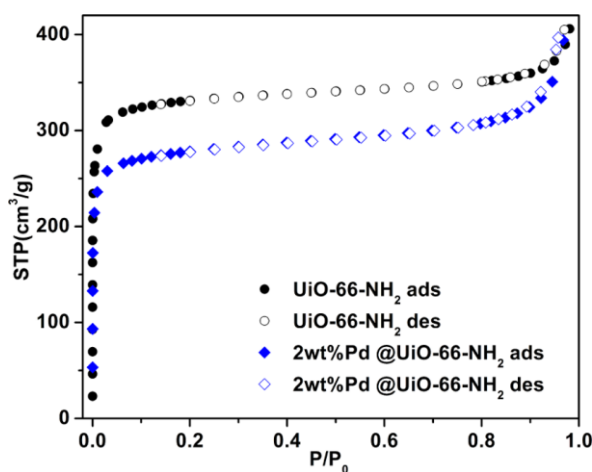


**Figure 6.** Nitrogen sorption isotherms of the as-synthesized UiO-66-NH<sub>2</sub> and 2.0 wt.% Pd@UiO-66-NH<sub>2</sub>.

The surface areas and pore volumes of the samples were measured by N<sub>2</sub> physisorption at -196 °C. Figure 6 shows the N<sub>2</sub> adsorption-desorption isotherm profiles of UiO-66-NH<sub>2</sub>, and 2.0 wt.% Pd@UiO-66-NH<sub>2</sub>. All adsorption-desorption isotherms show a type I shape, a characteristic of microporous materials. The BET

surface area and micropore volume of UiO-66-NH<sub>2</sub> were calculated to be 1194 m<sup>2</sup>g<sup>-1</sup> and 0.44 cm<sup>3</sup>g<sup>-1</sup>, respectively, which are close to the reported values.<sup>42</sup> Compared to UiO-66-NH<sub>2</sub>, the BET surface area and pore volume of 2.0 wt.% Pd@UiO-66-NH<sub>2</sub> decreased to 936 m<sup>2</sup>g<sup>-1</sup> and 0.36 cm<sup>3</sup>g<sup>-1</sup>, respectively, mainly because of the occupation of the cages of UiO-66-NH<sub>2</sub> by Pd NCs.<sup>11</sup>

We also tried to determine the oxidation state of Pd in UiO-66-NH<sub>2</sub> after reduction using X-ray photoelectron spectroscopy (XPS). However, due to the overlap between Pd 3d and Zr 3p peaks (from 330 to 350 eV) and the much higher concentration of Zr compared to Pd, we could not get a good fitting of the XPS spectra to determine the oxidation state of the Pd. Instead, we used extended X-ray absorption fine structure (EXAFS) spectroscopy to study the coordination environment of Pd before and after reducing the Pd (II)-loaded UiO-66-NH<sub>2</sub>. As shown in Figure 7a, the EXAFS spectrum of the sample before reduction is dominated by the Pd-O scattering. The Pd-O coordination number determined from fitting the EXAFS spectrum is  $3.6 \pm 0.3$ , which agrees with the structure of the Pd precursor, palladium acetate, although the interatomic distance ( $2.05 \pm 0.01$  Å) is slightly higher than that in Pd(OAc)<sub>2</sub> ( $2.00 \pm 0.01$  Å). After reduction with 10% H<sub>2</sub>/Ar at 200 °C, the scattering of Pd-Pd appears in Fourier transform as shown in Figure 8b. EXAFS fitting showed that Pd-Pd scattering has a coordination number of  $3.7 \pm 0.3$  with interatomic distance of  $2.78 \pm 0.01$  Å, indicating the formation of Pd NCs.

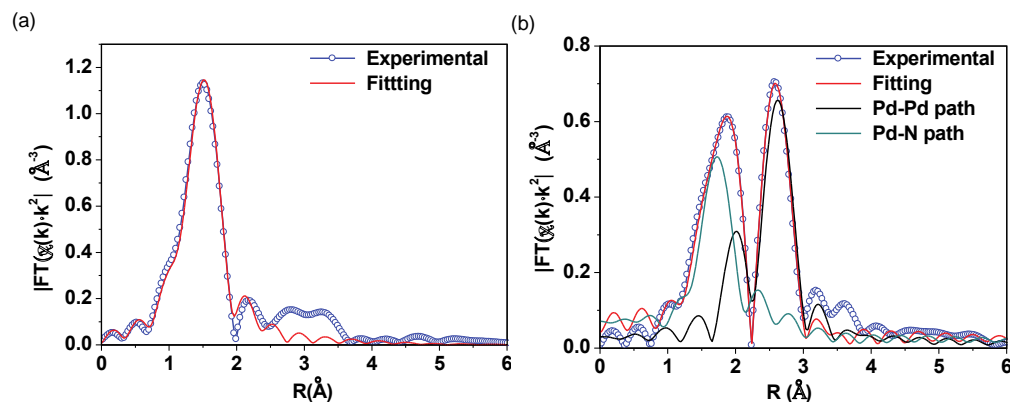


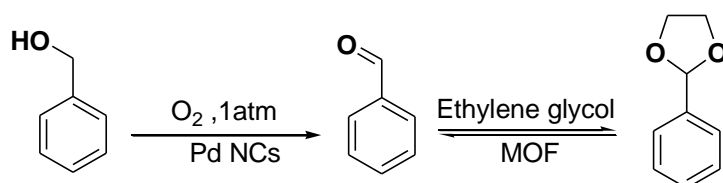
**Figure 7.** Fourier transform of EXAFS data extracted from Pd K edge (blue empty dot) and the computed fits (red line) in R space for 4.8 wt.% Pd@UiO-66-NH<sub>2</sub> samples: (a) before and (b) after reduction under 50 mL/min flow of 10% H<sub>2</sub>/Ar at 200 °C. FT peak positions are not corrected for phase shifts. The individual theoretical paths (Pd-Pd and Pd-N) used to fit the experimental data were also shown in (b). For comparison, only their magnitudes were shown.

Additionally, Fourier transform also indicates the presence of another scattering from Pd-N or Pd-O. The interatomic distance was found to be ~2.16-2.19 Å with fitting. This distance is obviously longer than that in PdO phase usually found in Pd catalysts (~2.0 Å).<sup>56,57</sup> However, in some catalysts with strong metal-support interaction, the metal-oxide distance was reported to be much longer (2.19 Å).<sup>58</sup> Besides, Pd-N bond length could vary between 2.0-2.2 Å, depending on the coordination environment.<sup>59,60</sup> Due to the presence of -NH<sub>2</sub> groups in UiO-66-NH<sub>2</sub>, it is more likely that the -NH<sub>2</sub> group coordinates with Pd NCs after the reduction.

The tandem oxidation-acetalization reactions of benzyl alcohol and ethylene glycol were carried out with 2.0 wt.% Pd@UiO-66-NH<sub>2</sub> and 1.9 wt.% Pd@UiO-66 under 0.1 MPa O<sub>2</sub> at 90 °C in cyclohexane. As shown in Table 1 (entry 1), Pd@UiO-66-NH<sub>2</sub> was an active catalyst for this one-pot tandem reaction and 99.9% conversion

of benzyl alcohol with 99.0% selectivity to benzaldehyde ethylene acetal was achieved.

**Table 1.** Performance of the heterogeneous tandem catalyst in the oxidation of benzyl alcohol and the subsequent acetalization with ethylene glycol.



Entry	Sample	Substrate	Solvent	time (h)	Conv. (%)	Alde (%)	Acetal <sup>f</sup> (%)	Ester <sup>g</sup> (%)
1 <sup>a</sup>	Pd@UiO-66-NH <sub>2</sub>	Benzyl alcohol	Cyclohexane	22	99.9	/	99.9	/
2 <sup>b</sup>	UiO-66-NH <sub>2</sub>	Benzyl alcohol	Cyclohexane	22	1.5	54.1	45.9	/
3 <sup>c</sup>	UiO-66-NH <sub>2</sub>	Benzaldehyde	Cyclohexane	6	99.9	/	99.9	/
4 <sup>a</sup>	Pd@UiO-66	Benzyl alcohol	Cyclohexane	22	91.0	5.0	95.0	/
5 <sup>d</sup>	Pd/C	Benzyl alcohol	Cyclohexane	22	99.0	40.3	59.7	/
6 <sup>e</sup>	Pd@UiO-66-NH <sub>2</sub>	Benzyl alcohol	Ethylene glycol	3	99.9	6.2	59.2	30.6
7 <sup>e</sup>	Pd@UiO-66-NH <sub>2</sub>	Benzyl alcohol	Toluene	22	98.7	45.9	54.1	/

<sup>a</sup> Reaction conditions: 90 °C, 0.1 MPa O<sub>2</sub>, benzyl alcohol (0.1 mmol), ethylene glycol (100 μL, 1.8 mmol), cyclohexane (2 mL), 5 mg 2.0 wt.% Pd@MOF, metal/substrate = 1 mol%. <sup>b</sup> 4.9 mg UiO-66-NH<sub>2</sub> was used. <sup>c</sup> 0.1 mmol benzaldehyde was used. <sup>d</sup> 2 mg 5%Pd/C was used. <sup>e</sup> 2 mL solvent was used. <sup>f</sup> Corresponding acetal benzaldehyde ethylene acetal. <sup>g</sup> Corresponding ester (2-hydroxyethyl benzoate).

On the contrary, UiO-66-NH<sub>2</sub> alone only gave 1.5% conversion of benzyl alcohol, which confirmed the oxidation of benzyl alcohol to benzaldehyde is catalysed by Pd NCs. To confirm that the acetalization of benzaldehyde and ethylene glycol is catalysed by UiO-66-NH<sub>2</sub>, we tested the activity of UiO-66-NH<sub>2</sub> in the acetalization reaction using benzaldehyde and ethylene glycol as the reactants. We found that the reaction reached 99.9% conversion and 99.9% selectivity after 6 h (Table 1, entry 3), which confirmed that UiO-66-NH<sub>2</sub> is a highly active and selective catalyst in the acetalization reaction. We also tested two control catalysts, 5.0 wt.% Pd/C and 1.9 wt.% Pd@UiO-66. We could not achieve high selectivity over Pd/C under the same reaction conditions (Table 1, entry 4). Using Pd@UiO-66, we could get a slightly worse result than that using Pd@UiO-66-NH<sub>2</sub> (entry 5). These catalysis results showed the superiority of using UiO-66-NH<sub>2</sub> as support and also suggested that both Pd NCs and Lewis acid sites on UiO-66-NH<sub>2</sub> are essential for the efficient tandem oxidation-acetalization reaction.

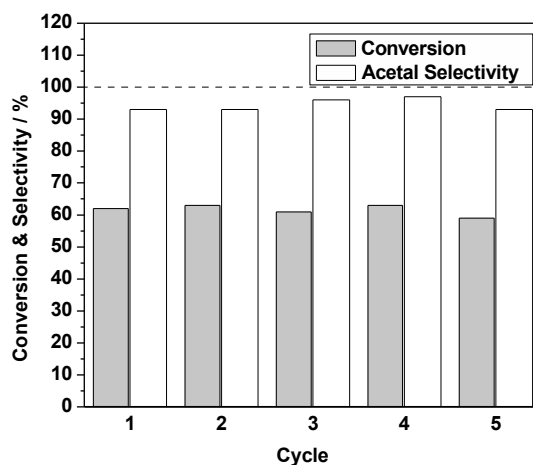


**Figure 8.** Recycling test with 2.0 wt.% Pd@UiO-66-NH<sub>2</sub> catalyst.

**Table 2.** Tandem reactions over 1.0 wt.%, 2.0 wt.% and 4.0 wt.% Pd@UiO-66-NH<sub>2</sub>.<sup>a</sup>

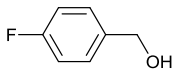
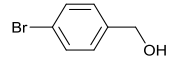
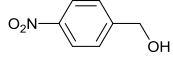
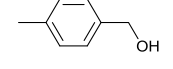
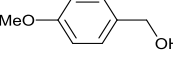
Entry	Sample	S/M	t (h)	Conv.	Alde.	Acetal	Ester
1	1.0 wt.% Pd@UiO-66-NH <sub>2</sub>	100	12	45%	12%	88%	0
2	2.0 wt.% Pd@UiO-66-NH <sub>2</sub>	100	3	30%	12%	88%	0
3	2.0 wt.% Pd@UiO-66-NH <sub>2</sub>	100	12	85%	5%	95%	0
4	4.0 wt.% Pd@UiO-66-NH <sub>2</sub>	100	3	44%	7%	93%	0
5	4.0 wt.% Pd@UiO-66-NH <sub>2</sub>	100	12	85%	6%	94%	0

<sup>a</sup> Reaction conditions: 90 °C, 0.1 MPa O<sub>2</sub>, benzyl alcohol (0.1 mmol), ethylene glycol (100 μL, 1.8 mmol), cyclohexane (2 mL), 2.5 mg, 5 mg and 10 mg of 4.0 wt.%, 2.0 wt.%, 1.0 wt.% Pd@UiO-66-NH<sub>2</sub>, respectively, metal/substrate = 1 mol%.

We synthesized 1.0 wt.%, 2.0 wt.% and 4.0 wt.% Pd@UiO-66-NH<sub>2</sub> and explored the effect of Pd loading in the MOF on the activity and selectivity in the tandem reaction (Table 2). At the same substrate to metal ratio, the catalysts with higher Pd loading are more active. We also investigated the effect of solvent and found that cyclohexane is the best solvent for this tandem reaction (Entries 1, 6 and 7 in Table 1). The high selectivity to benzaldehyde ethylene acetal in cyclohexane can be attributed to the low solubility of water in this nonpolar solvent. Since water is one of the products in the acetalization reaction, the low solubility of water in the reaction solvent could shift the equilibrium of the reaction to the acetalization product.<sup>66</sup> Furthermore, it is noteworthy that we did not detect any benzoic acid or the corresponding ester after the designated reaction time when we used cyclohexane as the reaction solvent, which shows the superior selectivity of Pd@UiO-66-NH<sub>2</sub> under appropriate reaction conditions. The inhibition of the further oxidation of

benzaldehyde could also be attributed to the low solubility of water in cyclohexane. The oxidation of alcohols to carboxylic acid normally proceeds through an aldehyde hydrate ( $R-CH(OH)_2$ ) which can be further oxidized to the carboxylic acid.<sup>62,63</sup> Since water is expelled from the cyclohexane, carboxylic acid cannot be formed.

**Table 3.** Tandem oxidation-acetalization reaction of various substituted benzyl alcohols catalysed by Pd@UiO-66-NH<sub>2</sub>.<sup>a</sup>

Entry	Substrates	t (h)	Conv. (%)	Acetal	Aldehyde
1		48	17.4	100	0
2		48	5.60	16.2	83.8
3		48	35.3	78.8	21.2
4		48	73.3	94.8	5.2
5		48	99.9	99.0	1.0

The reusability of the Pd@UiO-66-NH<sub>2</sub> and Pd@UiO-66 catalyst were also examined. After an initial reaction, the solid catalyst was isolated from the liquid phase by centrifugation and then reused in additional runs. The Pd@UiO-66-NH<sub>2</sub> catalyst could be recycled at least 5 times (Figure 8). The conversion was controlled below 70 % because complete conversion could mask the deactivation of the catalyst.<sup>69</sup> However, the recycle test of Pd@UiO-66 exhibited decay in activity after third run (Figure 9), and we found more severe aggregation of Pd NCs in Pd@UiO-66

after reaction (Figure 10), which further demonstrates the superiority of choosing UiO-66-NH<sub>2</sub> as support. The BET surface area of the used Pd@UiO-66-NH<sub>2</sub> decreased from 940 m<sup>2</sup>g<sup>-1</sup> to 830 m<sup>2</sup>g<sup>-1</sup>, which may be due to the residual reactants or products trapped inside the UiO-66-NH<sub>2</sub>. Furthermore, we measured the PXRD pattern of the used catalysts and found the crystalline structure of the UiO-66-NH<sub>2</sub> was still maintained after the 5th cycle (pattern e in Figure 4). TEM images of used Pd@UiO-66-NH<sub>2</sub> catalysts only show slight aggregation of Pd NCs (Figure 12), which does not affect the activity of the catalysts within 5 recycle runs.

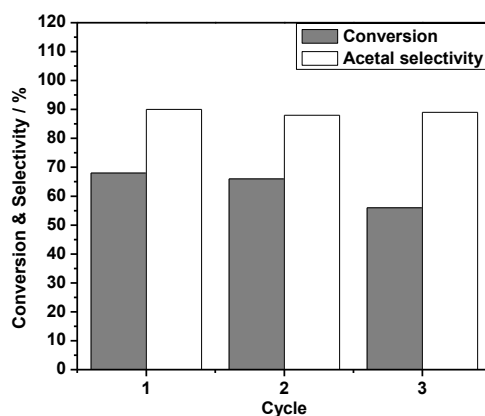


**Figure 9.** Recycle test for 1.9 wt.%Pd@UiO-66.

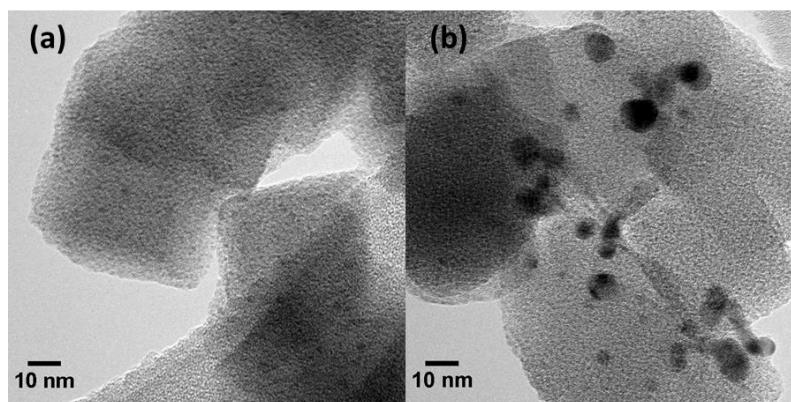


**Figure 10.** TEM image of 1.9 wt.% Pd@UiO-66, (a) before and (b) after reaction.



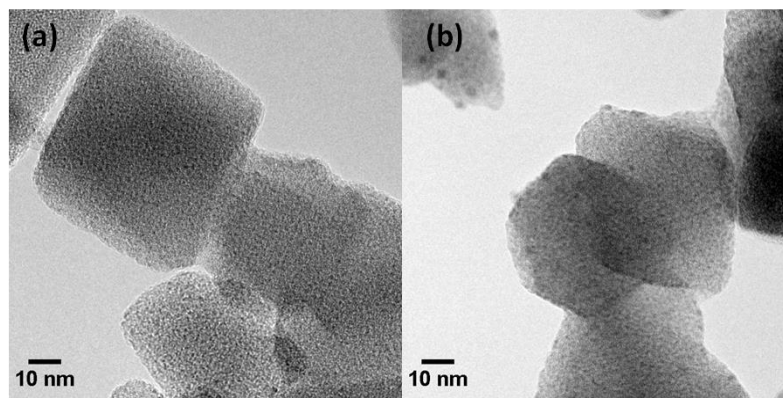


**Figure 11.** TEM image of 2.0 wt.% Pd@UiO-66-NH<sub>2</sub>, (a) before and (b) after reaction.

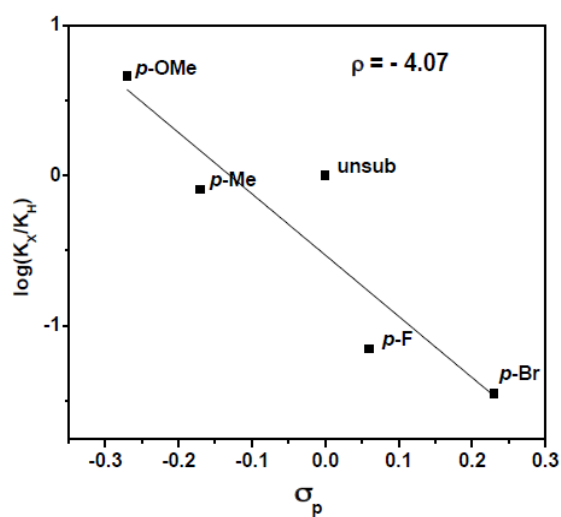


**Figure 12.** Hammett plot for tandem reaction of various substituted benzyl alcohol with ethylene glycol over 2.0 wt.% Pd@UiO-66-NH<sub>2</sub>.

The scope of the tandem catalytic system was investigated by performing the oxidation-acetalization reaction of various substituted benzyl alcohols. Table 3 summarizes the results of these tandem reactions. We found that benzyl alcohols with electron-withdrawing groups like fluoro- and bromo- gave low conversion and/or selectivity, while electron-donating groups ( $-\text{OCH}_3$  and  $-\text{CH}_3$ ) showed moderate to

high conversion and selectivity to the corresponding acetals. We used Hammett's equation to obtain the correlation between substituent constant and reaction rate (Figure 12). The negative value of  $\rho = -4.07$  indicates the tandem reaction is facilitated by the high electron density at the reaction center. Currently, we are studying bimetallic NCs encapsulated in this MOF for oxidation of aliphatic alcohols.

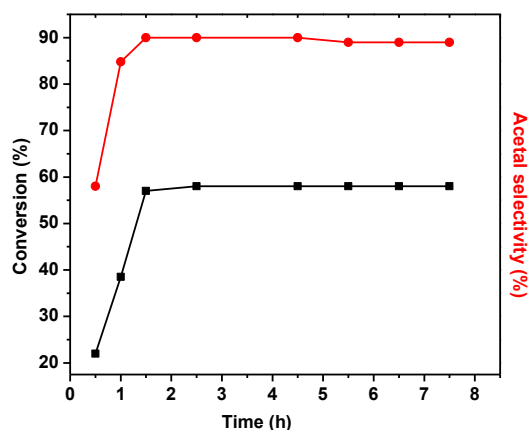


**Figure 13.** Leaching test for the tandem reaction of benzyl alcohol with ethylene glycol over 2.0 wt.% Pd@UiO-66-NH<sub>2</sub>. Reaction conditions: benzyl alcohol (0.1 mmol), ethylene glycol (100  $\mu$ L), mesitylene (8  $\mu$ L), cyclohexane (2 mL), 2.0 wt.% Pd@UiO-66-NH<sub>2</sub>, substrate/metal = 100, reflux at 90 °C. The solid catalyst was filtered from the reaction solution after 90 min, while the filtrate was transferred to a new vial and reaction was carried out under identical conditions for an additional 8 hours.

In order to confirm the heterogeneity of the catalyst, hot filtration test was carried out by stopping the tandem reaction after 90 min. The reaction reached 57% conversion and 90% selectivity to benzaldehyde ethylene acetal. The reaction solution was removed quickly from the solid catalyst and was transferred to another

flask under the same reaction conditions. No further increase in either the conversion of benzyl alcohol or the selectivity to benzaldehyde ethylene acetal was observed in the transferred solution after the solid catalyst was removed (Figure 13). These results demonstrate that the active sites for both the oxidation and the acetalization reactions were on the solid catalyst and there are no leached active species under the reaction conditions.

### Conclusions

We have developed a heterogeneous tandem catalyst for the oxidation of benzyl alcohol and the subsequent acetalization with ethylene glycol catalysed by UiO-66-NH<sub>2</sub> supported Pd nanoclusters. This bifunctional MOF catalyst exhibits high selectivity to give acetal products in this tandem oxidation-acetalization reaction and can be reused 5 times without any loss in activity and selectivity. We found that using the nonpolar solvent, cyclohexane, is essential for the high selectivity to acetal, which could promote the acetalization reaction and prevent the further oxidation of aldehydes to the corresponding esters. We also proved the superiority of choosing UiO-66-NH<sub>2</sub> instead of UiO-66 as support in the same tandem reaction system. This work demonstrates the potential of MOF-based catalysts in tandem heterogeneous catalysis. Under appropriate conditions, both high selectivity and stability of MOF-based catalysts can be achieved. Further work on exploring new tandem catalytic reactions with these catalytic systems and optimizing the performance of the multifunctional MOFs via preparing bimetallic nanoclusters is currently underway.

## Experimental Section

**BET, XRD, TEM, XPS, and TGA.** Surface area analysis of the catalyst was performed by nitrogen sorption isotherms in a Micromeritics Tristar 3000 surface area analyzer at 77 K. Powder X-ray diffraction patterns of the samples were obtained by a STOE Stadi P powder diffractometer using Cu  $K_{\alpha}$  radiation (40 kV, 40 mA,  $\lambda = 0.1541$  nm). The size and morphology of 2.0 wt.% Pd@UiO-66-NH<sub>2</sub> were investigated by using TEM and HAADF-STEM images recorded on a Tecnai G2 F20 electron microscope equipped with EDX detector (Oxford INCA EDS). XPS measurements were performed using a PHI 5500 Multi-technique system (Physical Electronics, Chanhassen, MN) with a monochromatized Al  $K_{\alpha}$  X-ray source ( $h\nu = 1486.6$  eV). TGA was carried out using STA 6000 simultaneous thermal analyzer (PerkinElmer). In the TGA experiment, 5.7 mg of Pd@UiO-66-NH<sub>2</sub> was analyzed under N<sub>2</sub> flow with a heating rate of 10 °C/min from room temperature to 900 °C.

**Inductively coupled plasma atomic emission spectroscopy (ICP-AES).** To determine the loading amount of palladium in UiO-66-NH<sub>2</sub>, ICP-AES (Optima 2100 DV) was performed. Since the zirconium in UiO-66-NH<sub>2</sub> has similar emission with palladium in ICP-AES, it is difficult to detect the palladium amount directly. Instead, we measured the amount of Pd that was washed away during the washing steps and calculated the actual Pd remaining in Pd@UiO-66-NH<sub>2</sub>. When loading the 2.0 wt.% Pd in UiO-66-NH<sub>2</sub>, the exact initial weight of the palladium precursor (palladium acetate) was recorded first. Every time after washing, the washing solution that contained the palladium acetate residue was collected. Finally, ICP-AES was performed for the washing solution and the palladium content was calculated. The

difference between added and removed Pd (during washing) is the actual palladium amount that was loaded in UiO-66-NH<sub>2</sub>. The same method was applied to determine the actual palladium amount in Pd@UiO-66.

**X-ray absorption spectroscopy (XAS) measurement.** The X-ray absorption spectra (XAS) were measured in transmission mode (Pd K edge = 24.350 keV) at 20-BM-B and 9-BM-B beamlines of the Advanced Photon Source at Argonne National Laboratory. XAS of reference samples were collected using pure finely ground powders homogeneously dispersed on polyimide Kapton tap, while the MOF samples were pressed into a pellet fit to a hole embedded in a Teflon substrate. A palladium foil spectrum was acquired simultaneously with each measurement for energy calibration. Multiple scans (8-10 scans) were collected for each sample, and merged into one data set for XAS analysis. For XAS analysis, the software at the beamline was used to perform dead-time correction, and energy calibration. The Athena program, which is an interface to IFEFFIT and FEFFIT, was used for glitch removal, pre-edge subtraction, post-edge normalization, and conversion to *k*-space.<sup>49,50</sup> The EXAFS data were fitted in *R*-space using the Artemis program from the same package, with theoretical models constructed from FEFF6.<sup>51-53</sup> All the EXAFS data fitting were performed with a *k*<sup>3</sup> weighting in *R* space.

**Synthesis of UiO-66-NH<sub>2</sub> and UiO-66.** The MOF was synthesized and purified according to a procedure reported by Lillerud and co-workers.<sup>48</sup> Zirconium(IV) chloride (0.40g, 1.71 mmol; 98%, Acros Organics) and 2-aminoterephthalic acid (NH<sub>2</sub>-H<sub>2</sub>BDC) (0.31 g, 1.71 mmol; >99%, Sigma-Aldrich; for UiO-66, terephthalic acid, 0.29 g, 1.71 mmol, 98%, Sigma-Aldrich) were dissolved in N, N'-

dimethylformamide (DMF; ACS grade, Macron) 100 mL at room temperature, then 100  $\mu$ L water was added (for preparing UiO-66, no water was added). The obtained mixture was sealed and placed in a pre-heated oven at 120 °C for 24 hours. The solid MOFs were washed with fresh DMF, chloroform and methanol three times every 12 hours. Then the MOFs were activated at 150 °C under vacuum (30 mTorr) for 6 hours.

**Synthesis of Pd NCs inside the cavities of MOFs.** 100 mg UiO-66-NH<sub>2</sub> was dispersed in 12 mL methylene chloride (Fisher, Optima™ grade). After sonication for 1 hour, a methylene chloride solution of palladium acetate (4.32 mg Pd(OAc)<sub>2</sub> in 5 mL methylene chloride, Kawaken Fine Chemicals) was added dropwise to the MOF solution under vigorous stirring. After 24 hours of stirring at room temperature, the as-prepared Pd<sup>2+</sup> infiltrated MOF was washed three times for 12 hours each time with fresh methylene chloride. The reduction process of the precursor loaded UiO-66-NH<sub>2</sub> was performed under a 50 mL/min flow of 10% H<sub>2</sub>/Ar at 200 °C for 2 hours. The same method was applied to synthesize Pd NCs@UiO-66.

**Typical procedure for the tandem reaction.** The tandem reaction was carried out under reflux in a 10 mL round-bottom flask equipped with a condenser whose temperature was maintained at 5 °C using a recirculating chiller (NESLAB, R134A). In a typical experiment, 10.5 mg of benzyl alcohol (0.1 mmol, Fisher Scientific), 100  $\mu$ L ethylene glycol (Fisher Scientific), 5.0 mg of 2.0 wt.% Pd@UiO-66-NH<sub>2</sub> (1 mol%) and 7 mg of mesitylene (internal GC standard, 99%, Acros Organics) were added into 2 mL cyclohexane in the round-bottom flask with an oxygen balloon at the top of the condenser. The flask was loaded in an oil bath which was preheated to 90

°C and then the reaction was refluxing under atmosphere with magnetic stirring at 600 rpm. After the reaction was finished, the products were analyzed using gas chromatograph equipped with a HP-5 capillary column (30 m × 0.32 mm × 0.25 μm) with a flame ionization detector and GC-MS(SHIMADZU 5050A) equipped with a HP-5ms capillary column (30 m × 0.32 mm × 0.25 μm).

**Recycling test.** The catalyst was isolated at the end of the reaction and the liquid was removed. The solid catalyst was reused in the second run. The catalytic activity and acetal selectivity of the catalyst did not show significant loss in the second run. PXRD of the used sample showed that the structure of the catalyst remained intact during the catalytic cycles.

**Leaching test.** The solid catalyst –Pd@UiO-66-NH<sub>2</sub> was separated from the hot solution right after reaction for 90 min. The reaction was continued with the filtrate in the absence of solid catalyst for an additional 8 h. No further increase in either the conversion of benzyl alcohol or the selectivity of acetal was observed, which indicates that the catalytically active sites for both oxidation and acetalization are on the solid catalyst.

**Acknowledgment.** We thank Ames Laboratory (Royalty Account) and Iowa State University for startup funds. The Ames Laboratory is operated for the U.S. Department of Energy by Iowa State University under Contract No. DE-AC02-07CH11358. We thank to Dale L. Brewster, Steve M. Heald, Trudy B. Bolin, Tianpin Wu, and Jeff Miller for the helps during XAS measurement at APS. Use of the Advanced Photon Source, an Office of Science User Facility operated for the U.S. Department of Energy (DOE) Office of Science by Argonne National Laboratory,

was supported by the U.S. DOE under Contract No. DE-AC02-06CH11357. We thank Robert J. Angelici for his advice during the writing of this manuscript. We thank Gordon J. Miller for use of PXRD, Brent Shanks for use of TGA, and Igor I. Slowing for use of gas adsorption analyzer and ICP-AES.

## References

- (1) Shiju, N. R.; Alberts, A. H.; Khalid, S.; Brown, D. R.; Rothenberg, G. *Angew. Chem. Int. Ed.* **2011**, *50*, 9615-9619.
- (2) Grondal, C.; Jeanty, M.; Enders, D. *Nat. Chem.* **2010**, *2*, 167-178.
- (3) Shin, J. Y.; Jung, D. J.; Lee, S.-g. *ACS Catal.* **2013**, *3*, 525-528.
- (4) Guan, Y.; Zhang, D.; Wang, Y. *Catal. Lett.* **2012**, *142*, 1225-1233.
- (5) Kim, J. H.; Lee, S.-g. *Org. Lett.* **2011**, *13*, 1350-1353.
- (6) Shylesh, S.; Wagener, A.; Seifert, A.; Ernst, S.; Thiel, W. R. *Angew. Chem. Int. Ed.* **2010**, *49*, 184-187.
- (7) Nicolaou, K. C.; Edmonds, D. J.; Bulger, P. G. *Angew. Chem. Int. Ed.* **2006**, *45*, 7134-7186.
- (8) Yang, G.; Kawata, H.; Lin, Q.; Wang, J.; Jin, Y.; Zeng, C.; Yoneyama, Y.; Tsubaki, N. *Chem. Sci.* **2013**, *4*, 3958-3964.
- (9) Farrusseng, D.; Aguado, S.; Pinel, C. *Angew. Chem. Int. Ed.* **2009**, *48*, 7502-7513.



- (10) Jiang, H.-L.; Akita, T.; Ishida, T.; Haruta, M.; Xu, Q. *J. Am. Chem. Soc.* **2011**, *133*, 1304-1306.
- (11) Aijaz, A.; Karkamkar, A.; Choi, Y. J.; Tsumori, N.; Rönnebro, E.; Autrey, T.; Shioyama, H.; Xu, Q. *J. Am. Chem. Soc.* **2012**, *134*, 13926-13929.
- (12) Zhu, Q.-L.; Li, J.; Xu, Q. *J. Am. Chem. Soc.* **2013**, *135*, 10210-10213.
- (13) Li, P.-Z.; Aranishi, K.; Xu, Q. *Chem. Commun.* **2012**, *48*, 3173-3175.
- (14) Yadav, M.; Xu, Q. *Chem. Commun.* **2013**, *49*, 3327-3329.
- (15) Liu, H.; Liu, Y.; Li, Y.; Tang, Z.; Jiang, H. *J. Phys. Chem. C* **2010**, *114*, 13362-13369.
- (16) Dhakshinamoorthy, A.; Garcia, H. *Chem. Soc. Rev.* **2012**, *41*, 5262-5284.
- (17) Hermansdoerfer, J.; Kempe, R. *Chem. Eur. J.* **2011**, *17*, 8071-8077.
- (18) Gu, X.; Lu, Z.-H.; Jiang, H.-L.; Akita, T.; Xu, Q. *J. Am. Chem. Soc.* **2011**, *133*, 11822-11825.
- (19) Esken, D.; Turner, S.; Lebedev, O. I.; Van Tendeloo, G.; Fischer, R. A. *Chem. Mater.* **2010**, *22*, 6393-6401.
- (20) Ishida, T.; Nagaoka, M.; Akita, T.; Haruta, M. *Chem. Eur. J.* **2008**, *14*, 8456-8460.
- (21) Cirujano, F. G.; Llabres i Xamena, F. X.; Corma, A. *Dalton Trans.* **2012**, *41*, 4249-4254.
- (22) Pan, Y.; Yuan, B.; Li, Y.; He, D. *Chem. Commun.* **2010**, *46*, 2280-2282.
- (23) Liu, H.; Chen, G.; Jiang, H.; Li, Y.; Luque, R. *ChemSusChem* **2012**, *5*, 1892-1896.
- (24) Liu, H.; Li, Y.; Jiang, H.; Vargas, C.; Luque, R. *Chem. Commun.* **2012**, *48*, 8431-8433.
- (25) Zhao, M.; Deng, K.; He, L.; Liu, Y.; Li, G.; Zhao, H.; Tang, Z. *J. Am. Chem. Soc.* **2014**, *136*, 1738-1741.
- (26) Dhakshinamoorthy, A.; Opanasenko, M.; Cejka, J.; Garcia, H. *Catal. Sci. Technol.* **2013**, *3*, 2509-2540.

- (27) Thavornprasert, K.-a.; Capron, M.; Jalowiecki-Duhamel, L.; Gardoll, O.; Trentesaux, M.; Mamede, A.-S.; Fang, G.; Faye, J.; Touati, N.; Vezin, H.; Dubois, J.-L.; Couturier, J.-L.; Dumeignil, F. *Appl. Catal., A* **2014**, *145*, 126-135.
- (28) Liu, H.; Iglesia, E. *J. Phys. Chem. B* **2003**, *107*, 10840-10847.
- (29) Liu, H.; Iglesia, E. *J. Phys. Chem. B* **2004**, *109*, 2155-2163.
- (30) Secordel, X.; Yoboue, A.; Cristol, S.; Lancelot, C.; Capron, M.; Paul, J.-F.; Berrier, E. *J. Solid State Chem.* **2011**, *184*, 2806-2811.
- (31) Yuan, Y. Z.; Liu, H. C.; Imoto, H.; Shido, T.; Iwasawa, Y. *J. Catal.* **2000**, *195*, 51-61.
- (32) Chan, A. S. Y.; Chen, W.; Wang, H.; Rowe, J. E.; Madey, T. E. *J. Phys. Chem. B* **2004**, *108*, 14643-14651.
- (33) Fu, Y.; Shen, J. *Chem. Commun.* **2007**, 2172-2174.
- (34) Cui, Y.; Yue, Y.; Qian, G.; Chen, B. *Chem. Rev.* **2011**, *112*, 1126-1162.
- (35) Liu, J.; Fu, Y.; Sun, Q.; Shen, J. *Microporous and Mesoporous Mater.* **2008**, *116*, 614-621.
- (36) Tanaka, T.; Takenaka, S.; Funabiki, T.; Yoshida, S. *photocatalytic oxidation of ethanol over tantalum oxide-supported on silica*, 1994; Vol. 90.
- (37) Tanaka, T.; Takenaka, S.; Funabiki, T.; Yoshida, S. *Chem.Lett.* **1994**, 809-812.
- (38) Heitler, C.; Scaife, D. B.; Thompson, B. W. *J. Chem. Soc.A* **1967**, 1409-1413.
- (39) Bueno, A. C.; Goncalves, J. A.; Gusevskaya, E. V. *Appl. Catal. A* **2007**, *329*, 1-6.
- (40) Smith, B. M.; Graham, A. E. *Tetrahedron Lett.* **2007**, *48*, 4891-4894.
- (41) Kim, M.; Cohen, S. M. *CrystEngComm* **2012**, *14*, 4096-4104.
- (42) Vermoortele, F.; Ameloot, R.; Vimont, A.; Serre, C.; De Vos, D. *Chem. Commun.* **2011**, *47*, 1521-1523.
- (43) Vermoortele, F.; Vandichel, M.; Van de Voorde, B.; Ameloot, R.; Waroquier, M.; Van Speybroeck, V.; De Vos, D. E. *Angew. Chem. Int. Ed.* **2012**, *51*, 4887-4890.

- (44) Timofeeva, M. N.; Panchenko, V. N.; Jun, J. W.; Hasan, Z.; Matrosova, M. M.; Jhung, S. H. *Applied Catalysis A: General* **2014**, *471*, 91-97.
- (45) Silva, P. H. R.; Goncalves, V. L. C.; Mota, C. J. A. *Bioresour. Technol.* **2010**, *101*, 6225-6229.
- (46) Ray, R.; Chowdhury, A. D.; Lahiri, G. K. *ChemCatChem* **2013**, *5*, 2158-2161.
- (47) Ajaikumar, S.; Pandurangan, A. *J. Mol. Catal. A: Chem* **2008**, *290*, 35-43.
- (48) Cavka, J. H.; Jakobsen, S.; Olsbye, U.; Guillou, N.; Lamberti, C.; Bordiga, S.; Lillerud, K. P. *J. Am. Chem. Soc.* **2008**, *130*, 13850-13851.
- (49) Newville, M. *J. Synchrot. Radiat.* **2001**, *8*, 322-324.
- (50) Ravel, B.; Newville, M. *J. Synchrot. Radiat.* **2005**, *12*, 537-541.
- (51) Rehr, J. J.; Kas, J. J.; Prange, M. P.; Sorini, A. P.; Takimoto, Y.; Vila, F. C. *R. Phys.* **2009**, *10*, 548-559.
- (52) Ravel, B.; Newville, M. *Phys. Scr.* **2005**, *2005*, 1007.
- (53) Zabinsky, S. I.; Rehr, J. J.; Ankudinov, A.; Albers, R. C.; Eller, M. J. *Phys. Rev. B* **1995**, *52*, 2995-3009.
- (54) Guo, Z.; Xiao, C.; Maligal-Ganesh, R. V.; Zhou, L.; Goh, T. W.; Li, X.; Tesfagaber, D.; Thiel, A.; Huang, W. *ACS Catal.* **2014**, *4*, 1340-1348.
- (55) Valenzano, L.; Civalieri, B.; Chavan, S.; Bordiga, S.; Nilsen, M. H.; Jakobsen, S.; Lillerud, K. P.; Lamberti, C. *Chem. Mater.* **2011**, *23*, 1700-1718.
- (56) Gaudet, J. R.; de la Riva, A.; Peterson, E. J.; Bolin, T.; Datye, A. K. *ACS Catal.* **2013**, *3*, 846-855.
- (57) Cho, S. J.; Kang, S. K. *J. Phys. Chem. B* **2000**, *104*, 8124-8128.
- (58) Kampers, F. W. H.; Koningsberger, D. C. *Faraday Discuss.* **1990**, *89*, 137-141.
- (59) Harkness, M. B.; Alvarado, E.; Badaj, A. C.; Skrela, B. C.; Fan, L.; Lavoie, G. *Organometallics* **2013**, *32*, 3309-3321.
- (60) Albrecht, M.; Stoeckli-Evans, H. *Chem. Commun.* **2005**, 4705-4707.

- (61) Liu, C.-H.; Yu, X.-Y.; Liang, X.-Z.; Wang, W.-J.; Yang, J.-G.; He, M.-Y. *Chin. J. Chem.* **2007**, *25*, 83-85.
- (62) Schmidt, A.-K. C.; Stark, C. B. W. *Org. Lett.* **2011**, *13*, 4164-4167.
- (63) Noyori, R.; Aoki, M.; Sato, K. *Chem. Commun.* **2003**, 1977-1986.
- (64) Jones, C. *Top. Catal.* **2010**, *53*, 942-952.

## CHAPTER 4

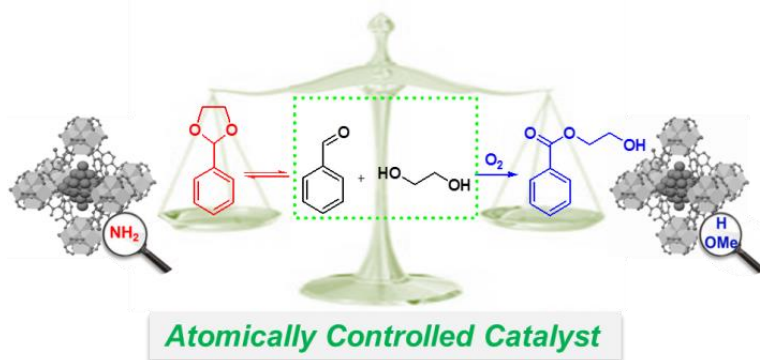
**CONTROLLING CATALYTIC PROPERTIES OF PD NANOCCLUSERS  
THROUGH THEIR CHEMICAL ENVIRONMENT AT THE ATOMIC  
LEVEL USING ISORETICULAR METAL-ORGANIC FRAMEWORKS**

A paper published in *ACS Catal.*, **2016**, 6, 3461–3468

Xinle Li, Tianwei Goh, Lei Li, Chaoxian Xiao, Xiaocheng Zeng, Wenyu Huang

**Abstract**

Judicious control of heterogeneous catalytic sites through their surrounding chemical environment at an atomic level is crucial to rational catalyst design. Herein we synthesize Pd NCs in different atomically tunable chemical environment using isorecticular metal-organic frameworks as the support (Pd@UiO-66-X, X = H, NH<sub>2</sub>, and OMe). In an aerobic reaction between benzaldehyde and ethylene glycol, these heterogeneous catalysts Pd@UiO-66-X show product distributions that are completely altered from the acetal to the ester when we change the functional groups on the MOF linkers from –NH<sub>2</sub> to –H/–OMe. Diffuse reflectance infrared Fourier transform spectroscopy (DRIFTS) studies, along with density functional theory (DFT) calculations, show that the coordination of the –NH<sub>2</sub> groups to the Pd NCs could enhance their chemical potential and weaken their oxidation capability to a greater extent than that of the –OMe group, which agrees with our experimental results.



## Introduction

Developing an atomic and electronic-level understanding of catalysis is necessary for the design of effective catalysts with atomic precision to exercise molecular control during catalytic reactions. These atomic and molecular-level controls have been partially realized in enzymatic and homogeneous catalysis. For example, the inherent activity of an enzyme can be modulated by protein engineering and immobilization.<sup>1,2</sup> In homogeneous catalysts, steric and electronic effects of the ligands play a decisive role in their activity and stereoselectivity, thus establishing structure–activity relationships between homogenous catalysts and their catalytic properties.<sup>3–6</sup> However, in heterogeneous catalysts, it is relatively hard to achieve an atomic-level understanding about the effect of the chemical environment surrounding the catalytic sites on their catalytic performance,<sup>7</sup> largely due to the lack of a catalyst support with atomic-level tunability. Unlike traditional catalyst supports, MOFs, featuring precisely controlled and tunable crystal structures and compositions, are an ideal platform to study the effect of the chemical environment surrounding the catalytic sites on their catalytic properties.<sup>8</sup>

MOFs are a burgeoning class of hybrid porous materials and have spurred tremendous research interest in the realm of heterogeneous catalysis.<sup>9-12</sup> The usage of MOFs as novel hosts for metal NPs has been extensively investigated.<sup>13-18</sup> Compared to other porous materials such as zeolites and mesoporous silica, the properties of MOFs are rationally ‘designable’ to study the effect of the chemical environment on the encapsulated metal NPs or NCs because the metal ions and the organic linkers of MOFs can be fine-tuned by either utilizing different building units or by the post-synthetic modification of pre-synthesized MOFs.<sup>19-21</sup> The introduction of different functional groups in isorecticular MOFs can dramatically affect the gas sorption capacity and uptake selectivity,<sup>22,23</sup> luminescence,<sup>24</sup> water stability,<sup>25</sup> and mechanical properties of the MOFs.<sup>26</sup> However, studies on the effects of introducing different functional groups in isorecticular MOFs on catalysis have been rarely reported.<sup>27-29</sup> In pioneering work carried out by De Vos’ and Jung’s group, it was found that Lewis acid catalysis can be affected by changing the organic linkers in Zirconium-based UiO-66 MOFs.<sup>30,31</sup> Nonetheless, varying product selectivity controlled through the well-defined chemical environment of isorecticular MOFs have scarcely been reported in heterogeneous catalysis to date.<sup>32,33</sup> In the present study, we provided spectroscopic and theoretical investigation for the first time, which could explain the different catalytic properties of Pd NCs when they are confined in different chemical environments of isorecticular MOFs.

Here we developed isorecticular MOFs containing palladium NCs (denoted as Pd@UiO-66-X, X = H, NH<sub>2</sub>, and OMe) as catalysts for the aerobic reaction between benzaldehyde and ethylene glycol. By varying the functional group on the organic

linkers of the UiO-66-X MOFs from  $-\text{NH}_2$  to  $-\text{H}/-\text{OMe}$ , the product selectivity was completely altered from an acetal to an ester. The distinct product distribution is attributed to the different oxidation capability derived from Pd NCs encapsulated in the isorecticular MOFs and  $\text{NH}_2$ -Pd interactions inhibiting the formation of ester. It is noteworthy that the  $\text{NH}_2$ -Pd interactions hindered but not completely impaired the oxidation capacity of Pd NCs. Modifying the organic linkers in UiO-66 results in geometrically identical cages with functionally diverse chemical environments. Pd NCs, encapsulated in these MOFs, are surrounded by different chemical environments, and thus exhibit different activity and selectivity in catalytic reactions.

## Results and Discussion

The Pd NCs@UiO-66-X (X = H,  $\text{NH}_2$ , and OMe) catalysts were synthesized using a protocol that has been previously reported by our group.<sup>41</sup> The PXRD analyses showed that UiO-66-X was successfully prepared and there were no obvious changes in the PXRD patterns of Pd@UiO-66-X after the impregnation and reduction of Pd(II) (Figure 1), consistent with reported literature.<sup>34</sup> The  $\text{N}_2$  sorption isotherms of all samples show a type I pattern (Figure 2). The appreciable decrease in the BET surface area and the pore volume of Pd@UiO-66-X compared to the pristine MOFs is likely due to the occupation of Pd NCs in MOF cavities and/or block of the MOF pores by these NCs, as in the case of metal NPs loaded into ZIF-8, MIL-101, and UiO-66- $\text{NH}_2$ .<sup>29,41,42</sup> The UiO-66-X MOFs reveal two major pores at 7-10 and  $\sim 12$  Å (Figure 3), which agree well with reported works.<sup>43,44</sup> Compared to pristine MOFs, Pd@UiO-66-X show decreased pore volumes due to the occupation of Pd NCs in the



cavities of the MOFs. Pd NCs with an average size of less than 1.2 nm (the diameter of the largest octahedral cages in UiO-66-X MOFs) are uniformly dispersed in UiO-66-X, as revealed by the TEM images (Figure 4). The fact that the size of the Pd NCs is smaller than the diameter of the cavities in the MOFs is a strong indication that the formed Pd NCs are well dispersed inside the cavities of the UiO-66-X MOFs.

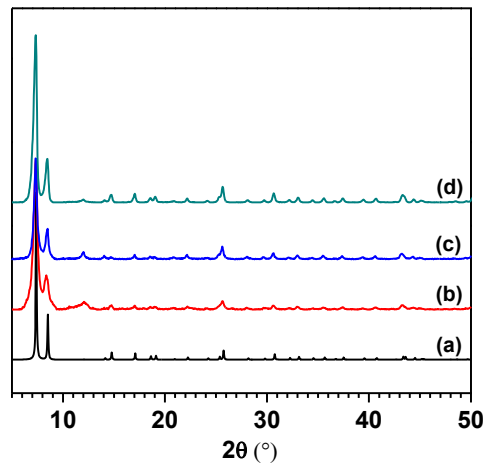


**Figure 1.** PXRD patterns of (a) simulated UiO-66; (b) 1.5 wt.% Pd@UiO-66; (c) 2.0 wt.% Pd@UiO-66-NH<sub>2</sub>; (d) 2.0 wt.% Pd@UiO-66-OMe.

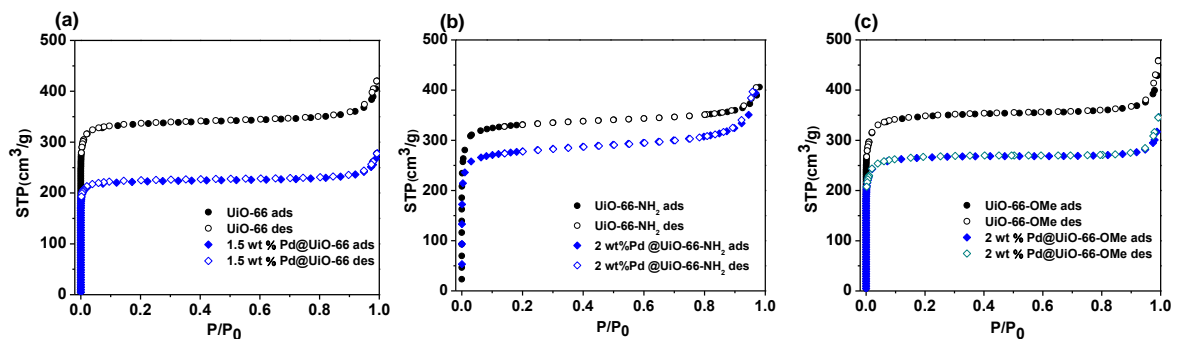


**Figure 2.** Nitrogen adsorption/desorption isotherms of the as-synthesized UiO-66-X and Pd@UiO-66-X. (a) UiO-66, and Pd@UiO-66; (b) UiO-66-NH<sub>2</sub>, and Pd@UiO-66-NH<sub>2</sub>; (c) UiO-66-OMe, and Pd@UiO-66-OMe.

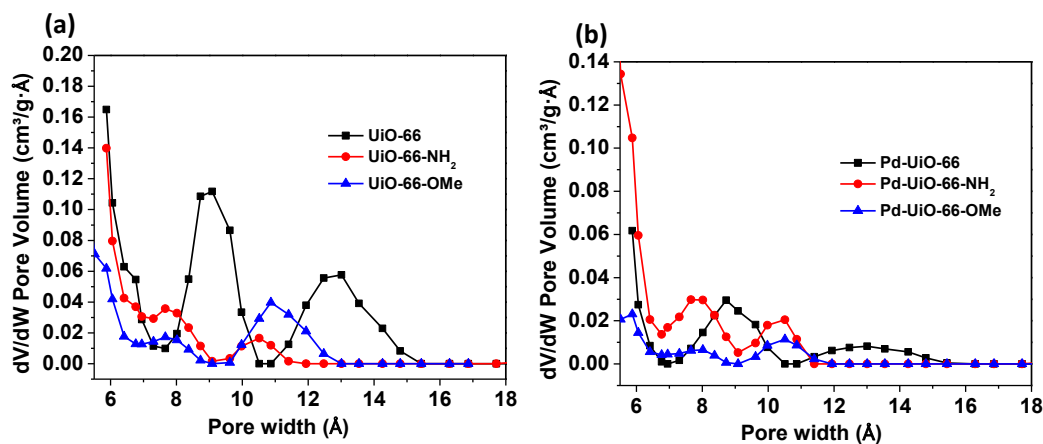


**Figure 3.** Pore size distributions calculated by NLDFT method from nitrogen sorption isotherms for activated UiO-66-X (a) and Pd@UiO-66-X (b) at 77 K.

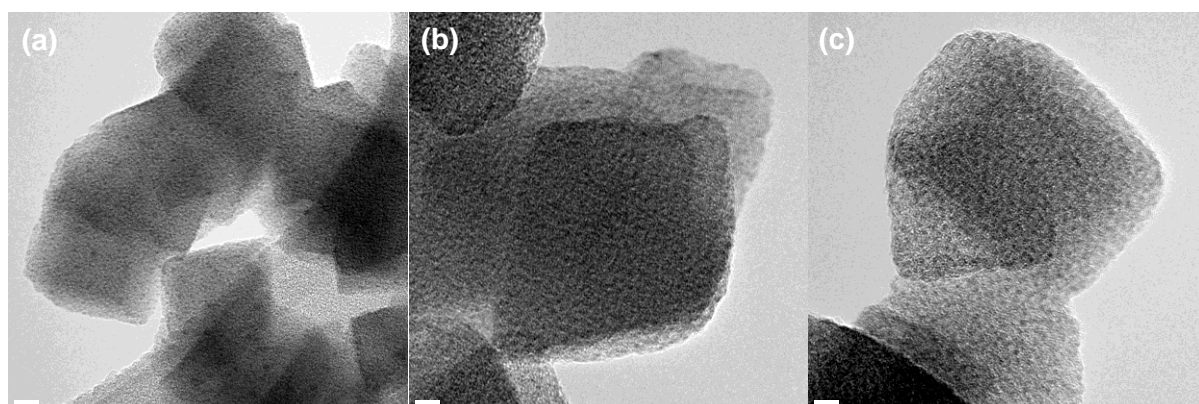
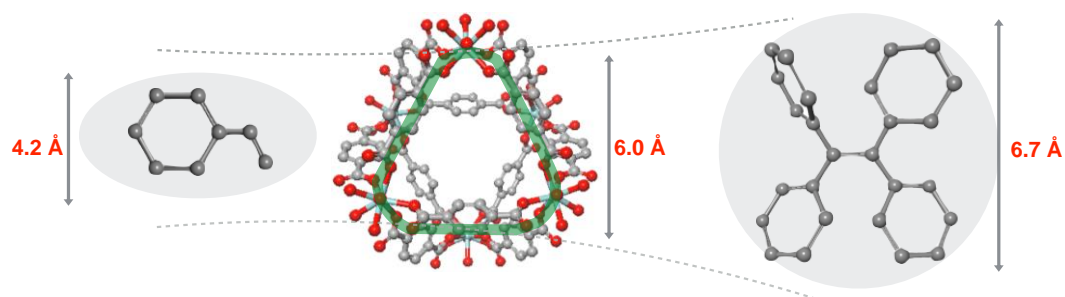


**Figure 4.** TEM images of Pd@UiO-66-X before reaction. (a) 1.5 wt.% Pd@UiO-66, (b) 2.0 wt.% Pd@UiO-66-NH<sub>2</sub>, (c) 2.0 wt.% Pd@UiO-66-OMe.



**Scheme 1.** Comparison of the size of two probe molecules and the triangular window of Zr-UiO-66-X.

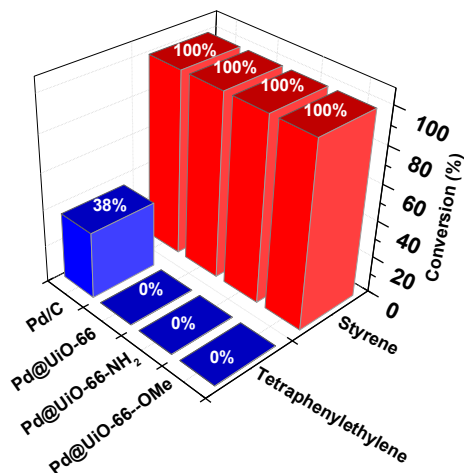


**Figure 5.** Comparison of Pd@UiO-66-X and 5.0% Pd/Carbon in the hydrogenation of styrene and tetraphenylethylene. Reaction conditions: alkene (0.1 mmol), Pd catalysts (Pd : substrate =1:100), EtOH (1.5 mL), 1 atm H<sub>2</sub> balloon, 50 °C,15 hours.

Probe molecules of different sizes have been extensively used to confirm the location of catalytically active sites inside MOFs,<sup>16,45-47</sup> and zeolites.<sup>48</sup> To further confirm the Pd NCs are confined in the cavities of MOFs, we utilized Pd@UiO-66-X and commercially available Pd/C to hydrogenate two probe molecules of different sizes, styrene (4.2 Å in atomic diameter; 6.0 Å in kinetic diameter)<sup>49</sup> and tetraphenylethylene (6.7 Å in atomic diameter)<sup>50</sup>. Tetraphenylethylene is too bulky to diffuse through the aperture of UiO-66-X (6.0 Å), and thus should not be hydrogenated by the Pd NCs confined inside the MOFs, whereas relatively smaller styrene molecule can readily access the encapsulated Pd NCs and undergo hydrogenation conveniently (Scheme 1). As expected (Figure 5), all Pd@UiO-66-X and Pd/C catalysts displayed high activity (100% conversion) in the hydrogenation of styrene. However, Pd@UiO-66-X showed no detectable activity in the hydrogenation

of tetraphenylethylene, while Pd/C and Pd NPs deposited on the external surface of UiO-66-NH<sub>2</sub> (Pd/UiO-66-NH<sub>2</sub>) still had relatively good activity (38% and 28% conversion, respectively), implying that the Pd NCs are indeed encapsulated inside the cavities of UiO-66-X MOFs.

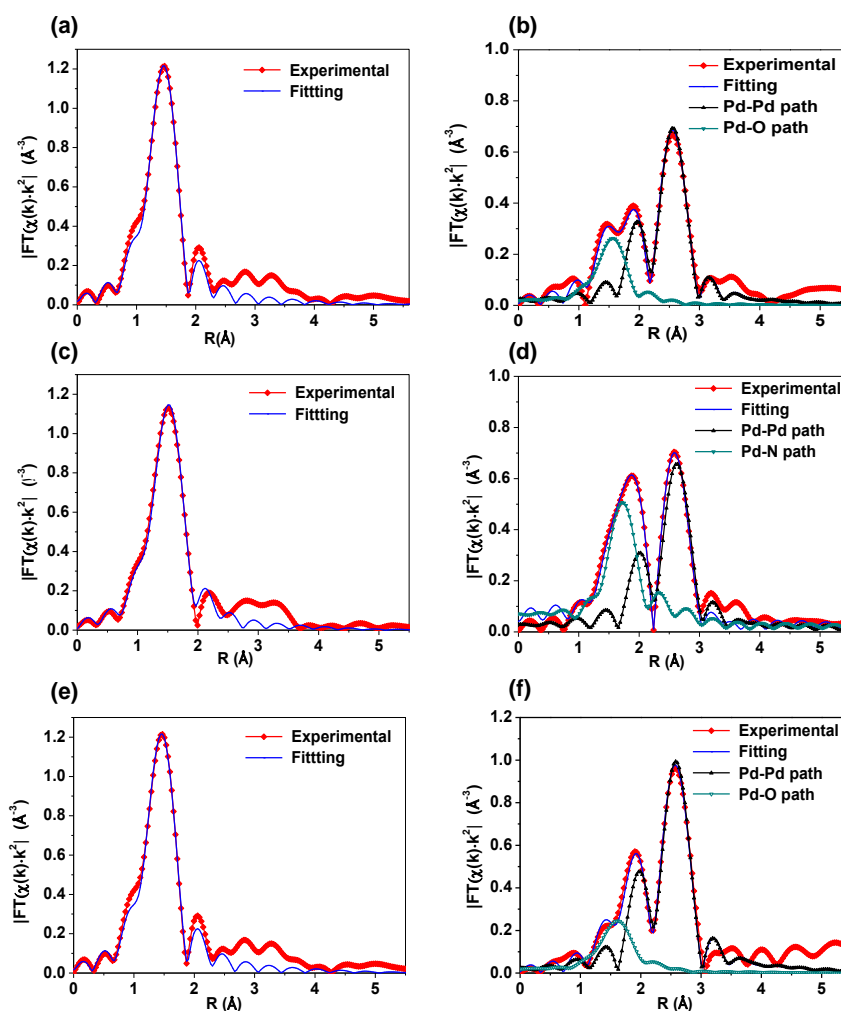


**Figure 6.** Fourier transform of EXAFS data extracted from Pd K edge (blue empty dot) and the computed fits (red line) in R space for 4.0 wt.% Pd@UiO-66 samples (a) before and (b) after reduction; 4.8 wt.% Pd@UiO-66-NH<sub>2</sub> (c) before and (d) after reduction, and 5.0 wt.% Pd@UiO-66-OMe samples (e) before and (f) after reduction under 50 mL/min flow of 10% H<sub>2</sub>/Ar at 200 °C.

We used EXAFS spectroscopy to explore the coordination environment of Pd in UiO-66-X before and after the reduction step. As shown in Figure 6a, c, and e, EXAFS spectra of the three catalysts before reduction have a dominant Pd-O scattering peak (2.0 Å), which is in good agreement with the structure of the Pd precursor, palladium acetate. After reduction with a 10% H<sub>2</sub>/Ar flow at 200 °C, the scattering of Pd-Pd appears in Fourier transform as shown in Figure 6b, d, and f. EXAFS fitting showed that Pd-Pd scattering has a interatomic distance of  $2.78 \pm 0.01$  Å, indicating the formation of Pd NCs.

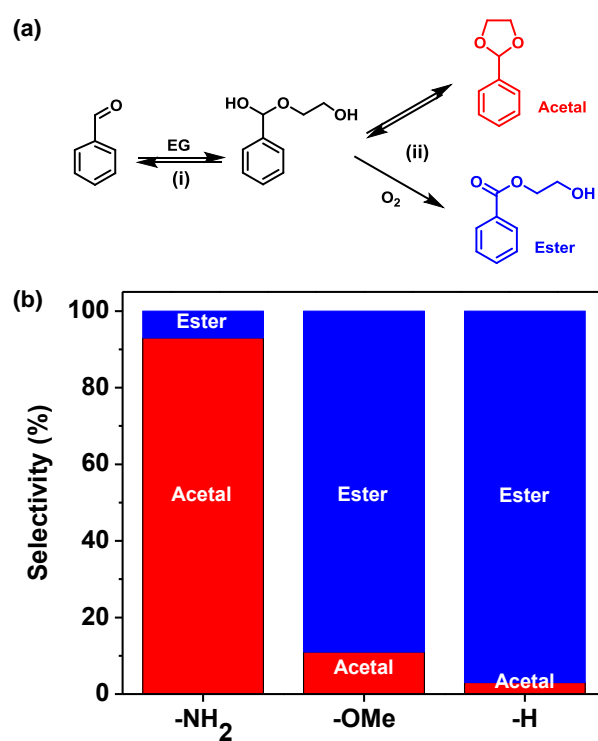


**Figure 7.** (a) Plausible mechanism for the aerobic reaction between benzaldehyde and ethylene glycol; (b) products distribution using Pd@UiO-66-X (X = H, NH<sub>2</sub>, and OMe).

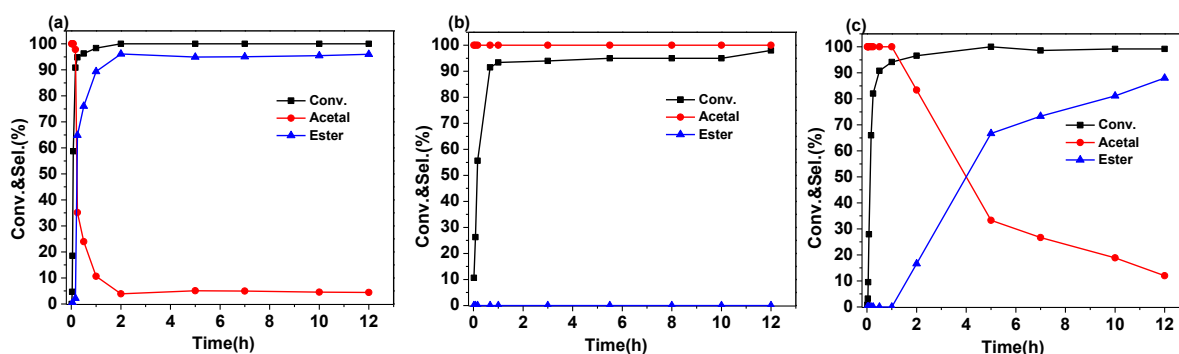


**Figure 8.** Kinetic study of aerobic reaction using Pd@UiO-66-X. (a) 1.5 wt.% Pd@UiO-66; (b) 2.0 wt.% Pd@UiO-66-NH<sub>2</sub>; (c) 2.0 wt.% Pd@UiO-66-OMe.

To investigate the effects of the chemical environment surrounding Pd NCs on their catalytic properties, we carried out an aerobic reaction between benzaldehyde and ethylene glycol over Pd@UiO-66-X (X = H, NH<sub>2</sub>, and OMe). As shown in Figure 7a, the plausible mechanism of this reaction involves two steps: i) condensation of benzaldehyde and ethylene glycol to yield hemiacetal, ii) further condensation to yield corresponding acetal or oxidation to yield ester. As shown in Figure 7b and Table 1 (Entry 1-3), Pd@UiO-66-X (X = H, NH<sub>2</sub>, and OMe) catalysts gave high activity (91-99%) with distinctly different product distribution, i.e., Pd@UiO-66-NH<sub>2</sub> gave the corresponding acetal, benzaldehyde ethylene acetal (sel. 94%), as the major product, while Pd@UiO-66-H and -OMe showed high selectivity (90% and 97%, respectively) to the corresponding ester, 2-hydroxyethyl benzoate. These product distributions, particularly for Pd@UiO-66-NH<sub>2</sub>, are still retained even if the reaction time was extended from 10 hours to 60 hours, indicating that Pd NCs in UiO-66-NH<sub>2</sub> do not have the ability to oxidize the hemiacetal to the ester.

**Table 1.** Series of control experiments starting with benzaldehyde and ethylene glycol.<sup>a</sup>

Entry	Catalyst	Condition	t (h)	Conv.	Acetal	Ester
1	1.5 wt.% Pd@UiO-66	1 atm O <sub>2</sub>	10	99%	3.3%	96.7%
2	2.0 wt.% Pd@UiO-66-NH <sub>2</sub>	1 atm O <sub>2</sub>	10	91%	93.4%	6.6%
3	2.0 wt.% Pd@UiO-66-OMe	1 atm O <sub>2</sub>	10	98%	11.6%	88.4%
4	UiO-66	1 atm O <sub>2</sub>	10	96%	99%	/
5	UiO-66-NH <sub>2</sub>	1 atm O <sub>2</sub>	10	90%	99%	/
6	UiO-66-OMe	1 atm O <sub>2</sub>	10	88%	99%	/
7 <sup>b</sup>	1.5 wt.% Pd@UiO-66	Ar, no O <sub>2</sub>	10	99%	99%	/
8 <sup>b</sup>	2.0 wt.% Pd@UiO-66-NH <sub>2</sub>	Ar, no O <sub>2</sub>	10	95%	99%	/
9 <sup>b</sup>	2.0 wt.% Pd@UiO-66-OMe	Ar, no O <sub>2</sub>	10	96%	99%	/
10 <sup>c</sup>	1.5 wt.% Pd@UiO-66	O <sub>2</sub> , aniline	10	99%	99%	/
11 <sup>c</sup>	2.0 wt.% Pd@UiO-66-OMe	O <sub>2</sub> , aniline	10	96%	99%	/
12	5.0 wt.% Pd/C	1 atm O <sub>2</sub>	10	96%	7%	93%

<sup>a</sup>Reaction conditions: benzaldehyde (0.1 mmol), 1.5 mL of ethylene glycol, S/M = 100/1, 90 °C.  
<sup>b</sup>A Freeze-Pump-Thaw method was applied to completely remove O<sub>2</sub> in the system.  
<sup>c</sup>Aniline/Pd = 1/1.

However, it is worth to mention that Pd@UiO-66-NH<sub>2</sub> is active for the oxidation of benzyl alcohol to benzaldehyde, which will be discussed later. In the kinetic studies, all catalysts achieved superior conversion of benzaldehyde within 1 hour and produced acetal as the predominant product. For Pd@UiO-66 and Pd@UiO-66-OMe, the acetal was gradually converted to the ester due to the reversible nature of the hemiacetal-acetal conversion, while for Pd@UiO-66-NH<sub>2</sub>, acetal quantities were always significantly greater than that of the ester. We used UiO-66-X alone to catalyze the aerobic reaction but only obtained acetal, confirming the Pd NCs are the active sites in the formation of ester (Table 1, entry 4-6). We also carried out anaerobic reactions with benzaldehyde and ethylene glycol using Pd@UiO-66-X in

the presence of argon, and we did not see any formation of ester but acetal (Table 1, entry 7-9), which implies that O<sub>2</sub> was indispensable in the formation of ester in the second step of the aerobic reaction, especially for Pd@UiO-66 and Pd@UiO-66-OMe.

Through the proposed reaction mechanism, we initially postulated that the final product distribution depends on the competition between hemiacetal oxidation and self-condensation. When the oxidation of hemiacetal precedes acetalization, the ester will be the predominant product and vice versa. From the kinetic studies (Figure 9), we determined that the rate constant of acetalization over Pd@UiO-66, -NH<sub>2</sub> and -OMe is 0.259 min<sup>-1</sup>, 0.199 min<sup>-1</sup>, and 0.123 min<sup>-1</sup>, respectively. The fact that UiO-66 is more active than UiO-66-NH<sub>2</sub> in our acetalization reaction is consistent with a recent study by Jung et al.,<sup>31</sup> but cannot explain why the ester is the major product for Pd@UiO-66.

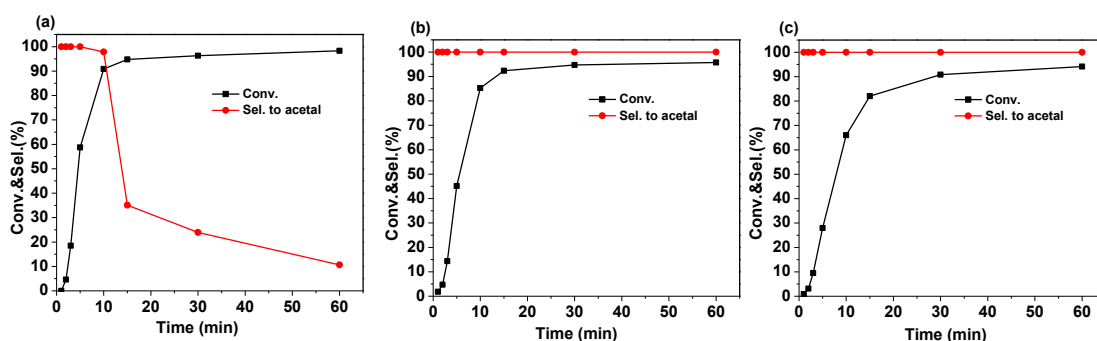


**Figure 9.** Kinetic study of acetalization reaction using Pd@UiO-66-X. (a) Pd@UiO-66 ;(b) Pd@UiO-66-NH<sub>2</sub>; (c) Pd@UiO-66-OMe. Reaction conditions: benzaldehyde (0.1 mmol), ethylene glycol (1.5 mL), mesitylene (8 μL), 5 mg of Pd@UiO-66-X, 90 °C, 0.1 MPa O<sub>2</sub>, 1 hour.



Given that the acetalization activity of the MOFs is not the key factor that determines whether acetal or ester is the major product, we proceeded to investigate the oxidation capacity of the encapsulated Pd NCs. Aniline (1 equiv. of Pd), which mimics the linker units in UiO-66-NH<sub>2</sub>, was added deliberately to the reactions catalyzed by Pd@UiO-66 and Pd@UiO-66-OMe (Table 1, entries 10-11). We found that the ester formation was totally precluded, indicating that the NH<sub>2</sub>-Pd interaction inhibits the oxidation capability of Pd NCs encapsulated in UiO-66 and UiO-66-OMe. Pd/C which does not contain NH<sub>2</sub>-Pd interaction, still gave the ester as the major product (Table 1, entry 12). However, Pd/C gave no ester at all in the presence of aniline (1 equiv. of Pd). Therefore, we speculated that the product distribution is determined by the different oxidation capability derived from Pd NCs encapsulated in the three isorecticular UiO-66-X MOFs. Since the Pd NCs are embedded in the cavities of the MOFs, the chemical environment endowed by the MOFs is prone to change the adsorption of reactants and the surface electronic property of the Pd NCs, thus controlling their oxidation capability. To verify our speculation, we employed aerobic benzyl alcohol oxidation in isopropanol as a test reaction to evaluate the oxidation capacity of Pd NCs residing in UiO-66-X (Figure 10). We found that these Pd NCs in different substituted MOFs displayed distinct oxidation capacity, and the trend for the oxidation capacity is consistent with the order (Pd@UiO-66 > Pd@UiO-66-OMe > Pd@UiO-66-NH<sub>2</sub>). We didn't detect any benzoic acid in this reaction, which agrees with a previous report.<sup>53</sup> Considering the blank test and pristine MOFs show negligible activity, we actually tuned the oxidation capacity of Pd NCs using isorecticular MOFs.

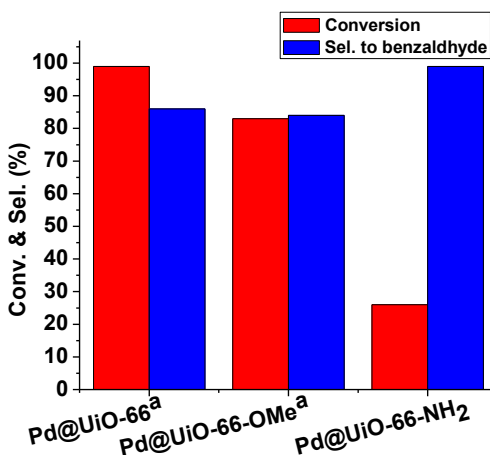


**Figure 10.** Aerobic oxidation of benzyl alcohol in isopropanol. Reaction condition: benzyl alcohol (0.1 mmol), isopropanol (1.5 mL), metal/substrate = 1/100, 0.1 MPa O<sub>2</sub> balloon, 90 °C, 10 hours. <sup>a</sup> Corresponding acetal, benzaldehyde isopropyl acetal was formed.

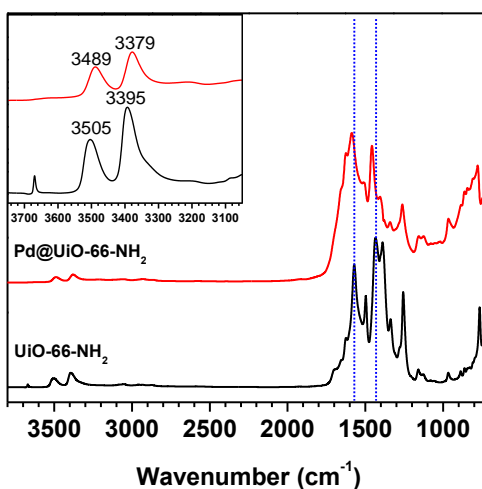


**Figure 11.** DRIFTS spectra of UiO-66-NH<sub>2</sub> (black) and 2.0 wt.% Pd@UiO-66-NH<sub>2</sub> (red). The inset show enlarged N-H vibration region.

We envision that confining metal NCs in the cavities of MOFs represents a new way to control the coordination of functional groups to metal surface because of

the define crystal structure of MOFs. In this work, the octahedral cage with 12 linkers in UiO-66-NH<sub>2</sub> has defined number of -NH<sub>2</sub> groups (12) that could coordinate to the confined Pd cluster. This new strategy is completely different from the metal nanoparticles prepared in colloidal solution, where the metal surface is saturated with ligands/functional groups and could be completely poisoned if all active sites are occupied. To validate this hypothesis, we intentionally added various amount of aniline (0.2, 0.4, 0.6, 0.8 and 1 equiv. of Pd) to Pd@UiO-66-NH<sub>2</sub> in the oxidation of benzyl alcohol under the identical conditions. As expected, the conversion of benzyl alcohol decreased as the aniline amount increased. Pd@UiO-66-NH<sub>2</sub> gives 90% conversion in 10 hours while the Pd-aniline@UiO-66-NH<sub>2</sub> was almost inactive (aniline/Pd = 1, 5% conversion in 10 hours). These control experiments highlight the advantages of using the under-coordinated Pd NCs confined in MOFs as catalysts, where we can tune the catalytic properties of these Pd NCs through ligand-surface interaction without completely blocking their surface active sites.

Bearing these findings in mind, we sought to investigate the Pd NCs-MOFs interaction, which may account for the different product distribution. Since such interaction could not be elucidated from EXAFS due to the close approximation between Pd-O and Pd-N (Figure 6), we used DRIFTS to probe the Pd NCs-MOF interaction. As shown in Figure 11, the peaks at ~1390 cm<sup>-1</sup> and ~1560 cm<sup>-1</sup> (indicated by the dashlines), corresponding to the respective O-C-O symmetric and asymmetric stretching vibrations, have shifted to higher wavenumbers, while peaks at 3395 cm<sup>-1</sup> and 3505 cm<sup>-1</sup>, corresponding to N-H symmetric and asymmetric stretch respectively, have shifted to lower energy.<sup>27,54</sup> These shifts in Pd@UiO-66-NH<sub>2</sub>

indicate that there could be an interaction between the Pd NCs with the  $-NH_2$  on benzenedicarboxylate moiety in the MOF upon loading.<sup>49</sup> The coordination of  $-NH_2$  on the linker of the MOF with Pd surface could affect the adsorption of reactants and thus the catalytic properties of these Pd NCs.

To further probe the surface electronic properties of encapsulated Pd NCs, we used DRIFTS to study the adsorbed CO molecules on the Pd@UiO-66-X (Figure 12). CO adsorption spectra of all three samples do not show any vibration peaks above  $2143\text{ cm}^{-1}$ , which indicates the absence of CO adsorption on any possible cationic species in the sample, such as  $Pd^{2+}$ .<sup>55</sup> Peaks in the  $2020 - 2075\text{ cm}^{-1}$  region correspond to C-O vibrations of linearly adsorbed CO, while peaks in the  $1850 - 1950\text{ cm}^{-1}$  correspond to the C-O vibration of 2-fold bridge carbonyls on  $Pd^0$  surface.<sup>56-60</sup> The DRIFTS spectra shows that the C-O vibration for CO adsorbed on Pd NCs in UiO-66- $NH_2$  exhibits a shift to a lower wavenumber ( $2059\text{ cm}^{-1}$ ) compare to that in UiO-66-OMe and UiO-66 ( $2071$  and  $2073\text{ cm}^{-1}$ , respectively).<sup>56</sup> The decrease in CO vibration wavenumber indicates that the C-O bond is weakened by the  $\pi$ -back donation from the electron -enriched surface of Pd NCs in UiO-66- $NH_2$  than those in UiO-66 and UiO-66-OMe. The presence of  $-NH_2$  group, with a lone pair of electrons could donate these electrons to the Pd NCs surface, which agrees with the lower N-H stretch vibration wavenumbers in Pd@UiO-66- $NH_2$  than in pristine UiO-66- $NH_2$  (Figure 11 inset). We also found that the IR spectrum for CO adsorbed on Pd@UiO-66- $NH_2$  contains less fine structures compared to those on Pd@UiO-66-OMe and Pd@UiO-66 (Figure 12). This could be due to the strong interaction of  $-NH_2$  with Pd

that can block the adsorption of CO at certain surface sites on Pd NCs confined in UiO-66-NH<sub>2</sub>.

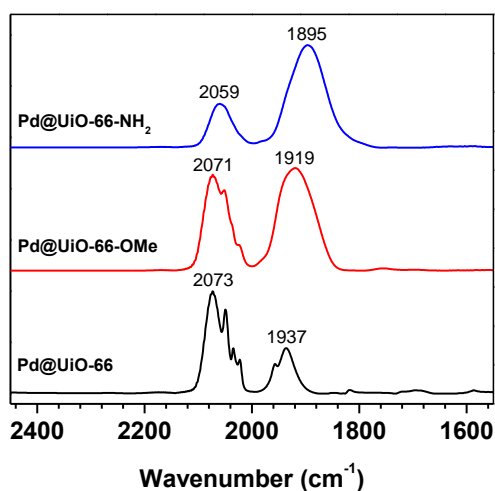


**Figure 12.** DRIFTS spectra of CO adsorption on 1.5 wt.% Pd@UiO-66 (black), 2.0 wt.% Pd@UiO-66-OMe (red), and 2.0 wt.% Pd@UiO-66-NH<sub>2</sub> (blue) at ambient temperature.

Our DRIFTS studies suggested that the interactions between –NH<sub>2</sub> and Pd NCs in UiO-66-NH<sub>2</sub>, affecting reactant adsorption and donating electrons to metal surface, could lead to their hindered activity in oxidation of hemiacetal to ester. More importantly, these interactions did not completely impair the oxidation capacity of Pd NCs, as evidenced by the fact that the Pd@UiO-66-NH<sub>2</sub> is still active for oxidation of benzyl alcohol to benzaldehyde under the same reaction condition but using benzyl alcohol as the starting material.

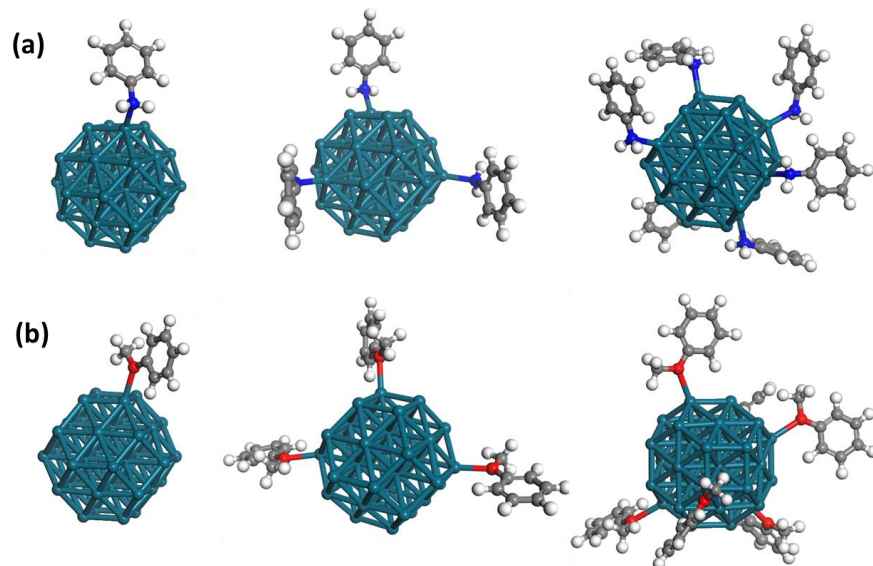


**Figure 13.** Optimized geometries of (a) the Pd<sub>38</sub>-NH<sub>2</sub> and (b) the Pd<sub>38</sub>-OMe model systems at DFT level. The dark green, gray, blue, red and white spheres represent palladium, carbon, nitrogen, oxygen and hydrogen atoms, respectively.

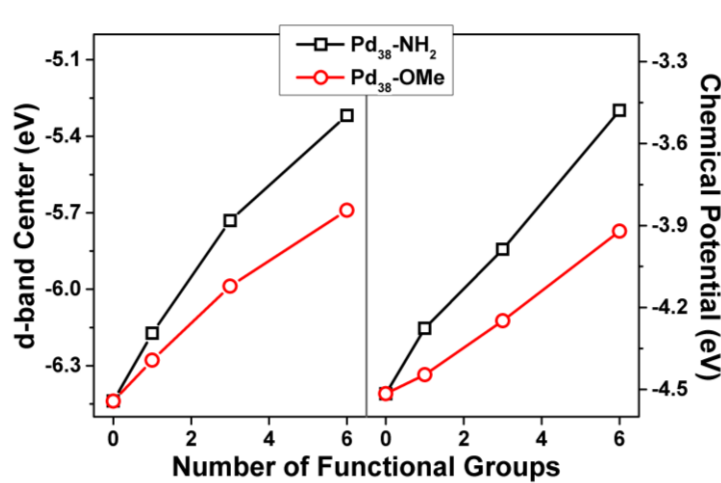


**Figure 14.** Black and red lines refer to variation of the d-band center (left panel) and the chemical potential (right panel) with different number of functional groups for Pd<sub>38</sub>-NH<sub>2</sub> and Pd<sub>38</sub>-OMe, respectively

In the oxidation reaction, the catalysts generally act as an electron reservoir which requires moderate oxidation capability of the catalysts to charge and discharge the reactants during the reaction cycle.<sup>61,62</sup> To gain deeper insight into the effect of different functional groups on the oxidation capability of Pd NCs, we computed evolution of the *d*-band center and the chemical potential change associated with the number of the functional groups ( $-\text{NH}_2$  or  $-\text{OMe}$ ) on the highly-symmetric  $\text{Pd}_{38}$  cluster as a prototype model system. All computations are performed at the level of DFT (see Figure 13 for detailed methods and two model systems, named as  $\text{Pd}_{38}\text{-NH}_2$  and  $\text{Pd}_{38}\text{-OMe}$ ). As shown in Figure 14, for both systems, the *d*-band center of the  $\text{Pd}_{38}$  clusters shifts towards higher energy levels with an increase in the number of functional groups due to the electron donation from the functional groups. Such a shift of the *d*-band center to higher energy-levels leads to increased chemical potential for the functionalized  $\text{Pd}_{38}$  clusters, thereby the tendency to lose more electrons. In other words, the increased chemical potential results in the impairment of the oxidation properties of Pd NCs. However, an important difference observed between the two systems is that with the same number of the functional groups, the  $-\text{NH}_2$ -functionalized MOF results in greater increase of the chemical potential than the  $-\text{OMe}$ -functionalized MOF. Additionally, such a difference between the two systems becomes more evident with an increase in the number of functional groups. Hence strong reduction coupled with weak oxidation is expected for the  $\text{Pd@UiO-66-NH}_2$  system, whereas the relatively weak oxidation property can impede drawing electrons from reactants, thus hindering completion of the reaction cycle. On the contrary, moderate oxidation capability can be achieved in the  $\text{Pd@UiO-66-OMe}$  system to

facilitate both the charging and discharging processes of the reactants. Hence, the Pd@UiO-66-OMe system exhibits higher catalytic activity towards the formation of ester.

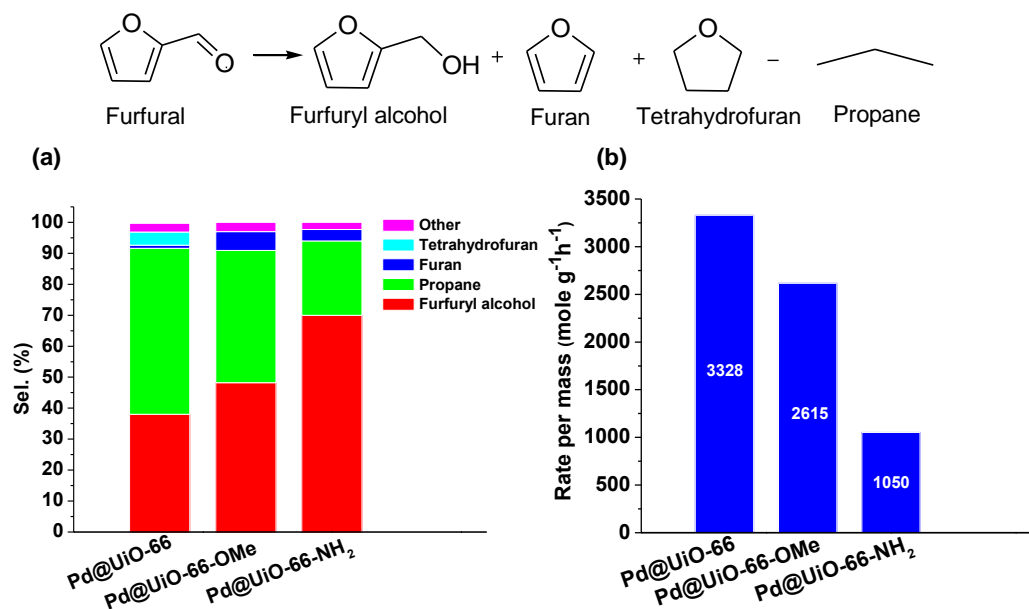


**Figure 15.** Gas-phase furfural hydrogenation product selectivity (a), and (b) Rate per mass (Rate per mass is expressed as mole of molecules reacted/gram of Pd/ hour) obtained at 140 °C by Pd@UiO-66-X. Prior to catalytic testing, the catalyst was reduced at 200 °C for 2 hours in 10% H<sub>2</sub>/Ar stream. The catalytic activity and selectivity were evaluated for total conversions at 9.5%. Reaction condition: He (bubbler)/H<sub>2</sub> = 17.2 (0.046 mL/min furfural)/2.8 mL/min, 140 °C.

We further extended our strategy to another catalytic transformation, gas-phase furfural hydrogenation catalyzed by Pd@UiO-66-X (X= H, NH<sub>2</sub> and OMe), where the desired product of the hydrogenation was furfuryl alcohol. Unsurprisingly, these chemical functionalities in the linker play a critical role in product selectivity and activity in the gas-phase furfural hydrogenation (Figure 15). We controlled the



conversion of furfural to be 9.5% for the three catalysts by using different amount of catalysts. At the same conversion, Pd@UiO-66-NH<sub>2</sub> gave the highest selectivity to furfuryl alcohol (ca. 70%) while Pd@UiO-66 showed highest selectivity to propane (ca. 55%). We are conducting more computational investigations currently to explore the reasons to account for such different selectivities to desired furfuryl alcohol, with regards to steric hindrance and electronic effects.

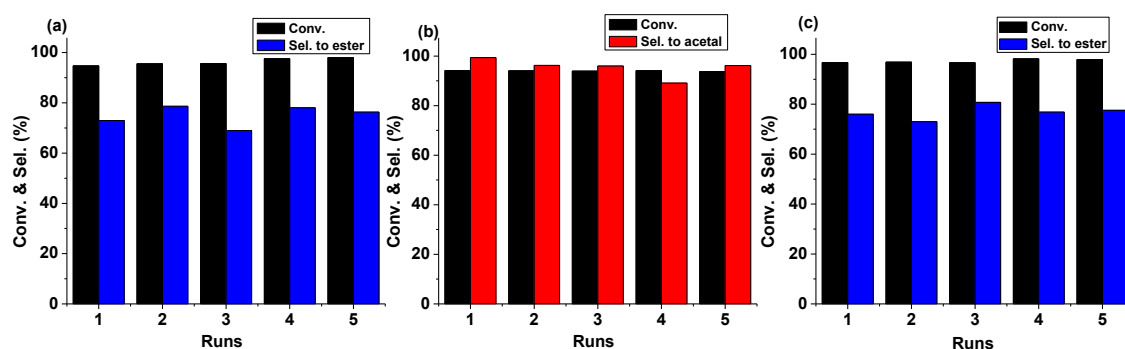


**Figure 16.** Recycling test with Pd@UiO-66-X (a) 1.5 wt.% Pd@UiO-66; (b) 2.0 wt.% Pd@UiO-66-NH<sub>2</sub> and (c) 2.0 wt.% Pd@UiO-66-OMe. Reaction conditions: benzaldehyde (0.1 mmol), ethylene glycol (1.5 mL), 0.1 MPa O<sub>2</sub> balloon, metal/substrate = 1/100, 90 °C for 5.5 hours.

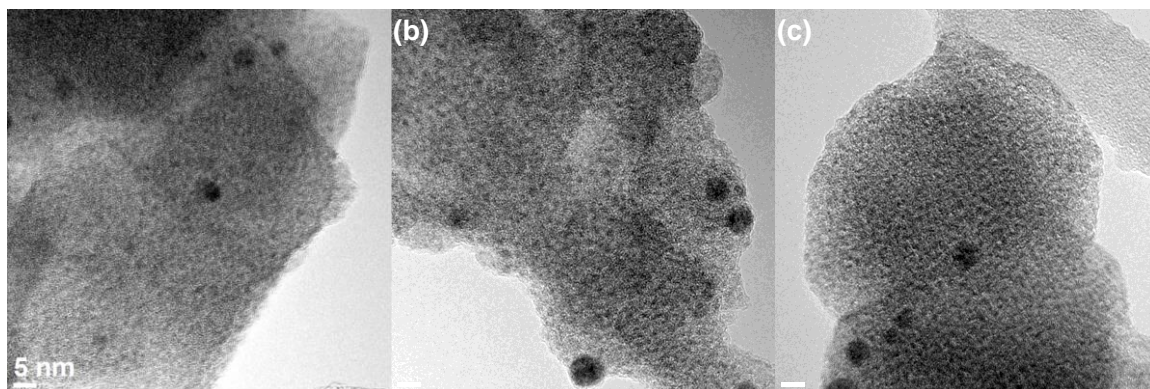


**Figure 17.** TEM images of catalysts after reaction. (a) 1.5 wt.% Pd@UiO-66; (b) 2.0 wt.% Pd@UiO-66-NH<sub>2</sub>; (c) 2.0 wt.% Pd@UiO-66-OMe.

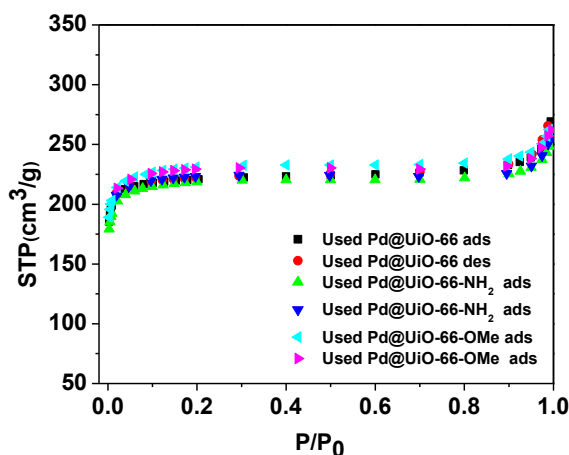


**Figure 18.** Nitrogen adsorption/desorption isotherms of the used Pd@UiO-66-X after catalysis.

Lastly, the durability of the Pd@UiO-66-X (X = H, NH<sub>2</sub>, and OMe) was evaluated. Pd@UiO-66-X could be recycled at least 5 times without significant change in activity and selectivity (Figure 16). Furthermore, the structural integrity of the catalysts was still maintained after reaction, as evidenced by PXRD. The slight aggregation of Pd NCs after reaction did not affect the recyclability of the catalysts (Figure 17). In order to confirm the majority of Pd NCs are still encapsulated inside MOFs, we also performed the encapsulation test by utilizing the used Pd@UiO-66-X as catalysts to hydrogenate two probe molecules, styrene and tetraphenylethylene. The used Pd@UiO-66-X showed high activity in the hydrogenation of styrene, but no detectable activity in the hydrogenation of tetraphenylethylene, suggesting that the majority of the Pd NCs are still encapsulated inside the cavities of UiO-66-X. We speculate that the slight aggregation of Pd NCs in used catalysts may result from the loss of MOF restriction associated with the linker dissociation in the MOF at elevated reaction temperature.<sup>63</sup> The N<sub>2</sub> sorption analysis showed that the used Pd@UiO-66-X

catalysts are still highly porous and the slight decrease of BET surface area and pore volume could be due to the residual reactants or products trapped inside the UiO-66-X (Figure 18), which is consistent with our previous work.<sup>64</sup> Pd leaching was assessed after reaction by ICP-MS analysis of the metal content in the reaction solution after removing the catalysts by centrifugation. The leached Pd in the solution was found to be negligible (< 0.1% of total Pd in the added catalysts).

## Conclusions

In conclusion, we have developed Pd NCs encapsulated in isorecticular MOFs of different chemical environments (Pd@UiO-66-X, X = H, NH<sub>2</sub>, and OMe), which were used to catalyze the aerobic reaction between benzaldehyde and ethylene glycol. Notably, the linker modification in MOFs can atomically tune the product distribution in this reaction. We found that Pd@UiO-66-NH<sub>2</sub> favors the formation of acetal, while Pd@UiO-66 and Pd@UiO-66-OMe have a higher selectivity to ester. DRIFTS studies revealed that -NH<sub>2</sub> groups coordinate to the Pd surface and donate electrons to the Pd NCs in Pd@UiO-66-NH<sub>2</sub>. These NH<sub>2</sub>-Pd interactions decrease (but do not completely eliminate) the oxidation capability of encapsulated Pd NCs and lead to the high acetal selectivity by Pd@UiO-66-NH<sub>2</sub> in the reaction. DFT calculations show the Pd-NH<sub>2</sub> NCs system possess higher chemical potential and thus weaker oxidation capability than the Pd-OMe NCs, which agrees with the experimental results. This strategy can be extended to gas-phase furfural hydrogenation and linker modification in MOFs is decisive to the product distribution as well. The present work demonstrates the control of heterogeneous catalytic sites through their surrounding chemical environment at an atomic level, thus opening up fascinating opportunities

for the development of tunable metal-MOF catalysts for selective chemical transformations.

### **Experimental section**

**Instruments.** Surface area analysis of the catalysts was performed by N<sub>2</sub> adsorption/desorption isotherms using a Micromeritics 3Flex surface characterization analyzer at 77 K. Powder X-ray diffraction patterns of the samples were obtained by a STOE Stadi P powder diffractometer using Cu K $\alpha$  radiation (40 kV, 40 mA,  $\lambda$  = 0.1541 nm). The size and morphology of Pd@UiO-66-X were investigated using TEM recorded on a Tecnai G2 F20 electron operated at 200 kV. ICP-MS (X Series II, Thermo Scientific) was performed to determine the actual loading of palladium in UiO-66-X. The ICP-MS sample was prepared by dissolving the Pd@UiO-66-X samples in boiling aqua regia until the solid was completely dissolved. The XAS were measured in transmission mode (Pd K-edge = 24.350 keV) at 20-BM-B and 9-BM-B beam lines of the Advanced Photon Source at Argonne National Laboratory. XAS of reference samples were collected using pure finely ground powders homogeneously dispersed on polyimide Kapton tape. While the MOF samples were pressed into a pellet fit to a hole embedded in a Teflon substrate. A palladium foil spectrum was acquired simultaneously with each measurement for energy calibration. Multiple scans (8-10 scans) were collected for each sample, and merged into one data set for XAS analysis. For XAS analysis, the software at the beam line in Argonne National Lab was used to perform dead-time correction, and energy calibration. The Athena program, which is an interface to IFEFFIT and FEFFIT, was used for glitch removal,

pre-edge subtraction, post-edge normalization, and conversion to k-space. The EXAFS data were fitted in R-space by using the Artemis program from the same package, with theoretical models constructed from FEFF6. DRIFTS measurements were performed using an Agilent Cary 670 FTIR equipped with a linearized MCT detector, a Harrick diffuse reflectance accessory, and a Praying Mantis high-temperature reaction chamber. MOFs samples were packed in the sample cup, followed by an activation process under high vacuum ( $10^{-6}$  mTorr) at 150 °C for 1 hour to remove the absorbed water. After the sample was cooled down to ambient temperature, the spectra were recorded at  $2\text{ cm}^{-1}$  resolution within the range of 4000–700  $\text{cm}^{-1}$ . Kubelka–Munk correction was applied to generate the spectra for qualitative analysis.

**Computational Methods.** DFT methods are used to perform geometry optimization and computation of the electronic properties. More specifically, the plane-wave basis sets and projected augmented wave (PAW) pseudopotentials implemented in the Vienna ab initio simulation package (VASP 5.3) are adopted.<sup>35-38</sup> The exchange-correlation interaction is treated within the generalized gradient approximation (GGA) in the Perdew-Burke-Ernzerhof (PBE) form.<sup>39,40</sup> Spin-restricted computation with the energy cutoff at 400 eV is selected. Aniline, anisole and the Pd<sub>38</sub> cluster with high octahedral symmetry are chosen to simulate –NH<sub>2</sub> and –OMe functional groups and Pd NCs, respectively. For all computations, a  $\sim 15\text{ \AA}$  vacuum spacing is set along *x*, *y* and *z* directions to neglect the interaction between neighboring clusters. All the structures are fully relaxed until the force on each atom is less than 0.02 eV/Å. The chemical potential is calculated as follows:

$$\mu = -\frac{I + A}{2} = \frac{E(N+1) - E(N-1)}{2}$$

where  $I$ ,  $A$ ,  $E(N+1)$  and  $E(N-1)$  represent ionization energy, electron affinity, the energies of the  $N+1$  and  $N-1$  electron systems, respectively. The  $N+1$  and the  $N-1$  electron systems are corresponding to the same system with one positive and negative net charge, respectively.

**General procedure for aerobic reaction.** Typically, 10.5 mg of benzaldehyde (0.1 mmol, >99%, Aldrich), 1.5 mL of ethylene glycol (Fisher Scientific), Pd@UiO-66-X (Pd/substrate=1/100) and 7 mg of mesitylene (internal GC standard, 99%, Acros Organics) were added in a 20 mL glass vial. The air in the vial was removed by using a modified freeze-pump method. The vial with an oxygen balloon on top was loaded in an oil bath which was preheated to 90 °C and then the reaction was carried out with magnetic stirring at 600 rpm. After the reaction was finished, the products were analyzed using a gas chromatograph equipped with a HP-5 capillary column (30 m × 0.32 mm × 0.25 μm) with a flame ionization detector and SHIMADZU 5050A GC-MS equipped with a HP-5ms capillary column (30 m × 0.32 mm × 0.25 μm).

**Probe alkene hydrogenation.** Styrene (0.1 mmol, 98%, Aldrich) and palladium catalyst (Pd/substrate=1/100) were added to 1.5 mL of ethanol and the reaction mixture was stirred at 50 °C with a hydrogen balloon for 15 hours. Upon the completion of styrene hydrogenation, the solid catalyst was removed from the solution by filtration and the liquid phase was analyzed using a gas chromatograph equipped with a HP-5 capillary column (30 m × 0.32 mm × 0.25 μm) with a flame ionization detector; For tetraphenylethylene (0.1 mmol, Aldrich), the catalyst was removed from the solution by filtration and the solid catalyst was washed with

ethanol 5 times. The ethanol was removed by rotary evaporation and the yield was calculated using  $^1\text{H}$  NMR with mesitylene as the external standard.

**CO adsorption studies of the Pd@UiO-66-X catalyst.** The Pd@UiO-66-X (X = H, NH<sub>2</sub> and OMe) sample was packed in a Praying Mantis high-temperature reaction chamber. The sample was activated *in-situ* under dynamic vacuum ( $10^{-6}$  mTorr) at 150 °C for 1 hour. The sample was then pre-treated with 10% H<sub>2</sub>/He (total flow rate: 50 mL/min) at 200 °C for 2 hours and subsequently purged with Helium at 200 °C for 30 min. The samples were then cooled to 30 °C. A background spectrum was collected as reference prior to the introduction of CO into the chamber at 30 °C. CO was introduced to the chamber at 10 mL/min for 30 min, and subsequently flushed with Helium to remove any gas phase CO. The IR spectra were collected with subtracted background.

**Recycling of Pd@UiO-66-X catalyst.** The solid catalyst was separated from the reaction mixture by centrifugation and washed thoroughly with acetone. After it was dried at 80 °C under vacuum, the catalyst was reused in the second run. The catalytic activity and product selectivity of the catalyst did not show significant change in the following run. PXRD analysis showed that the crystal structure of the used catalyst remained intact during the catalytic cycles and catalysts remained effective within 5 cycles of the reaction.

**Acknowledgment.** We are grateful for the startup funds support from the Ames Laboratory (Royalty Account) and Iowa State University. The Ames Laboratory is operated for the U.S. Department of Energy by Iowa State University under Contract No. DE-AC02-07CH11358. We thank Dale L. Brewé, Steve M. Heald, Trudy B.

Bolin, Tianpin Wu, and Jeff Miller for their assistance during XAS measurements at APS. Use of the Advanced Photon Source was supported by the U. S. Department of Energy, Office of Science, Office of Basic Energy Sciences, under Contract No. DE-AC02-06CH11357. We thank Robert J. Angelici for his advice during the writing of this manuscript and we also thank Gordon J. Miller for the use of X-ray Diffractometer.

## References

- (1) Woodley, J. M. *Curr. Opin. Chem. Biol.* **2013**, *17*, 310-316.
- (2) Rodrigues, R. C.; Ortiz, C.; Berenguer-Murcia, A.; Torres, R.; Fernandez-Lafuente, R. *Chem. Soc. Rev.* **2013**, *42*, 6290-6307.
- (3) Jacobsen, E. N.; Zhang, W.; Guler, M. L. *J. Am. Chem. Soc.* **1991**, *113*, 6703-6704.
- (4) Miller, J. J.; Sigman, M. S. *Angew. Chem. Int. Ed.* **2008**, *120*, 783-786.
- (5) Jensen, K. H.; Sigman, M. S. *Angew. Chem. Int. Ed.* **2007**, *119*, 4832-4834.
- (6) Wang, W.; Hammond, G. B.; Xu, B. *J. Am. Chem. Soc.* **2012**, *134*, 5697-5705.
- (7) Ribeiro, F. R.; Alvarez, F.; Henriques, C.; Lemos, F.; Lopes, J. M.; Ribeiro, M. *F. J. Mol. Catal. A: Chem.* **1995**, *96*, 245-270.
- (8) Allendorf, M. D.; Stavila, V. *CrystEngComm* **2015**, *17*, 229-246.
- (9) Valvekens, P.; Vermoortele, F.; De Vos, D. *Catal. Sci. Tech.* **2013**, *3*, 1435-1445.
- (10) Dhakshinamoorthy, A.; Alvaro, M.; Garcia, H. *Catal. Sci. Tech.* **2011**, *1*, 856-867.
- (11) Dhakshinamoorthy, A.; Opanasenko, M.; Čejka, J.; Garcia, H. *Adv. Synth. Catal.* **2013**, *355*, 247-268.
- (12) Dhakshinamoorthy, A.; Opanasenko, M.; Cejka, J.; Garcia, H. *Catal. Sci. Technol.* **2013**, *3*, 2509-2540.



- (13) Aijaz, A.; Karkamkar, A.; Choi, Y. J.; Tsumori, N.; Rönnebro, E.; Autrey, T.; Shioyama, H.; Xu, Q. *J. Am. Chem. Soc.* **2012**, *134*, 13926-13929.
- (14) Hu, P.; Morabito, J. V.; Tsung, C.-K. *ACS Catal.* **2014**, *4*, 4409-4419.
- (15) Na, K.; Choi, K. M.; Yaghi, O. M.; Somorjai, G. A. *Nano Lett.* **2014**, *14*, 5979-5983.
- (16) Lu, G.; Li, S.; Guo, Z.; Farha, O. K.; Hauser, B. G.; Qi, X.; Wang, Y.; Wang, X.; Han, S.; Liu, X. *Nat. Chem.* **2012**, *4*, 310-316.
- (17) Chen, Y.-Z.; Xu, Q.; Yu, S.-H.; Jiang, H.-L. *Small* **2015**, *11*, 70-70.
- (18) Chen, Y.-Z.; Zhou, Y.-X.; Wang, H.; Lu, J.; Uchida, T.; Xu, Q.; Yu, S.-H.; Jiang, H.-L. *ACS Catal.* **2015**, *5*, 2062-2069.
- (19) Corma, A.; García, H.; Llabrés i Xamena, F. X. *Chem. Rev.* **2010**, *110*, 4606-4655.
- (20) Wang, Z.; Cohen, S. M. *Chem. Soc. Rev.* **2009**, *38*, 1315-1329.
- (21) Zhang, Z.; Zhang, L.; Wojtas, L.; Nugent, P.; Eddaoudi, M.; Zaworotko, M. J. *J. Am. Chem. Soc.* **2011**, *134*, 924-927.
- (22) Yang, Q.; Guillerm, V.; Ragon, F.; Wiersum, A. D.; Llewellyn, P. L.; Zhong, C.; Devic, T.; Serre, C.; Maurin, G. *Chem. Commun.* **2012**, *48*, 9831-9833.
- (23) Biswas, S.; Zhang, J.; Li, Z.; Liu, Y.-Y.; Grzywa, M.; Sun, L.; Volkmer, D.; Van Der Voort, P. *Dalton Trans.* **2013**, *42*, 4730-4737.
- (24) Bauer, C. A.; Timofeeva, T. V.; Settersten, T. B.; Patterson, B. D.; Liu, V. H.; Simmons, B. A.; Allendorf, M. D. *J. Am. Chem. Soc.* **2007**, *129*, 7136-7144.
- (25) Burtch, N. C.; Jasuja, H.; Walton, K. S. *Chem. Rev.* **2014**, *114*, 10575-10612.
- (26) Tan, J. C.; Cheetham, A. K. *Chem. Soc. Rev.* **2011**, *40*, 1059-1080.
- (27) Goh, T. W.; Xiao, C.; Maligal-Ganesh, R. V.; Li, X.; Huang, W. *Chem. Eng. Sci.* **2015**, *124*, 45-51.
- (28) Shen, L.; Liang, R.; Luo, M.; Jing, F.; Wu, L. *Phys Chem Chem Phys* **2015**, *17*, 117-121.
- (29) Esken, D.; Turner, S.; Lebedev, O. I.; Van Tendeloo, G.; Fischer, R. A. *Chem. Mater.* **2010**, *22*, 6393-6401.

- (30) Vermoortele, F.; Vandichel, M.; Van de Voorde, B.; Ameloot, R.; Waroquier, M.; Van Speybroeck, V.; De Vos, D. E. *Angew. Chem. Int. Ed.* **2012**, *51*, 4887-4890.
- (31) Timofeeva, M. N.; Panchenko, V. N.; Jun, J. W.; Hasan, Z.; Matrosova, M. M.; Jhung, S. H. *Appl. Catal., A* **2014**, *471*, 91-97.
- (32) Choi, K. M.; Na, K.; Somorjai, G. A.; Yaghi, O. M. *J. Am. Chem. Soc.* **2015**, *137*, 7810-7816.
- (33) Zhang, D.; Guan, Y.; Hensen, E. J. M.; Xue, T.; Wang, Y. *Catal. Sci. Tech.* **2014**, *4*, 795-802.
- (34) Cavka, J. H.; Jakobsen, S.; Olsbye, U.; Guillou, N.; Lamberti, C.; Bordiga, S.; Lillerud, K. P. *J. Am. Chem. Soc.* **2008**, *130*, 13850-13851.
- (35) Kresse, G.; Furthmüller, J. *Comp. Mat. Sci.* **1996**, *6*, 15-50.
- (36) Kresse, G.; Furthmüller, J. *Phys. Rev. B* **1996**, *54*, 11169.
- (37) Blöchl, P. E. *Phys. Rev. B* **1994**, *50*, 17953.
- (38) Kresse, G.; Joubert, D. *Phys. Rev. B* **1999**, *59*, 1758.
- (39) Perdew, J. P.; Burke, K.; Ernzerhof, M. *Phys. Rev. Lett.* **1996**, *77*, 3865.
- (40) Perdew, J. P.; Burke, K.; Ernzerhof, M. *Phys. Rev. Lett.* **1997**, *78*, 1396-1396.
- (41) Manna, K.; Zhang, T.; Lin, W. *J. Am. Chem. Soc.* **2014**, *136*, 6566-6569.
- (42) Li, H.; Zhu, Z.; Zhang, F.; Xie, S.; Li, H.; Li, P.; Zhou, X. *ACS Catal.* **2011**, *1*, 1604-1612.
- (43) Chun, J.; Kang, S.; Park, N.; Park, E. J.; Jin, X.; Kim, K.-D.; Seo, H. O.; Lee, S. M.; Kim, H. J.; Kwon, W. H. *J. Am. Chem. Soc.* **2014**, *136*, 6786-6789.
- (44) Katz, M. J.; Brown, Z. J.; Colon, Y. J.; Siu, P. W.; Scheidt, K. A.; Snurr, R. Q.; Hupp, J. T.; Farha, O. K. *Chem. Commun.* **2013**, *49*, 9449-9451.
- (45) Gui, B.; Yee, K.-K.; Wong, Y.-L.; Yiu, S.-M.; Zeller, M.; Wang, C.; Xu, Z. *Chem. Commun.* **2015**, *51*, 6917-6920.
- (46) Guo, Z.; Xiao, C.; Maligal-Ganesh, R. V.; Zhou, L.; Goh, T. W.; Li, X.; Tesfagaber, D.; Thiel, A.; Huang, W. *ACS Catal.* **2014**, *4*, 1340-1348.

- (47) Kuo, C.-H.; Tang, Y.; Chou, L.-Y.; Sneed, B. T.; Brodsky, C. N.; Zhao, Z.; Tsung, C.-K. *J. Am. Chem. Soc.* **2012**, *134*, 14345-14348.
- (48) Goel, S.; Wu, Z.; Zones, S. I.; Iglesia, E. *J. Am. Chem. Soc.* **2012**, *134*, 17688-17695.
- (49) Chen, L.; Chen, H.; Luque, R.; Li, Y. *Chem. Sci.* **2014**, *5*, 3708-3714.
- (50) Zhang, W.; Lu, G.; Cui, C.; Liu, Y.; Li, S.; Yan, W.; Xing, C.; Chi, Y. R.; Yang, Y.; Huo, F. *Adv. Mater.* **2014**, *26*, 4056-4060.
- (51) Su, F.-Z.; Ni, J.; Sun, H.; Cao, Y.; He, H.-Y.; Fan, K.-N. *Chem. Eur. J.* **2008**, *14*, 7131-7135.
- (52) Enache, D.; Knight, D.; Hutchings, G. *Catal Lett.* **2005**, *103*, 43-52.
- (53) Chen, G.; Wu, S.; Liu, H.; Jiang, H.; Li, Y. *Green Chem.* **2013**, *15*, 230-235.
- (54) Valenzano, L.; Civalieri, B.; Chavan, S.; Bordiga, S.; Nilsen, M. H.; Jakobsen, S.; Lillerud, K. P.; Lamberti, C. *Chem. Mater.* **2011**, *23*, 1700-1718.
- (55) Skotak, M.; Karpiński, Z.; Juszczak, W.; Pielaszek, J.; Kępiński, L.; Kazachkin, D. V.; Kovalchuk, V. I.; d'Itri, J. L. *J. Catal.* **2004**, *227*, 11-25.
- (56) Groppo, E.; Liu, W.; Zavorotynska, O.; Agostini, G.; Spoto, G.; Bordiga, S.; Lamberti, C.; Zecchina, A. *Chem. Mater.* **2010**, *22*, 2297-2308.
- (57) Groppo, E.; Agostini, G.; Piovano, A.; Muddada, N. B.; Leofanti, G.; Pellegrini, R.; Portale, G.; Longo, A.; Lamberti, C. *J. Catal.* **2012**, *287*, 44-54.
- (58) Anderson, S. L.; Mizushima, T.; Udagawa, Y. *J. Phys. Chem.* **1991**, *95*, 6603-6610.
- (59) Kaden, W. E.; Kunkel, W. A.; Kane, M. D.; Roberts, F. S.; Anderson, S. L. *J. Am. Chem. Soc.* **2010**, *132*, 13097-13099.
- (60) Kaden, W. E.; Kunkel, W. A.; Roberts, F. S.; Kane, M.; Anderson, S. L. *J. Chem. Phys.* **2012**, *136*, 204705.
- (61) Wang, Y.-G.; Yoon, Y.; Glezakou, V.-A.; Li, J.; Rousseau, R. *J. Am. Chem. Soc.* **2013**, *135*, 10673-10683.
- (62) Chen, L.; Rangan, S.; Li, J.; Jiang, H.; Li, Y. *Green Chem.* **2014**, *16*, 3978-3985.

- (63) Morabito, J. V.; Chou, L.-Y.; Li, Z.; Manna, C. M.; Petroff, C. A.; Kyada, R. J.; Palomba, J. M.; Byers, J. A.; Tsung, C.-K. *J. Am. Chem. Soc.* **2014**, *136*, 12540-12543.
- (64) Li, X.; Guo, Z.; Xiao, C.; Goh, T. W.; Tesfagaber, D.; Huang, W. *ACS Catal.* **2014**, *4*, 3490-3497.

**CHAPTER 5**  
**IMPACT OF LINKER ENGINEERING ON THE CATALYTIC ACTIVITY**  
**OF METAL–ORGANIC FRAMEWORKS CONTAINING Pd(II)-**  
**BIPYRIDINE COMPLEXES**

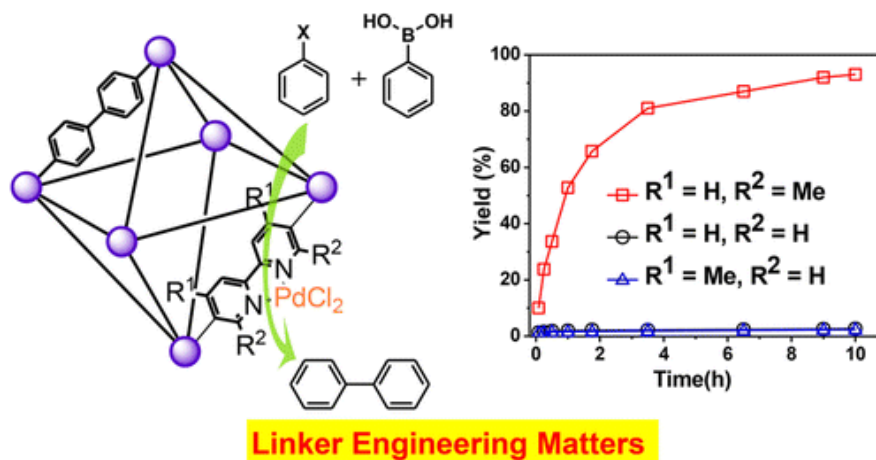
A paper published in *ACS Catal.* 2016, 6, 6324–6328

Xinle Li, Ryan Van Zeeland, Levi Stanley, and Wenyu Huang

**Abstract**

The first example detailing the impact of systematic variation of the stereoelectronic properties of ancillary ligands on organometallic catalysis in MOFs is described. A series of mixed-linker bipyridyl MOF-supported palladium (II) catalysts was used to elucidate the electronic and steric effects of linker substitution on the activity of these catalysts in the context of Suzuki–Miyaura cross-coupling reactions. *m*-6,6′-Me<sub>2</sub>bpy-MOF-PdCl<sub>2</sub> exhibited a 110-fold and 496-fold enhancement in the activity compared to non-functionalized *m*-bpy-MOF-PdCl<sub>2</sub> and *m*-4,4′-Me<sub>2</sub>bpy-MOF-PdCl<sub>2</sub>. This result clearly demonstrates that the stereoelectronic properties of metal-binding linker units are critical to the activity of single-site organometallic catalysts in MOFs and highlights the importance of linker engineering in the design and development of efficient MOF catalysts. Control experiments show that the reactions proceed through cross-coupling of the organic electrophile and organometallic nucleophile without homocoupling of either reaction partner. In addition, a hot filtration test and ICP-MS analysis of supernatant solution show that there was no leaching of active Pd species

during the reaction, and the catalyst, m-6,6'-Me<sub>2</sub>bpy-MOF-PdCl<sub>2</sub>, can be reused without deactivation.



## Introduction

In palladium-catalysed cross-coupling reactions, the steric and electronic properties of ancillary ligands bound to the metal center significantly impact the catalytic properties of palladium complexes.<sup>1</sup> Previous studies detail how the steric and electronic properties of phosphine,<sup>2</sup> *N*-heterocyclic carbene,<sup>3,4</sup> and Schiff base<sup>5</sup> ligands impact palladium-catalysed Suzuki-Miyaura reactions. However, these studies are primarily limited to homogeneous catalyst systems, and analogous studies on heterogeneous palladium catalysts have rarely been reported.<sup>6</sup> The lack of systematic studies on the impact of ancillary ligands on heterogeneous palladium catalysts likely results from a lack of catalyst supports that enable facile tuning of ligand structures at the atomic level.

MOFs have recently gained attention due to their high surface area and porosity, structural tunability, as well as applications in diverse areas.<sup>7-13</sup> Of particular importance to our studies, MOFs have been established as a versatile platform for the

immobilization of homogeneous organometallic catalysts. These catalytic entities are attractive because they integrate the benefits of the well-defined stereoelectronic properties of homogeneous organometallic catalysts with the uniform active sites and recyclability of MOFs. Recent studies have greatly expanded the types of organometallic transformations catalyzed by metalated bipyridyl-MOFs.<sup>14-20</sup> However, there remains minimal understanding of how the steric and electronic properties of the bipyridyl linker unit impact the properties of these heterogeneous catalysts.

In comparison to conventional porous supports, MOFs feature the advantages of adjustable pore structures and broad synthetic diversity accessible through an array of structural building units. In addition, MOFs are well suited to establishing clear structure-function relationships through rational functionalization of linkers in isorecticular MOFs.<sup>21-25</sup> Recent studies have investigated how the identity of linker units in MOFs impacts heterogeneous catalysis.<sup>26-30</sup> The steric and electronic properties of ancillary ligands are crucial to improving activity in cross-coupling reactions promoted by homogeneous palladium complexes.<sup>31,32</sup> We envisioned that anchoring homogeneous palladium catalysts in MOFs may allow the heterogeneous catalytic behavior to be fine-tuned in a similar fashion to ligand modification in homogeneous catalyst systems. To the best of our knowledge, studies to elucidate the effects of metal-binding linker units in MOFs on palladium-catalyzed Suzuki-Miyaura cross-coupling have not been reported.

Herein we report the immobilization of palladium chloride within a series of bipyridyl-MOFs (m-bpy-MOF-PdCl<sub>2</sub>, m-6,6'-Me<sub>2</sub>bpy-MOF-PdCl<sub>2</sub> and m-4,4'-Me<sub>2</sub>bpy-MOF-PdCl<sub>2</sub>) synthesized via a mixed-linker approach to afford

heterogeneous catalysts for Suzuki-Miyaura cross-coupling reactions (Figure 1). Mixed-linker MOFs (m-MOFs) hold multiple advantages. They possess high surface areas and stability. The bipyridine sites are capable of coordinating palladium complexes,<sup>33-36</sup> and the linkers without bipyridine sites facilitate the separation of the active palladium centers in MOFs, preventing deactivation by dimerization of the palladium catalysts.<sup>14,37</sup> These metalated isorecticular MOFs are crystalline, porous and robust. Importantly, m-6,6'-Me<sub>2</sub>bpy-MOF-PdCl<sub>2</sub> exhibited a 110-fold and 496-fold enhancement in the catalytic activity in Suzuki-Miyaura cross-coupling reactions of iodobenzene compared to m-bpy-MOF-PdCl<sub>2</sub> and m-4,4'-Me<sub>2</sub>bpy-MOF-PdCl<sub>2</sub>. m-6,6'-Me<sub>2</sub>bpy-MOF-PdCl<sub>2</sub> also exhibited the highest activity and remarkable enhancement in activity for the Suzuki-Miyaura reactions of bromobenzene. This work constitutes the first example detailing the systematic study of the stereoelectronic properties of ancillary ligands on organometallic catalysis in MOFs.

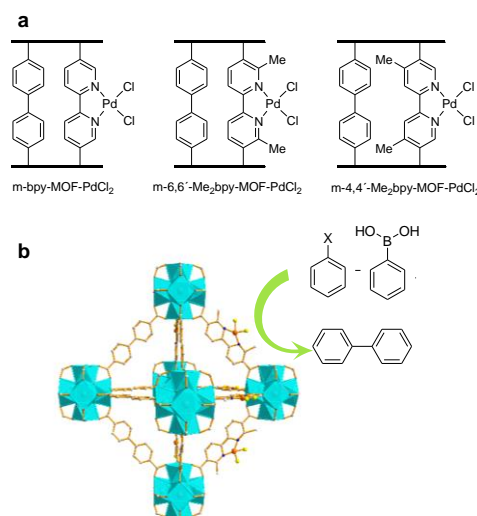


**Figure 1.** (a) Schematic structures of m-MOF-PdCl<sub>2</sub> precatalysts. (b) Idealized structure of m-6,6'-Me<sub>2</sub>bpy-MOF-PdCl<sub>2</sub> as a precatalyst for the model Suzuki-Miyaura cross-coupling reaction.

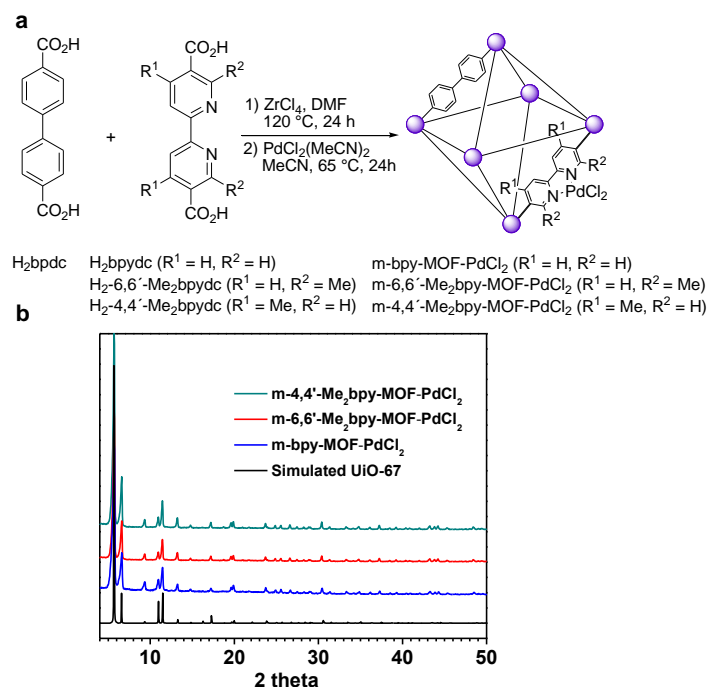


## Results and Discussion

At the outset of our studies, we synthesized a series of 2,2'-bipyridine-5,5'-dicarboxylic acid derivatives. 2,2'-bipyridine-5,5'-dicarboxylic acid ( $H_2bdydc$ ) was prepared according to a literature procedure.<sup>38</sup> The novel 6,6'-dimethyl-[2,2'-bipyridine]-5,5'-dicarboxylic acid ( $H_2-6,6'-Me_2bpydc$ ) and 4,4'-dimethyl-[2,2'-bipyridine]-5,5'-dicarboxylic acid ( $H_2-4,4'-Me_2bpydc$ ) derivatives were prepared by a sequence involving nickel-catalyzed reductive homocoupling of ethyl 6-chloro-2-methylnicotinate and methyl 6-chloro-4-methylnicotinate,<sup>39</sup> respectively, and subsequent hydrolysis of the resulting diesters. Using this series of bipyridyl linkers, we prepared mixed-linker MOFs (m-bpy-MOF, m-6,6'- $Me_2bpy$ -MOF, and m-4,4'- $Me_2bpy$ -MOF) from equimolar amounts of the bipyridyl and biphenyl linkers (Figure 2a).<sup>16</sup> PXRD patterns of the MOFs are in good agreement with simulated patterns for UiO-67, indicating that these MOFs have isorecticular crystalline structures. Linker ratios were quantified by  $^1H$  NMR spectroscopy upon digestion of the MOF with HF in  $d_6$ -DMSO. m-bpy-MOF, m-6,6'- $Me_2bpy$ -MOF, and m-4,4'- $Me_2bpy$ -MOF contained 50%, 40%, and 40% of the bipyridyl linkers, respectively.

The m-MOF- $PdCl_2$  precatalysts were synthesized by postsynthetic metalation of the mixed-linker MOFs with  $PdCl_2(CH_3CN)_2$  in acetonitrile. PXRD analyses of the metalated MOFs show that the m-MOF- $PdCl_2$  complexes remain crystalline during the post-synthetic metalation (Figure 2b). We determined the loading of palladium in the metalated MOFs by ICP-MS. The palladium loadings are 2.8 wt.% for m-bpy-MOF- $PdCl_2$ , 2.9 wt.% for m-6,6'- $Me_2bpy$ -MOF- $PdCl_2$ , and 3.0 wt.% for m-4,4'- $Me_2bpy$ -MOF- $PdCl_2$ . These loadings are consistent with palladium coordination to

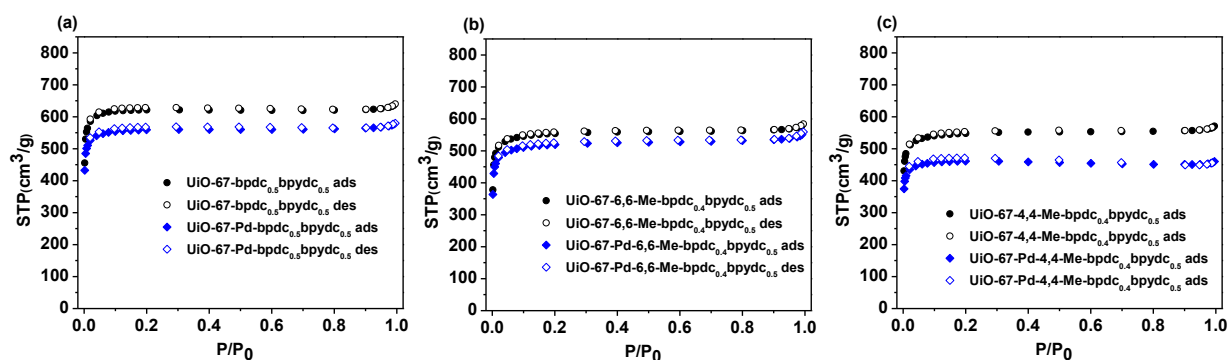
19.3%, 25.8% and 26.7% of the total bipyridine sites in m-bpy-MOF-PdCl<sub>2</sub>, m-6,6'-Me<sub>2</sub>bpy-MOF-PdCl<sub>2</sub>, and m-4,4'-Me<sub>2</sub>bpy-MOF-PdCl<sub>2</sub>.



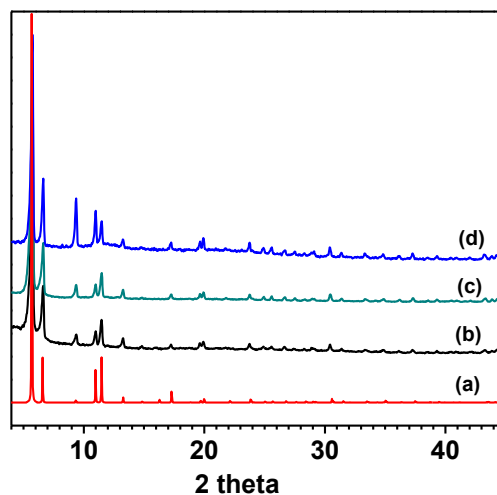
**Figure 2.** (a) Hydrothermal synthesis of m-MOFs; (b) PXRD of simulated UiO-67 and m-MOFs-PdCl<sub>2</sub>.

N<sub>2</sub> adsorption-desorption isotherm profiles of mixed-linker MOFs and m-MOF-PdCl<sub>2</sub> complexes all exhibit a type I curve, which is characteristic of microporous materials (Figure 3). The BET surface area and micropore volume of m-bpy-MOF are calculated to be 2600 m<sup>2</sup> g<sup>-1</sup> and 0.91 cm<sup>3</sup> g<sup>-1</sup>, which are in close agreement with reported values.<sup>16</sup> The introduction of methyl groups at the 4,4' or 6,6' positions of the bipyridyl linker leads to a decrease in the BET surface areas of the corresponding mixed-linker MOFs. The surface areas of m-6,6'-Me<sub>2</sub>bpy-MOF and m-4,4'-Me<sub>2</sub>bpy-MOF are 2300 m<sup>2</sup> g<sup>-1</sup> and 2200 m<sup>2</sup> g<sup>-1</sup>. The BET surfaces areas of m-

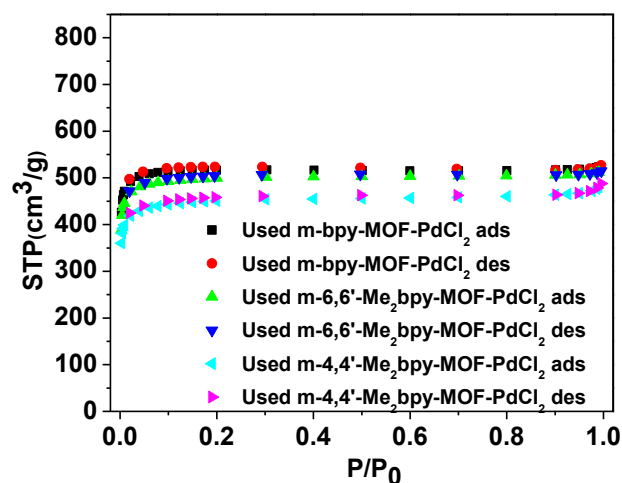
bpy-MOF-PdCl<sub>2</sub>, m-6,6'-Me<sub>2</sub>bpy-MOF-PdCl<sub>2</sub>, and m-4,4'-Me<sub>2</sub>bpy-MOF-PdCl<sub>2</sub> decrease to 2300 m<sup>2</sup> g<sup>-1</sup>, 2100 m<sup>2</sup> g<sup>-1</sup>, and 1900 m<sup>2</sup> g<sup>-1</sup>, primarily due to incorporation of PdCl<sub>2</sub> into the cages of the MOFs.



**Figure 3.** Nitrogen sorption isotherms of (a) m-bpy-MOF and 2.8 wt.% m-bpy-MOF-PdCl<sub>2</sub>; (b) m-6,6'-Me<sub>2</sub>bpy-MOF, and 2.9 wt.% m-6,6'-Me<sub>2</sub>bpy-MOF-PdCl<sub>2</sub>; (c) m-4,4'-Me<sub>2</sub>bpy-MOF, and 3.0 wt.% m-4,4'-Me<sub>2</sub>bpy-MOF-PdCl<sub>2</sub>

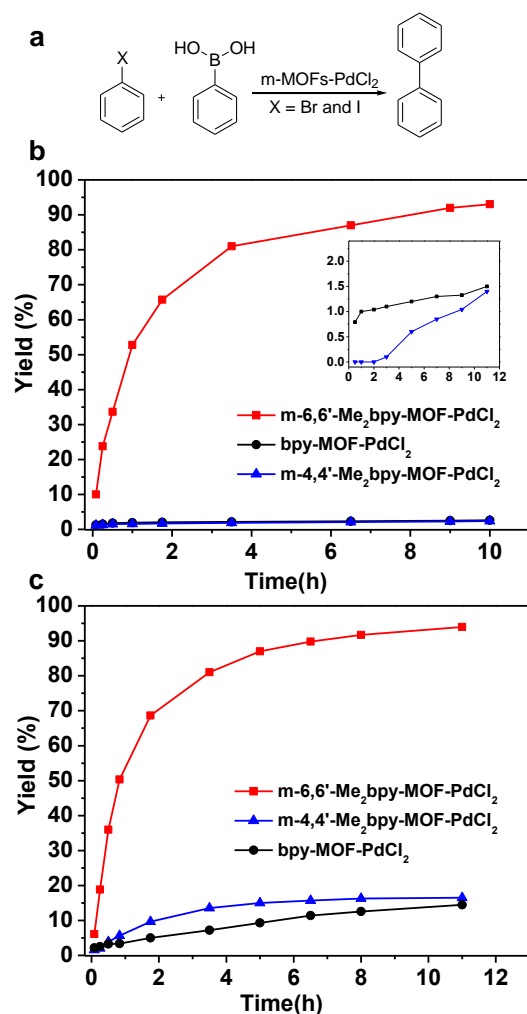


**Figure 4.** PXRD patterns of (a) simulated UiO-67; (b) used m-bpy-MOF-PdCl<sub>2</sub>; (c) used m-6,6'-Me<sub>2</sub>bpy-MOF-PdCl<sub>2</sub>; (d) used m-4,4'-Me<sub>2</sub>bpy-MOF-PdCl<sub>2</sub> after one cycle of catalysis.



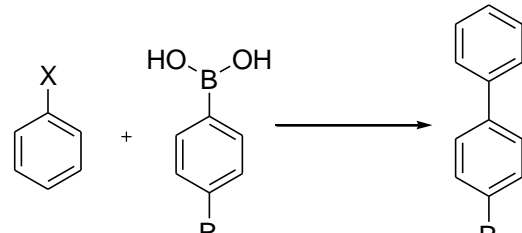
**Figure 5.** Nitrogen sorption isotherms of used m-MOFs-PdCl<sub>2</sub> after one cycle of catalysis.

We chose the coupling of iodobenzene with phenylboronic acid as a model reaction to evaluate the effect of linker substitution in Suzuki-Miyaura reactions catalyzed by m-MOFs-PdCl<sub>2</sub> (Figure 6). During our initial identification of reaction conditions, a range of common solvent and base combinations for Suzuki-Miyaura reactions, including DMF/H<sub>2</sub>O (1:1), toluene/H<sub>2</sub>O (9:1), EtOH, EtOH/H<sub>2</sub>O (1:1) with either potassium carbonate or potassium fluoride as the base, were evaluated. However, the metalated MOFs collapsed within 4 hours in the presence of these polar, protic reaction media. Decomposition of the metalated MOFs is not observed when the model coupling reaction is run in toluene with K<sub>2</sub>CO<sub>3</sub> as the base. The PXRD and N<sub>2</sub> sorption analyses (Figure 4 and 5) of the recovered catalysts showed that the crystalline integrity and high surface area of the bpy-UiO MOFs was retained after the catalysis, indicating the robust nature of the palladium-doped MOF catalysts.



**Figure 6.** (a) Suzuki-Miyaura cross-coupling reaction catalyzed by m-MOF-PdCl<sub>2</sub>; (b) Catalytic difference of m-MOF-PdCl<sub>2</sub> in coupling reaction of iodobenzene. The inset shows the reaction yield by m-bpy-MOF-PdCl<sub>2</sub> and m-4,4'-Me<sub>2</sub>bpy-MOF-PdCl<sub>2</sub>; (c) Catalytic difference of m-MOF-PdCl<sub>2</sub> in coupling reaction of bromobenzene. Reaction conditions: Aryl halide (0.1 mmol), phenylboronic acid (0.15 mmol), K<sub>2</sub>CO<sub>3</sub> (0.2 mmol), Toluene (0.5 mL), m-MOF-PdCl<sub>2</sub> (1.0 mol% Pd), Ar atmosphere, 85 °C.

**Table 1.** Suzuki-Miyaura cross-coupling reactions.<sup>a</sup>

							
Entry	Catalysts	X	R	Pd	Time (h)	Conv. (%)	Sel. (%)
1	m-6,6'-Me <sub>2</sub> bpy-MOF	I	H	/	12	/	/
2	m-6,6'-Me <sub>2</sub> bpy-MOF-PdCl <sub>2</sub>	I	Me	1.0 mol%	12	95%	99%
3	m-6,6'-Me <sub>2</sub> bpy-MOF-PdCl <sub>2</sub>	I	H	1.0 mol%	12	99%	99%
4	m-6,6'-Me <sub>2</sub> bpy-MOF-PdCl <sub>2</sub>	I	H	2.5 mol%	8	99%	99%
5	m-6,6'-Me <sub>2</sub> bpy-MOF-PdCl <sub>2</sub>	I	H	5.0 mol%	6	99%	99%

<sup>a</sup> Reaction conditions: iodobenzene (0.1 mmol), phenylboronic acid (0.15 mmol), K<sub>2</sub>CO<sub>3</sub> (0.20 mmol), toluene (0.5 mL), Ar atmosphere, 85 °C.

m-bpy-MOF-PdCl<sub>2</sub>, m-4,4'-Me<sub>2</sub>bpy-MOF-PdCl<sub>2</sub>, and m-6,6'-Me<sub>2</sub>bpy-MOF-PdCl<sub>2</sub> exhibit dramatic differences in their catalytic activity in the model coupling reaction (Figure 6b). Assuming pseudo-first-order kinetics, we calculated the rate constants for the coupling reaction over m-bpy-MOF-PdCl<sub>2</sub>, m-4,4'-Me<sub>2</sub>bpy-MOF-PdCl<sub>2</sub> and m-6,6'-Me<sub>2</sub>bpy-MOF-PdCl<sub>2</sub> to be 0.24 min<sup>-1</sup>, 0.05 min<sup>-1</sup> and 26.3 min<sup>-1</sup>, respectively. The m-6,6'-Me<sub>2</sub>bpy-MOF-PdCl<sub>2</sub> exhibited a remarkable 110-fold and 496-fold enhancement in the activity compared to non-functionalized m-bpy-MOF-PdCl<sub>2</sub> and m-4,4'-Me<sub>2</sub>bpy-MOF-PdCl<sub>2</sub>. In addition, m-6,6'-Me<sub>2</sub>bpy-MOF-PdCl<sub>2</sub> exhibited superior activity in comparison to Pd/carbon (Figure 7). m-6,6'-Me<sub>2</sub>bpy-MOF-PdCl<sub>2</sub> showed much higher activity than bpy-MOF-PdCl<sub>2</sub> and m-4,4'-Me<sub>2</sub>bpy-MOF-PdCl<sub>2</sub> regardless of the Pd loading. Among m-6,6'-Me<sub>2</sub>bpy-MOF-PdCl<sub>2</sub>

catalysts with different Pd loading, m-6,6'-Me<sub>2</sub>bpy-MOF-PdCl<sub>2</sub> with 2.9 wt.% and 5.0 wt.% Pd loading showed similar catalytic activities while m-6,6'-Me<sub>2</sub>bpy-MOF-PdCl<sub>2</sub> with 1.0 wt.% Pd loading showed slightly inferior activity for Suzuki-Miyaura cross-coupling reaction when the same amount of Pd (1.0 mol % to substrate) was used in the coupling reaction (Figure 8). The model coupling reaction of iodobenzene with phenylboronic acid in the presence of m-6,6'-Me<sub>2</sub>bpy-MOF-PdCl<sub>2</sub> (1 mol % palladium relative to iodobenzene) forms biphenyl in 99% yield in 12 h. The m-MOFs without palladium were catalytically inactive, consistent with ligated palladium centers as the active sites for the Suzuki-Miyaura coupling reaction (Table 1, entry 1).

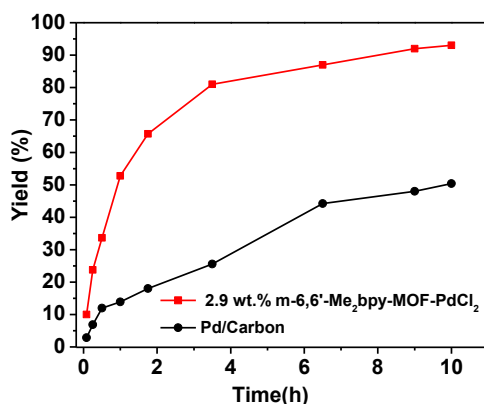


**Figure 7.** Comparison of 5% Pd/carbon with 2.9 wt.% m-6,6'-Me<sub>2</sub>bpy-MOF-PdCl<sub>2</sub> in Suzuki-Miyaura cross-coupling reaction.

It is reported that biphenyl could be synthesized from palladium-catalyzed homocoupling of aryl halides,<sup>40</sup> or arylboronic acids.<sup>41</sup> To verify the origin of biphenyl product, we conducted the Suzuki-Miyaura coupling reaction of iodobenzene and 4-methylphenylboronic acid with m-6,6'-Me<sub>2</sub>bpy-MOF-PdCl<sub>2</sub> under

standard reaction conditions and obtained 4-methyl-1,1'-biphenyl as only product (Table 1, entry 2). This result clearly shows that biaryl coupling products are not formed through homocoupling of either the arylboronic acid or the iodoarene coupling partners.

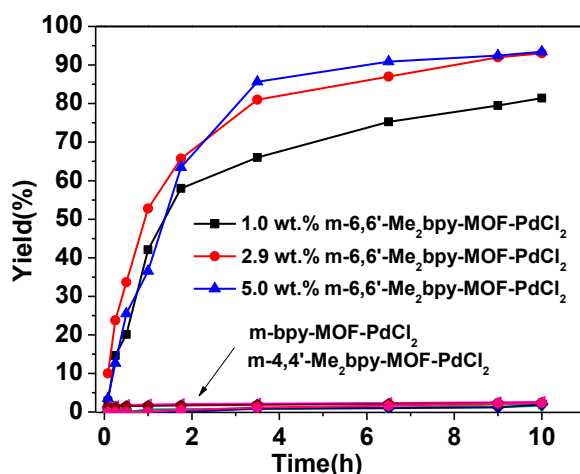


**Figure 8.** Effect of Pd loading on the catalytic performance of m-bpy-MOF-PdCl<sub>2</sub> in Suzuki-Miyaura cross-coupling reaction. Reaction conditions: iodobenzene (0.1 mmol), phenylboronic acid (0.15 mmol), K<sub>2</sub>CO<sub>3</sub> (0.2 mmol), toluene (0.5 mL), Pd/substrate = 1/100, Ar atmosphere, 85 °C.

The difference in activity between the metalated mixed-linker MOFs led us to investigate the coupling of bromobenzene with phenylboronic acid in the presence of these catalysts (Figure 6c). As expected, m-6,6'-Me<sub>2</sub>bpy-MOF-PdCl<sub>2</sub> displayed the highest activity among the three m-MOF-PdCl<sub>2</sub> catalysts and leads to the formation of biphenyl in 92% yield. However, m-bpy-MOF-PdCl<sub>2</sub> and m-4,4'-Me<sub>2</sub>bpy-MOF-PdCl<sub>2</sub> showed enhanced catalytic activity in coupling of bromobenzene relative to



iodobenzene. For example, the reaction of bromobenzene catalyzed by m-4,4'-Me<sub>2</sub>bpy-MOF-PdCl<sub>2</sub> forms biphenyl in 17% yield, while the reaction of iodobenzene under otherwise identical reaction conditions forms biphenyl in 3% yield. The low yields of the biaryl product in coupling reactions of iodobenzene catalysed by m-bpy-MOF-PdCl<sub>2</sub> and m-4,4'-Me<sub>2</sub>bpy-MOF-PdCl<sub>2</sub> prompted us to evaluate the potential for a deactivation pathway that is operative with iodobenzene as the electrophile, but not with bromobenzene. We ran the Suzuki-Miyaura coupling reaction of bromobenzene in the presence of iodobenzene (1 equiv.) over m-bpy-MOF-PdCl<sub>2</sub> and m-4,4'-Me<sub>2</sub>bpy-MOF-PdCl<sub>2</sub>. We found the yield of the biaryl product decreased from ca.17% to 2%, indicating that catalysts derived from m-bpy-MOF-PdCl<sub>2</sub> and m-4,4'-Me<sub>2</sub>bpy-MOF-PdCl<sub>2</sub> may be deactivated in couplings of iodobenzene. However, such deactivation was not observed in reactions catalysed by m-6,6'-Me<sub>2</sub>bpy-MOF-PdCl<sub>2</sub>, demonstrating the importance of linker engineering in the design of transition metal-functionalized MOF catalysts. On the basis of these results, we hypothesize that the identity of the linker plays a key role in preventing catalyst deactivation that requires further studies to elucidate.

Given the fact that the most active m-6,6'-Me<sub>2</sub>bpy-MOF-PdCl<sub>2</sub> did not possess either the highest BET surface area or pore volume and all m-MOF-PdCl<sub>2</sub> catalysts exhibited similar pore size distributions (Figure 9), mass transfer/diffusion should not account for the activity difference. Compared to non-functionalized m-bpy-MOF-PdCl<sub>2</sub>, m-6,6'-Me<sub>2</sub>bpy-MOF-PdCl<sub>2</sub> contains a relatively hindered and electron-rich metal center and is a more active catalyst. We found the activity of m-4,4'-Me<sub>2</sub>bpy-MOF-PdCl<sub>2</sub> to be similar to m-bpy-MOF-PdCl<sub>2</sub> in coupling reactions of both

iodobenzene and bromobenzene (Figure 6b and 6c), suggesting the electronic character of the new linker units has minimal impact on the activity of the metalated MOF catalysts. Our data is consistent with reductive elimination, which is favored at sterically congested metal centers, as the turnover-limiting step of the catalytic cycle for this Suzuki-Miyaura coupling reaction.<sup>3</sup>

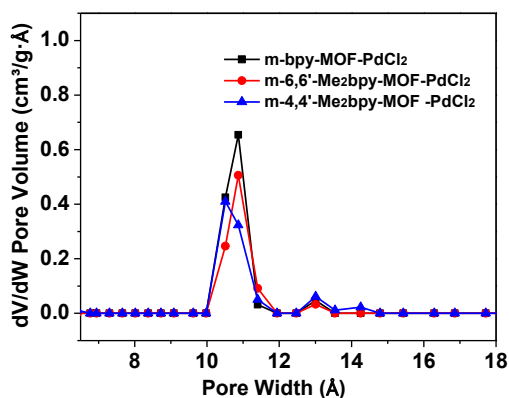


**Figure 9.** Pore size distributions of m-bpy-MOFs-PdCl<sub>2</sub> (NLDFT method).

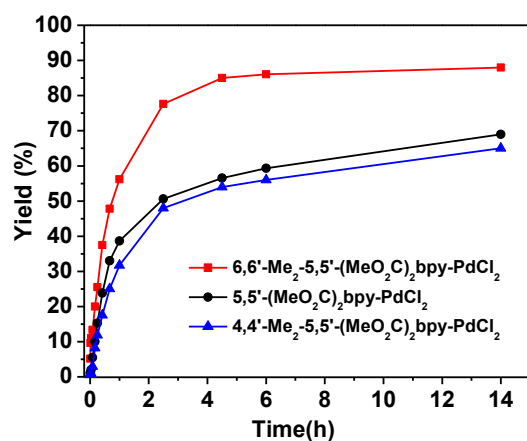


**Figure 10.** Suzuki-Miyaura cross-coupling reaction catalyzed by homogeneous counterparts. Reaction conditions: iodobenzene (0.1 mmol), phenylboronic acid (0.15 mmol), K<sub>2</sub>CO<sub>3</sub> (0.2 mmol), toluene (0.5 mL), Pd/substrate = 1/100, Ar atmosphere, 85 °C.

We utilized the homogeneous counterparts (denoted as 5,5'-(MeO<sub>2</sub>C)<sub>2</sub>bpy-PdCl<sub>2</sub>, 4,4'-Me<sub>2</sub>-5,5'-(MeO<sub>2</sub>C)<sub>2</sub>bpy-PdCl<sub>2</sub>, and 6,6'-Me<sub>2</sub>-5,5'-(MeO<sub>2</sub>C)<sub>2</sub>bpy-PdCl<sub>2</sub>) as control catalysts for Suzuki-Miyaura reaction. As shown in Figure 10, the homogeneous analog catalysts displayed higher activity. Moreover, the initial slopes indicate that the activity of 6,6'-Me<sub>2</sub>-5,5'-(MeO<sub>2</sub>C)<sub>2</sub>bpy-PdCl<sub>2</sub> is higher than the activities of 5,5'-(MeO<sub>2</sub>C)<sub>2</sub>bpy-PdCl<sub>2</sub> and 4,4'-Me<sub>2</sub>-5,5'-(MeO<sub>2</sub>C)<sub>2</sub>bpy-PdCl<sub>2</sub>. These results are consistent with the relative rates observed for the heterogeneous MOF catalysts, but the rate differences in these homogeneous catalysts are much less.

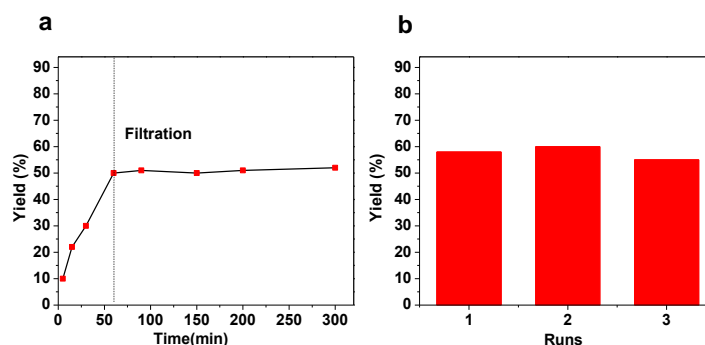


**Figure 11.** Filtration and recycle test of m-6,6'-Me<sub>2</sub>bpy-MOF-PdCl<sub>2</sub> in the Suzuki-Miyaura cross-coupling reaction. Reaction conditions: iodobenzene (0.1 mmol), phenylboronic acid (0.15 mmol), K<sub>2</sub>CO<sub>3</sub> (0.2 mmol), toluene (0.5 mL), m-6,6'-Me<sub>2</sub>bpy-MOF-PdCl<sub>2</sub> (1.0 mol% Pd), Ar atmosphere, 85 °C for 1.5 hours.

Since the Suzuki-Miyaura cross-coupling reactions could proceed with a trace amount of a soluble palladium species,<sup>42</sup> it is important to verify that palladium does not leach from the MOF during catalysis. The heterogeneity of the most active catalyst, m-6,6'-Me<sub>2</sub>bpy-MOF-PdCl<sub>2</sub>, was assessed by a hot filtration test. We did not observe a further increase in the yield of biphenyl upon the removal of the solid

catalyst at 50% conversion (Figure 11a). Moreover, the palladium content in the reaction solution was determined by ICP-MS, and <0.1% of added Pd was detected. These results suggest that the Suzuki-Miyaura cross-coupling reaction in the presence of m-6,6'-Me<sub>2</sub>bpy-MOF-PdCl<sub>2</sub> is indeed catalyzed by heterogeneous palladium species. To probe deactivation of the catalyst under our reaction conditions, we evaluated the reusability of the m-6,6'-Me<sub>2</sub>bpy-MOF-PdCl<sub>2</sub> in coupling reactions run to approximately 60% conversion.<sup>43</sup> The m-6,6'-Me<sub>2</sub>bpy-MOF-PdCl<sub>2</sub> catalyst can be used at least three times without significant decrease in the yield of biphenyl (Figure 11b).

## Conclusion

We have developed a series of functionalized mixed-linker bipyridyl MOF-supported palladium catalysts. We have demonstrated for the first time that simple and systematic modifications to the stereoelectronic properties of linker units in MOFs can significantly impact the activity of metalated MOF catalysts in important organometallic cross-coupling reactions. m-6,6'-Me<sub>2</sub>bpy-MOF-PdCl<sub>2</sub> exhibits dramatically enhanced activity compared to m-bpy-MOF-PdCl<sub>2</sub> and m-4,4'-Me<sub>2</sub>bpy-MOF-PdCl<sub>2</sub> in model Suzuki-Miyaura cross-coupling reactions due to the steric properties at the bpy-palladium sites. m-6,6'-Me<sub>2</sub>bpy-MOF-PdCl<sub>2</sub> is also more robust and prevents deactivation pathways observed when m-bpy-MOF-PdCl<sub>2</sub> and m-4,4'-Me<sub>2</sub>bpy-MOF-PdCl<sub>2</sub> are used as catalysts of Suzuki-Miyaura cross-coupling reactions of iodobenzene. Control experiments confirm that these reactions proceed through cross-coupling of the haloarene and arylboronic acid reactions without homocoupling

of either reaction partner. We showed that the m-6,6'-Me<sub>2</sub>bpy-MOF-PdCl<sub>2</sub> is a heterogeneous catalyst of the Suzuki-Miyaura cross-coupling reaction via a hot filtration test and ICP-MS analysis of supernatant solution, and the catalyst can be used three times without obvious deactivation. The present work demonstrates the first systematic example of linker engineering of metalated units in bipyridyl MOFs and highlights the importance of linker design for immobilization of homogeneous catalysts in MOFs. This strategy for linker engineering of metalated units in bipyridyl MOFs for application to additional catalytic organometallic reactions holds great promise and such studies are currently underway in our laboratories.

## **Experimental Section**

### **Synthesis of 2,2'-bipyridine-5,5'-dicarboxylic acid derivatives.**

#### **General Experimental Details**

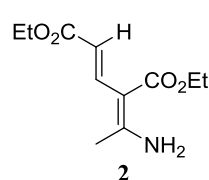
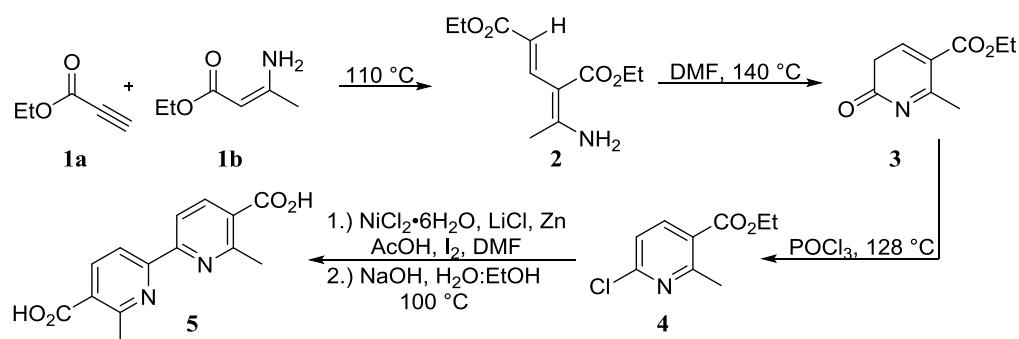
All reactions were performed under air unless otherwise noted. Reactions involving air-sensitive reagents were conducted under inert atmosphere in a nitrogen-filled dry box or by standard Schlenk techniques. Glassware for moisture sensitive reactions was dried at 140 °C in an oven for at least one hour prior to use. Flash column chromatography was performed on Siliflash® P60 silica gel (230-400 mesh) using hexane/ethyl acetate or dichloromethane/methanol mixtures as the eluent. Products were visualized on TLC by UV light. NMR spectra were acquired on Varian MR-400 and Bruker Advance III 600 spectrometers at the Iowa State Chemical Instrumentation Facility. Chemical shifts are reported relative to a residual solvent

peak ( $\text{CDCl}_3 = 7.26$  ppm for  $^1\text{H}$ , and  $77.10$  ppm for  $^{13}\text{C}$ ,  $\text{DMSO} = 2.50$  ppm for  $^1\text{H}$  and  $39.5$  ppm for  $^{13}\text{C}$ ). Coupling constants are reported in hertz.

## Materials

Ethyl-3-amino crotonate **1a**, dimethylformamide, phosphorous oxychloride, nickel (II) chloride hexahydrate, zinc dust, copper (I) cyanide, thionyl chloride, and anhydrous methanol were purchased from Sigma-Aldrich and used without further purification. Ethyl propiolate **1b** and 5-bromo-4-methylpyridin-2-amine **6** were purchased from AK Scientific and used without further purification. Lithium chloride, acetic acid, sodium hydroxide, potassium permanganate and sodium nitrite were purchased from Fisher Scientific and used without further purification. 5,5'-dimethyl-2,2'-bipyridine was purchased from Alfa Aesar and used without further purification.

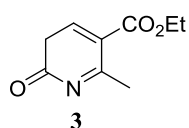
## Synthesis of New Organic Linkers for UiO-bpy MOFs



### Diethyl (2E,4Z)-4-(1-aminoethylidene)pent-2-enedioate (**2**)

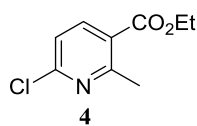
Compound **2** was prepared according a modified literature procedure.<sup>44</sup> To a 250 mL round-bottom flask was added ethyl-3-

amino crotonate **1a** (15.6 g, 120 mmol, 1.00 equiv.) and ethyl propiolate **1b** (12.2 mL, 120 mmol, 1.00 equiv.). This mixture was heated at 108 °C for 4 hours under N<sub>2</sub>. After cooling, the resulting solid was recrystallized from methanol to give diethyl (2*E*,4*Z*)-4-(1-aminoethylidene)pent-2-enedioate **2** (23.9 g, 105 mmol, 88% yield). Characterization data is consistent with a previous report.<sup>45</sup> <sup>1</sup>H NMR (400 MHz, CDCl<sub>3</sub>): δ 1.29 (t, *J* = 7.0 Hz, 3H), 1.36 (t, *J* = 7.0 Hz, 3H), 2.27 (s, 3H), 4.19 (q, *J* = 7.0 Hz, 2H), 4.26 (q, *J* = 7.0 Hz, 2H), 6.15 (d, *J* = 15.6 Hz, 1H), 7.65 (d, *J* = 15.6 Hz, 1H).



#### Ethyl-2-methyl-6-oxo-5,6-dihydropyridine-3-carboxylate (**3**)

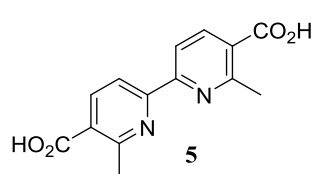
Compound **3** was prepared according a modified literature procedure.<sup>44</sup> A mixture of diethyl (2*E*,4*Z*)-4-(1-aminoethylidene)pent-2-enedioate **2** (23.0 g, 100.8 mmol, 1.00 equiv.) and DMF (114 mL) were heated to 140 °C for 14 hours under N<sub>2</sub>. After cooling, the resulting solid was collected by vacuum filtration, washed with ice cold ether (3x) and dried to give ethyl-2-methyl-6-oxo-5,6-dihydropyridine-3-carboxylate **3** (8.6 g, 47.5 mmol, 47% yield). <sup>1</sup>H NMR data is consistent with previous reports.<sup>1</sup> <sup>1</sup>H NMR (400 MHz, CDCl<sub>3</sub>): δ 1.35 (t, *J* = 7.0 Hz, 3H), 2.73 (s, 3H), 4.29 (q, *J* = 7.0 Hz, 2H), 6.40 (d, *J* = 9.6 Hz, 1H), 8.03 (d, *J* = 9.6 Hz, 1H) 13.28 (br s, 1H).



#### Ethyl-6-chloro-2-methylnicotinate (**4**)

Compound **4** was prepared according a modified literature procedure.<sup>44</sup> A mixture of ethyl-2-methyl-6-oxo-5,6-dihydropyridine-3-carboxylate **3**

(7.5 g, 41.4 mmol, 1.00 equiv.) and phosphorous oxychloride (18.0 mL, 193 mmol, 4.66 equiv.) was heated at 128 °C for 4 hours. The reaction was cooled to room temperature, then poured onto ice water, made basic with 8M NaOH and extracted three times with EtOAc (100 mL). The combined organics were washed with brine, dried over Na<sub>2</sub>SO<sub>4</sub>, and concentrated under reduce pressure to give ethyl-6-chloro-2-methylnicotinate **4** (7.41 g, 41.3 mmol, 99% yield). <sup>1</sup>H NMR data is consistent with previous reports.<sup>1</sup> <sup>1</sup>H NMR (400 MHz, CDCl<sub>3</sub>): δ 1.40 (t, *J* = 7.2 Hz, 3H), 2.82 (s, 3H), 4.38 (q, *J* = 7.2 Hz, 2H), 7.24 (d, *J* = 8.0 Hz, 1H), 8.16 (d, *J* = 8.0 Hz, 1H)



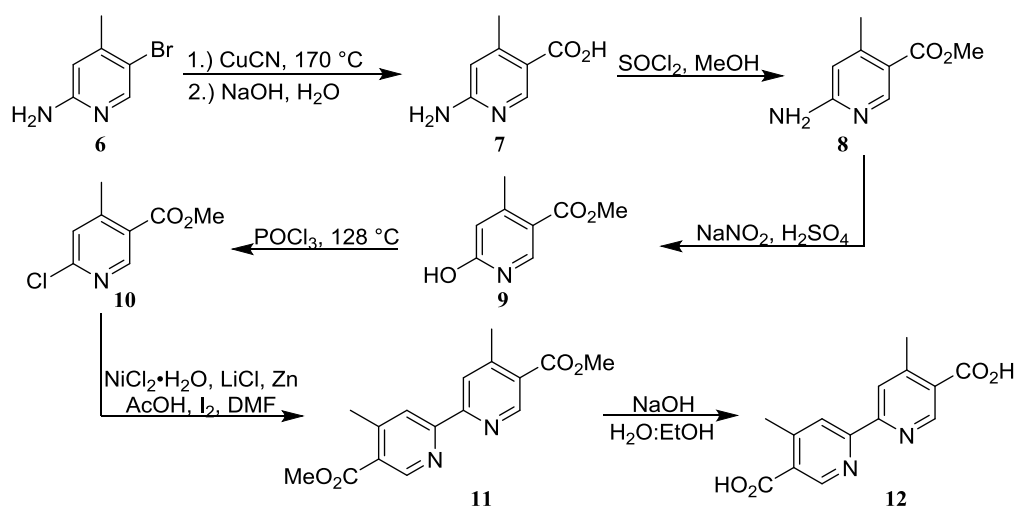
**6,6'-dimethyl-[2,2'-bipyridine]-5,5'-dicarboxylic acid**  
**(5)**

Compound **5** was prepared according a modified literature procedure.<sup>46</sup> A 250 mL round-bottom flask was charged with NiCl<sub>2</sub>·6H<sub>2</sub>O (0.475 g, 2.00 mmol, 0.100 equiv.) and DMF (120 mL). The resulting solution was stirred and heated to 40 °C, and ethyl-6-chloro-2-methylnicotinate **4** (3.60 g, 20.0 mmol, 1.00 equiv), anhydrous LiCl, (0.848 g, 20.0 mmol, 1.00 equiv.), and zinc dust (1.57 g, 24.0 mmol, 1.20 equiv.) were added. When the temperature rose to 50 °C, a grain of iodine crystal and two drops of acetic acid were added to the mixture. The mixture was stirred at 60 °C for 16 hours. The reaction was cooled to room temperature and 10% HCl added (25 mL), the resulting mixture was made basic with 25% aqueous ammonia and extracted with DCM. The organic layers were combined, washed with brine, dried over Na<sub>2</sub>SO<sub>4</sub>, and concentrated under reduced pressure. The crude material was purified by flash chromatography to give dimethyl 6,6'-dimethyl-[2,2'-bipyridine]-5,5'-dicarboxylate (2.13 g, 6.5 mmol, 65% yield). <sup>1</sup>H NMR data is

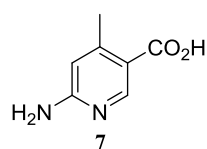


consistent with a previous report.<sup>47</sup> <sup>1</sup>H NMR (400 MHz, CDCl<sub>3</sub>): δ 1.32 (t, *J* = 7.2 Hz, 6H), 2.74 (s, 6H), 4.30 (q, *J* = 7.2 Hz, 4H), 7.16 (d, *J* = 8.4 Hz, 2H), 8.08 (d, *J* = 8.4 Hz, 2H).

To a round-bottom flask was added dimethyl 6,6'-dimethyl-[2,2'-bipyridine]-5,5'-dicarboxylate (2.0 g, 6.1 mmol, 1 equiv.), KOH (3.43 g, 61.0 mmol, 10.0 equiv.), water (70 mL) and EtOH (70 mL). The mixture was heated at 100 °C for 16 hours. The reaction was allowed to cool to room temperature and then made acidic with 1M HCl. The resultant precipitate was filtered and washed three times with ether (50 mL), and dried to give 6,6'-dimethyl-[2,2'-bipyridine]-5,5'-dicarboxylic acid **5** (1.61 g, 5.90 mmol, 98% yield). <sup>1</sup>H NMR data is consistent with a previous report.<sup>47</sup> <sup>1</sup>H NMR (400 MHz, *d*<sub>6</sub>-DMSO): δ 2.83 (s, 6H), 8.33-8.37 (m, 4H).



### 6-amino-4-methylnicotinic acid (**7**)

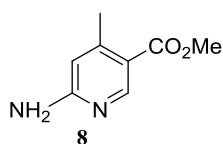


Prepared according to a literature procedure.<sup>48</sup> To a 250 mL round-bottom flask, copper(I) cyanide (28.8 g, 321 mmol, 3.00 equiv.)

was added to a solution of 5-bromo-4-methylpyridin-2-amine **6** (20.0 g, 107 mmol,

1.00 equiv.) in DMA 120 mL, and the reaction was stirred under N<sub>2</sub> at 170 °C for 14 hours. After cooling to room temperature, the reaction mixture was added to a solution of ethylenediamine (60 mL) and water (240 mL) and stirred for 15 minutes. The mixture was diluted with EtOAc, washed with water and brine, dried over Na<sub>2</sub>SO<sub>4</sub>, filtered and concentrated to give 6-amino-4-methylnicotinonitrile (11.0 g, 82.6 mmol, 77% yield). The crude product was used without further purification in the next step. <sup>1</sup>H NMR data is consistent with a previous report.<sup>5</sup> <sup>1</sup>H NMR (400 MHz, *d*<sub>6</sub>-DMSO): δ 2.37 (s, 3H), 6.25 (s, 1H), 6.59 (br s, 2H), 8.45 (s, 1H).

In a 500 mL round-bottom flask, 6-amino-4-methylnicotinonitrile (11.0 g, 82.6 mmol, 1.00 equiv) was suspended in a 4M aqueous NaOH solution. The reaction mixture was heated to 100 °C for 6 hours. The mixture was cooled to room temperature and made acidic with 6M HCl. The precipitate was filtered, washed with water and dried to give 6-amino-4-methylnicotinic acid **7** (11.5 g, 75.6 mmol, 91% yield). <sup>1</sup>H NMR data is consistent with a previous report.<sup>48</sup> <sup>1</sup>H NMR (400 MHz, *d*<sub>6</sub>-DMSO): δ 2.37 (s, 3H), 6.25 (s, 1H), 6.59 (br s, 2H), 8.45 (s, 1H).

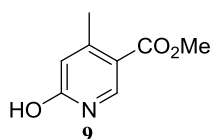


### Methyl 6-amino-4-methylnicotinate (**8**)

Prepared according to a literature procedure.<sup>44</sup> To a heterogeneous mixture of 6-amino-4-methylnicotinic acid **7** (12.7g, 83.5 mmol,

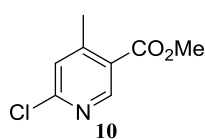
1.00 equiv.) in methanol (250 mL) was added thionyl chloride (7.6 mL, 104 mmol, 1.25 equiv.). The mixture was refluxed for 14 hours, cooled to room temperature, and the solvent was removed under reduced pressure. The resulting solid was dissolved in water and the pH adjusted to 13 with 1M aqueous NaOH. The resulting solid was

collected by vacuum filtration, washed with water and air dried to give methyl 6-amino-4-methylnicotinate **8** (9.20g, 55.4 mmol, 66% yield).  $^1\text{H}$  NMR data is consistent with previous reports.<sup>44</sup>  $^1\text{H}$  NMR (400 MHz,  $d_6$ -DMSO):  $\delta$  2.37 (s, 3H), 3.73 (s, 3H), 6.26 (s, 1H), 6.64 (br s, 2H), 8.45 (s, 1H).



#### Methyl 6-hydroxy-4-methylnicotinate (**9**)

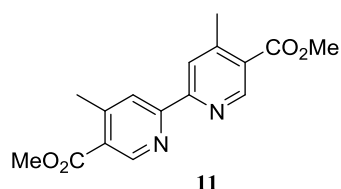
Prepared according to a literature procedure.<sup>44</sup> To ice cold 15% aqueous sulfuric acid (180 mL) was added methyl 6-amino-4-methylnicotinate **8** (9.20 g, 55.4 mmol, 1.00 equiv.) followed by portionwise addition of sodium nitrite (7.66 g, 111 mmol, 2.00 equiv.). The reaction mixture was stirred at 0 °C for 2 hours, and the resulting solid was collected by vacuum filtration, rinsed sequentially with water (100 mL) and diethyl ether (100 mL) and dried to give methyl 6-hydroxy-4-methylnicotinate **9** (5.21 g, 31.2 mmol, 56% yield).  $^1\text{H}$  NMR data is consistent with previous reports.<sup>1</sup>  $^1\text{H}$  NMR (400 MHz,  $d_6$ -DMSO):  $\delta$  2.35 (s, 3H), 3.73 (s, 3H), 6.21 (s, 1H), 8.00 (s, 1H).



#### Methyl 6-chloro-4-methylnicotinate (**10**)

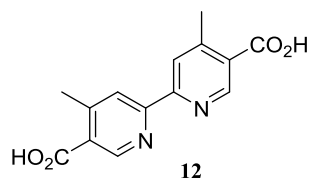
Prepared according to a literature procedure.<sup>44</sup> To a suspension of methyl 6-hydroxy-4-methylnicotinate **9** (5.1 g, 30.5 mmol, 1.00 equiv.) was added phosphorous oxychloride (20 mL). The mixture was heated at 128 °C for 4 hours, cooled to room temperature and poured onto ice water. The mixture was neutralized with aqueous 3M NaOH, extracted with dichloromethane, washed with brine, dried over  $\text{Na}_2\text{SO}_4$ , and concentrated under reduced pressure to give methyl 6-chloro-4-methylnicotinate **10** (4.47 g, 24.1 mmol, 79% yield).  $^1\text{H}$  NMR data

is consistent with previous reports.<sup>44</sup> <sup>1</sup>H NMR (400 MHz, CDCl<sub>3</sub>): δ 2.61 (s, 3H), 3.93 (s, 3H), 7.24 (s, 1H), 8.86 (s, 1H).



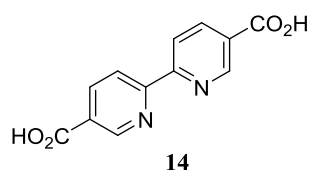
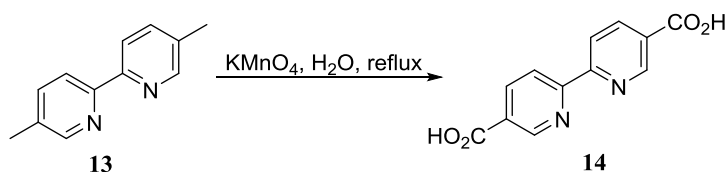
**Dimethyl 4,4'-dimethyl-[2,2'-bipyridine]-5,5'-dicarboxylate (11)**

Adapted from a literature procedure,<sup>46</sup> a 250 mL round-bottom flask was charged with NiCl<sub>2</sub>·6H<sub>2</sub>O (2.82 g, 11.9 mmol, 0.50 equiv.), and DMF (48 mL). The resulting solution was stirred and heated to 40 °C, and methyl-6-chloro-4-methylnicotinate **10** (4.40 g, 23.7 mmol, 1.00 equiv.), anhydrous LiCl, (1.00 g, 23.7 mmol, 1.00 equiv.), and zinc dust (3.88 g, 59.3 mmol, 2.50 equiv.) were added. When the temperature rose to 50 °C, a grain of iodine crystal and two drops of acetic acid were added to the mixture. The mixture was stirred at 60 °C for 16 hours. The reaction was cooled to room temperature and 10% HCl added (25 mL), the resulting mixture was made alkaline with 25% aqueous ammonia and extracted with DCM. The organic layers were combined, washed with brine, dried over Na<sub>2</sub>SO<sub>4</sub>, and concentrated under reduced pressure. The crude material was purified by flash chromatography to give dimethyl 4,4'-dimethyl-[2,2'-bipyridine]-5,5'-dicarboxylate **11** (1.05 g, 3.5 mmol, 30% yield). <sup>1</sup>H NMR (400 MHz, CDCl<sub>3</sub>): δ 2.73 (s, 6H), 3.97 (s, 6H), 8.36 (s, 2H), 9.14 (s, 2H). <sup>13</sup>C NMR (150 MHz, CDCl<sub>3</sub>): δ 166.6, 157.2, 151.5, 150.8, 126.1, 124.4, 52.3, 21.6. HRMS (ESI) *m/z*: [M+H]<sup>+</sup> Calcd. for C<sub>16</sub>H<sub>17</sub>N<sub>2</sub>O<sub>4</sub><sup>+</sup> 301.1183; found: 301.1178.



**4,4'-dimethyl-[2,2'-bipyridine]-5,5'-dicarboxylic acid**  
**(12)**

To a round-bottom flask was added dimethyl 4,4'-dimethyl-[2,2'-bipyridine]-5,5'-dicarboxylate **11** (1.05 g, 3.50 mmol, 1 equiv.), NaOH (0.140 g, 35.0 mmol, 10.0 equiv.), water (6 mL) and EtOH (6 mL). The mixture was heated at 100 °C for 16 hours. The reaction was allowed to cool to room temperature and then made acidic with 1M HCl. The resultant precipitate was filtered and washed with 50 mL ether (3x), and dried to give 4,4'-dimethyl-[2,2'-bipyridine]-5,5'-dicarboxylic acid **12** (0.952 g, 3.5 mmol, 99% yield). <sup>1</sup>H NMR (400 MHz, DMSO): δ 2.66 (s, 6H), 8.37 (s, 2H), 9.04 (s, 2H), 13.4 (s, 2H). <sup>13</sup>C NMR (150 MHz, CDCl<sub>3</sub>): δ 167.0, 156.0, 150.8, 149.7, 126.9, 123.4, 20.8. HRMS (ESI) *m/z*: [M-H]<sup>-</sup> Calcd. for C<sub>14</sub>H<sub>11</sub>N<sub>2</sub>O<sub>4</sub><sup>-</sup> 271.0724; found: 271.0717.



**2,2'-bipyridine-5,5'-dicarboxylic acid (14)**

Prepared according to a literature procedure.<sup>49</sup> 5,5'-dimethyl-2,2'-bipyridine (5.75 g, 27.1 mmol, 1.00 equiv.) and potassium permanganate (29.2 g, 185 mmol, 6.80 equiv.) were added to 300 mL of water. The resulting mixture was heated to 100 °C with stirring for 18 hours. After the mixture cooled to room temperature, a brown precipitate was removed by filtration and the filtrate was extracted with 100 mL diethyl ether (3x). The resulting aqueous solution was acidified to pH = 2 with 1M HCl, which led to the formation of

a white precipitate. The precipitate was collected by vacuum filtration, washed with diethyl ether (100 mL) and dried to give 2,2'-bipyridine-5,5'-dicarboxylic acid **14** (4.03 g, 19.0 mmol, 70%).  $^1\text{H}$  NMR data is consistent with previous reports.<sup>6</sup>  $^1\text{H}$  NMR (600 MHz,  $d_6$ -DMSO):  $\delta$  8.45 (d,  $J = 8.4$  Hz, 2H), 8.57 (d,  $J = 8.4$  Hz, 2H), 9.20 (s, 2H).

**Synthesis of mixed-linker MOFs.** These m-MOFs were synthesized and purified according to a modified version of a reported procedure.<sup>50</sup> As a representative example,  $\text{ZrCl}_4$  (24.5 mg, 0.105 mmol, 98%, Acros Organics), glacial acetic acid (189 mg, 3.15 mmol), biphenyl-4,4'-dicarboxylic acid ( $\text{H}_2\text{bpdc}$ , 13.0 mg, 0.053 mmol), and 2,2'-bipyridine-5,5'-dicarboxylic acid ( $\text{H}_2\text{bpydc}$ , 13.0 mg, 0.053 mmol) were placed in a scintillation vial with 4 mL of  $N,N'$ -dimethylformamide (DMF, ACS grade, Fisher, anhydrous). The reagents were dispersed via sonication for 10 min, followed by incubation in an oven at 120 °C for 24 hours. The solid MOFs were washed with DMF three times, followed by soaking in methanol for 3 days. Subsequently, the MOFs were collected via centrifugation and activated at 150 °C under vacuum (30 mTorr) for 12 hours. The yield is 35 mg and 94% based on Zr). m-6,6'- $\text{Me}_2\text{bpy}$ -MOF (34 mg, 87%) and m-4,4'- $\text{Me}_2\text{bpy}$ -MOF (33 mg, 83%) were synthesized by analogous procedures in which  $\text{H}_2\text{bpydc}$  was replaced by 4,4'-dimethyl-2,2'-bipyridine-5,5'-dicarboxylic acid for m-6,6'- $\text{Me}_2\text{bpy}$ -MOF and 6,6'-dimethyl-2,2'-bipyridine-5,5'-dicarboxylic acid for m-4,4'- $\text{Me}_2\text{bpy}$ -MOF.

**Synthesis of m-MOF- $\text{PdCl}_2$ .** 100 mg of m-MOFs was dispersed in 5 mL of acetonitrile (Fisher, Optima<sup>TM</sup> grade). After sonication for 10 min, an acetonitrile solution of  $\text{PdCl}_2(\text{CH}_3\text{CN})_2$  (9.2 mg  $\text{PdCl}_2(\text{CH}_3\text{CN})_2$  in 3 mL  $\text{CH}_3\text{CN}$ ) was added to

the MOF solution, and mixture was incubated at 65 °C for 24 hours. After 24 hours, the solid was isolated by centrifugation and washed three times with acetonitrile (5 mL). The solids were suspended in methanol for 3 days, and the methanol (5 mL) was exchanged every 24 hours. After 3 days, the solids were collected via centrifugation and dried at 80 °C under vacuum for further use.

**Synthesis of homogeneous counterpart catalysts.** PdCl<sub>2</sub>(CH<sub>3</sub>CN)<sub>2</sub> (65 mg, 0.25 mmol) and 2,2'-bipyridine-5,5'-dicarboxylic acid dimethyl ester (0.25 mmol) were added in 4 mL of acetonitrile and then stirred vigorously (600 rpm) at 65 °C for 24 hours. The resultant yellow solid was separated by centrifugation and was washed thoroughly with copious amounts of acetonitrile, and finally dried at 80 °C for 12 hours under vacuum. 6,6'-Me<sub>2</sub>-5,5'-(MeO<sub>2</sub>C)<sub>2</sub>bpy-PdCl<sub>2</sub> and 4,4'-Me<sub>2</sub>-5,5'-(MeO<sub>2</sub>C)<sub>2</sub>bpy-PdCl<sub>2</sub> were synthesized by analogous procedures.

**Quantitative analysis of linkers by <sup>1</sup>H NMR.** m-MOFs samples (10 mg) were dried under vacuum and digested by sonication in 570 μL DMSO-*d*<sub>6</sub> and 30 μL of 40% HF to facilitate <sup>1</sup>H NMR analysis of the linkers.

**General.** All reagents and solvents were of ACS certified grade or higher and were used as received from commercial suppliers. Powder X-ray diffraction data were recorded on a STOE Stadi P powder diffractometer using Cu *K*<sub>α</sub> radiation (40 kV, 40 mA, λ = 0.1541 nm). Surface area analysis of the catalysts was performed by nitrogen adsorption–desorption isotherms in a Micromeritics 3Flex surface area analyzer at 77 K. UiO-67-X-bpydc<sub>0.5</sub>/bpdc<sub>0.5</sub> samples (ca. 25 mg) were degassed under vacuum (5 x 10<sup>-5</sup> torr) at 200 °C for 12 hours prior to measurement. Surface area was calculated in pressure range of 0.002 and 0.02 the basis of two consistency criteria.<sup>51</sup> ICP-MS was

performed on Thermo Fisher Scientific X Series 2 ICP-MS and the UiO-67-Pd-X-bpydc<sub>0.5</sub>/bpdc<sub>0.5</sub> was heated in a boiling aqua regia solution until the solid was completely dissolved.

**Typical procedure of catalytic reaction.** The Suzuki-Miyaura cross-coupling was carried out in Argon atmosphere. In a typical catalytic reaction, 4-iodobenzene (0.1 mmol, Fisher Scientific), 30 mg of phenylboronic acid (0.11 mmol, Aldrich), K<sub>2</sub>CO<sub>3</sub> (0.15 mmol), an appropriate amount of UiO-67-Pd-bpydc<sub>0.5</sub>/bpdc<sub>0.5</sub> (1.5 mol%) and 10 mg of mesitylene (Internal GC standard, Acros Organics) were added to in a 20 mL vial containing 2 mL of toluene. The vial was incubated in an oil bath which was preheated to 85 °C. Upon the completion of reaction, the product was separated via centrifugation and analyzed using gas chromatography (Hewlett Packard 5890 II, FID detector) and GC-MS (Shimadzu QP5050).

**Recycling test.** The MOFs were isolated from the reaction medium by centrifugation at the end of the reaction. The solid catalyst was washed with diluted HCl (pH = 1) to remove the undissolved K<sub>2</sub>CO<sub>3</sub> and then washed with methanol thrice, Finally, the MOFs were dried in vacuum at 80 °C and reused under the identical reaction conditions in the next run.

**Leaching test.** The MOF catalyst was separated from the hot solution right after the reaction was run for 3 hours. The reaction was continued with the filtrate in the absence of solid catalyst for an additional 4 hours. No further increase in either the conversion of iodobenzene was observed, which indicates that the catalytically active sites for cross coupling reaction are on the solid catalyst.



**Acknowledgment.** We thank Ames Laboratory (Royalty Account) and Iowa State University for startup funds. The Ames Laboratory is operated for the U.S. Department of Energy by Iowa State University under Contract No. DE-AC02-07CH11358. We thank Gordon J. Miller for use of PXRD in his group.

## References

- (1) Fleckenstein, C. A.; Plenio, H. *Chem. Soc. Rev.* **2010**, *39*, 694-711.
- (2) Lu, G.-P.; Voigttritter, K. R.; Cai, C.; Lipshutz, B. H. *J. Org. Chem.* **2012**, *77*, 3700-3703.
- (3) Hadei, N.; Kantchev, E. A. B.; O'Brie, C. J.; Organ, M. G. *Org. Lett.* **2005**, *7*, 1991-1994.
- (4) Szilvási, T.; Veszprémi, T. s. *ACS Catal.* **2013**, *3*, 1984-1991.
- (5) Das, P.; Linert, W. *Coord. Chem. Rev.* **2016**, *311*, 1-23.
- (6) Paul, S.; Clark, J. H. *J. Mol. Catal. A: Chem.* **2004**, *215*, 107-111.
- (7) Li, J.-R.; Kuppler, R. J.; Zhou, H.-C. *Chem. Soc. Rev.* **2009**, *38*, 1477-1504.
- (8) Suh, M. P.; Park, H. J.; Prasad, T. K.; Lim, D.-W. *Chem. Rev.* **2011**, *112*, 782-835.
- (9) Betard, A.; Fischer, R. A. *Chem. Rev.* **2012**, *112*, 1055-1083.
- (10) Della Rocca, J.; Liu, D.; Lin, W. *Acc. Chem. Res.* **2011**, *44*, 957-968.
- (11) Dhakshinamoorthy, A.; Opanasenko, M.; Cejka, J.; Garcia, H. *Catal. Sci. Technol.* **2013**, *3*, 2509-2540.
- (12) Pascanu, V.; Yao, Q.; Bermejo Gómez, A.; Gustafsson, M.; Yun, Y.; Wan, W.; Samain, L.; Zou, X.; Martín-Matute, B. *Chem. Eur. J.* **2013**, *19*, 17483-17493.
- (13) Jiang, H.-L.; Yi, F.-Y.; Chen, D.; Wu, M.-K.; Han, L. *ChemPlusChem* **2016**, DOI: 10.1002/cplu.201600137.
- (14) Chen, L.; Gao, Z.; Li, Y. *Catal.Today* **2015**, *245*, 122-128.

- (15) Chen, L.; Rangan, S.; Li, J.; Jiang, H.; Li, Y. *Green Chem.* **2014**, *16*, 3978-3985.
- (16) Fei, H.; Cohen, S. M. *Chem. Commun.* **2014**, *50*, 4810-4812.
- (17) Fei, H.; Sampson, M. D.; Lee, Y.; Kubiak, C. P.; Cohen, S. M. *Inorg. Chem.* **2015**, *54*, 6821-6828.
- (18) Manna, K.; Zhang, T.; Greene, F. X.; Lin, W. *J. Am. Chem. Soc.* **2015**, *137*, 2665-2673.
- (19) Manna, K.; Zhang, T.; Lin, W. *J. Am. Chem. Soc.* **2014**, *136*, 6566-6569.
- (20) Van Zeeland, R.; Li, X.; Huang, W.; Stanley, L. M. *RSC Adv.* **2016**, *6*, 56330-56334.
- (21) Yang, Q.; Guillerm, V.; Ragon, F.; Wiersum, A. D.; Llewellyn, P. L.; Zhong, C.; Devic, T.; Serre, C.; Maurin, G. *Chem. Commun.* **2012**, *48*, 9831-9833.
- (22) Bauer, C. A.; Timofeeva, T. V.; Settersten, T. B.; Patterson, B. D.; Liu, V. H.; Simmons, B. A.; Allendorf, M. D. *J. Am. Chem. Soc.* **2007**, *129*, 7136-7144.
- (23) Hendon, C. H.; Tiana, D.; Fontecave, M.; Sanchez, C.; D'arras, L.; Sassoeye, C.; Rozes, L.; Mellot-Draznieks, C.; Walsh, A. *J. Am. Chem. Soc.* **2013**, *135*, 10942-10945.
- (24) Burtch, N. C.; Jasuja, H.; Walton, K. S. *Chem. Rev.* **2014**, *114*, 10575-10612.
- (25) Tan, J. C.; Cheetham, A. K. *Chem. Soc. Rev.* **2011**, *40*, 1059-1080.
- (26) Vermoortele, F.; Vandichel, M.; Van de Voorde, B.; Ameloot, R.; Waroquier, M.; Van Speybroeck, V.; De Vos, D. E. *Angew. Chem. Int. Ed.* **2012**, *51*, 4887-4890.
- (27) Zhong, J.; Chen, J.; Chen, L. *Catal. Sci. Technol.* **2014**, *4*, 3555-3569.
- (28) Choi, K. M.; Na, K.; Somorjai, G. A.; Yaghi, O. M. *J. Am. Chem. Soc.* **2015**, *137*, 7810-7816.
- (29) Goh, T. W.; Xiao, C.; Maligal-Ganesh, R. V.; Li, X.; Huang, W. *Chem. Eng. Sci.* **2015**, *124*, 45-51.
- (30) Li, X.; Goh, T. W.; Li, L.; Xiao, C.; Guo, Z.; Zeng, X. C.; Huang, W. *ACS Catal.* **2016**, *6*, 3461-3468.

- (31) Gorin, D. J.; Sherry, B. D.; Toste, F. D. *Chem. Rev.* **2008**, *108*, 3351-3378.
- (32) Tolman, C. A. *Chem. Rev.* **1977**, *77*, 313-348.
- (33) Puthraya, K. H.; Srivastava, T. S.; Amonkar, A. J.; Adwankar, M. K.; Chitnis, M. P. *J. Inorg. Biochem* **1985**, *25*, 207-215.
- (34) Mansouri-Torshizi, H.; Eslami-Moghadam, M.; Divsalar, A.; Saboury, A.-A. *Acta Chim Slov* **2011**, *58*, 811-822.
- (35) Klein, A.; Lepski, R. Z. *Anorg. Allgem. Chem* **2009**, *635*, 878-884.
- (36) Chen, L.; Huang, B.; Qiu, X.; Wang, X.; Luque, R.; Li, Y. *Chem. Sci.* **2016**, *7*, 228-233.
- (37) Chen, L.; Chen, X.; Liu, H.; Li, Y. *small* **2015**, *11*, 2642-2648.
- (38) Uhlich, N. A.; Sommer, P.; Bühr, C.; Schürch, S.; Reymond, J.-L.; Darbre, T. *Chem. Commun.* **2009**, 6237-6239.
- (39) Liao, L.-Y.; Kong, X.-R.; Duan, X.-F. *J. Org. Chem.* **2014**, *79*, 777-782.
- (40) Hennings, D. D.; Iwama, T.; Rawal, V. H. *Org. Lett.* **1999**, *1*, 1205-1208.
- (41) Adamo, C.; Amatore, C.; Ciofini, I.; Jutand, A.; Lakmini, H. *J. Am. Chem. Soc.* **2006**, *128*, 6829-6836.
- (42) Li, X.; Zhang, J.; Zhao, X.; Zhao, Y.; Li, F.; Li, T.; Wang, D. *Nanoscale* **2014**, *6*, 6473-6477.
- (43) Jones, C. W. *Top Catal* **2010**, *53*, 942-952.
- (44) Watterson, S. H.; Xiao, Z.; Dodd, D. S.; Tortolani, D. R.; Vaccaro, W.; Potin, D.; Launay, M.; Stetsko, D. K.; Skala, S.; Davis, P. M.; Lee, D.; Yang, X.; McIntyre, K. W.; Balimane, P.; Patel, K.; Yang, Z.; Marathe, P.; Kadiyala, P.; Tebben, A. J.; Sherrif, S.; Chang, C. Y. Y.; Ziemba, T.; Zhang, H.; Chen, B.-C.; DelMonte, A. J.; Aranibar, N.; McKinnon, M.; Barrish, J. C.; Suchard, S. J.; Dhar, T. G. M.; *J. Med. Chem.* **2010**, *53*, 3814-3830.
- (45) Anghelid, N.; Draghici, C.; Raileanu, D., *Tetrahedron.* **1974**, *30*, 623-632.
- (46) Liao, L.-Y.; Kong, X.-R.; Duan, X.-F.; *J. Org. Chem.* **2014**, *79*, 777-782.
- (47) Constable, E. C.; Redondo, A. H.; Housecroft, C. E.; Neuburger, M.; Schaffner, S.; *Dalton Trans.* **2009**, 6634-6644.

- (48) Betschart, C.; Cotesta, S.; Hintermann, S.; Wagner, J.; Roy, B. L.; Gerspacher, M.; Von Matt, A.; WO2011073316(A1), June 2011.
- (49) Qi, H.; Teesdale, J. J.; Pupillo, R. C.; Rosenthal, J.; Bard, A. J.; *J. Am. Chem. Soc.* **2013**, *135*, 13558-13566.
- (50) Fei, H.; Cohen, S. M. *Chem. Commun.* **2014**, *50*, 4810-4812.
- (51) Walton, K. S.; Snurr, R. Q. *J. Am. Chem. Soc.* **2007**, *129*, 8552-8556.

## CHAPTER 6

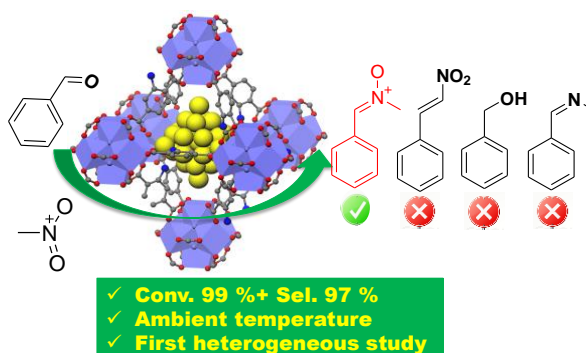
**PLATINUM NANOCLUSTERS IN AMINE-FUNCTIONALIZED METAL-  
ORGANIC FRAMEWORKS: COOPERATIVE MULTIFUNCTIONAL  
CATALYSTS FOR NITRONE SYNTHESIS**

A paper to be submitted

Xinle Li, Linlin Tang, Shuyan Qi, and Wenyu Huang

**Abstract**

Nitrones are well recognized as key intermediates in organic and pharmaceutical chemistry but there have been few attempts for the synthesis of nitrones using heterogeneous catalysts, which is preferred from a practical and green chemistry perspective. In this work, ultrasmall platinum nanoparticles are encapsulated in amine-functionalized UiO-66-NH<sub>2</sub> (Pt@UiO-66-NH<sub>2</sub>) and used as multifunctional catalysts in the one-pot tandem nitron synthesis. Pt@UiO-66-NH<sub>2</sub> exhibits high activity, enhanced selectivity, and excellent stability in the tandem nitron synthesis, in comparison to Pt/carbon, Pt@UiO-66, Pt/UiO-66-NH<sub>2</sub> and Pd@UiO-66-NH<sub>2</sub>. As far as we know, this delineates the first attempt for the one-pot synthesis of nitron using heterogeneous multifunctional catalysts.



## Introduction

Nitrones are widely recognized as key intermediates in the synthesis of biologically active alkaloids and pharmaceuticals.<sup>1</sup> The common procedures for the preparation of nitrones include oxidation of *N,N'*-substituted hydroxylamines/secondary amines/imines,<sup>2-4</sup> alkylation of oximes,<sup>5</sup> condensation of *N*-methylhydroxylamine hydrochloride with aromatic aldehydes,<sup>6</sup> reduction of *N*-hydroxyamides,<sup>7</sup> and Cope-type hydroamination of alkenes,<sup>8</sup> etc. However, most of the reported methods are mainly limited to homogeneous catalysis, which faces the twin hurdles of metal contamination and limited recyclability. To circumvent such obstacles associated with homogenous catalysis, it is advantageous to develop heterogeneous catalysts which can lead to facile separation and recycling. Nevertheless, there have been very few attempts for the synthesis of nitrones using heterogeneous catalysts.

Tandem reactions, where two or more individual reactions are carried out in a single pot, can maximize spatial and temporal productivity, minimizing the cost of resources and avoiding tedious and costly intermediate purification/separation processes.<sup>9</sup> In comparison to homogenous multifunctional catalysts, the design of heterogeneous multifunctional catalysts is highly desired not only to avoid stop-and-go syntheses and achieve high atomic efficiency, but also to ensure recyclability. Heterogeneous catalysts that can facilitate tandem reactions can also potentially serve as promising platforms for continuous flow processes.

MOFs have been widely utilized as a host matrix for metal NPs in heterogeneous catalysis (metal NPs@MOF).<sup>10</sup> Metal NPs@MOF system offers

multiple merits: (i) the uniform cavities of MOFs can limit the migration and aggregation of metal NPs; (ii) they possess multiple active sites which is a prerequisite to the design of multifunctional catalysts; (iii) the highly porous nature of the MOFs facilitates the transportation of substrates and ensures accessibility to the active metal sites; (iv) the nanoconfinement effects endowed by MOFs lead to enhanced catalytic performance. Despite intensive scientific efforts directed towards studying the role of metal NPs@MOFs in catalysis,<sup>11-14</sup> there have only been a limited number of studies on bifunctional catalysts to implement tandem reactions up to now.<sup>15-20</sup> In light of these reports, the development of an NPs@MOF multifunctional catalytic system for tandem catalysis will exert a significant impact on chemical processes.

In this context, we have synthesized ultrasmall and monodispersed platinum NCs inside a Zr-MOF, UiO-66-NH<sub>2</sub>. The Pt@UiO-66-NH<sub>2</sub> cooperatively catalyzes a tandem reaction on the basis of both Lewis acidity/basicity from MOF and redox properties from Pt NPs. Impressively, the multifunctional catalyst, Pt@UiO-66-NH<sub>2</sub>, could catalyze the one-pot multistep tandem reaction for the synthesis of nitron with high activity and selectivity, by coupling the reduction activity of Pt NCs and the condensation activity of the Lewis acid/base sites on UiO-66-NH<sub>2</sub>. To the best of our knowledge, this delineates the first attempt for the one-pot synthesis of nitron using heterogeneous multifunctional catalysts.

## Results and Discussion

UiO-66-NH<sub>2</sub> was prepared via a solvothermal synthetic protocol and PXRD pattern of the as-synthesized UiO-66-NH<sub>2</sub> was identical to the simulated UiO-66 (Figure 1), revealing the successful synthesis of MOFs. Using UiO-66-NH<sub>2</sub> as the support, we immobilized Pt NPs confined inside its cavities via a solution impregnation method developed by our group.<sup>21</sup> The actual Pt content was quantitatively determined to be 2.0 wt. % by ICP-MS analysis. As shown in Figure 2, TEM images confirmed that the Pt NCs residing inside UiO-66-NH<sub>2</sub> are extremely small. Both the TEM and HAADF-STEM images clearly show that the Pt NPs in UiO-66-NH<sub>2</sub> are highly dispersed with mean diameters of  $1.2 \pm 0.2$  nm. Pt NPs with sizes smaller than the diameters of MOF cages (the octahedral cage size is 1.1 nm) have been successfully confined inside the MOF as predesigned.

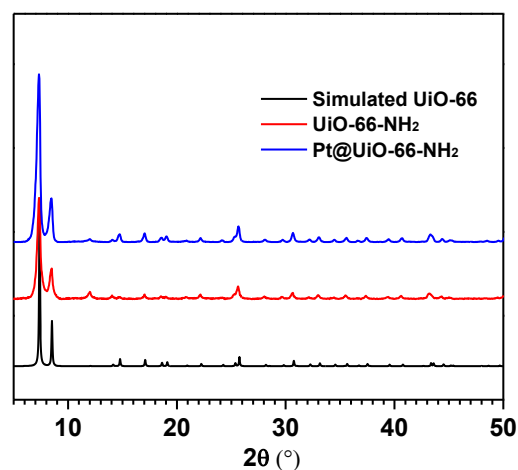


**Figure 1.** PXRD patterns of simulated UiO-66, UiO-66-NH<sub>2</sub> and 2.0 wt.% Pt@UiO-66-NH<sub>2</sub>.



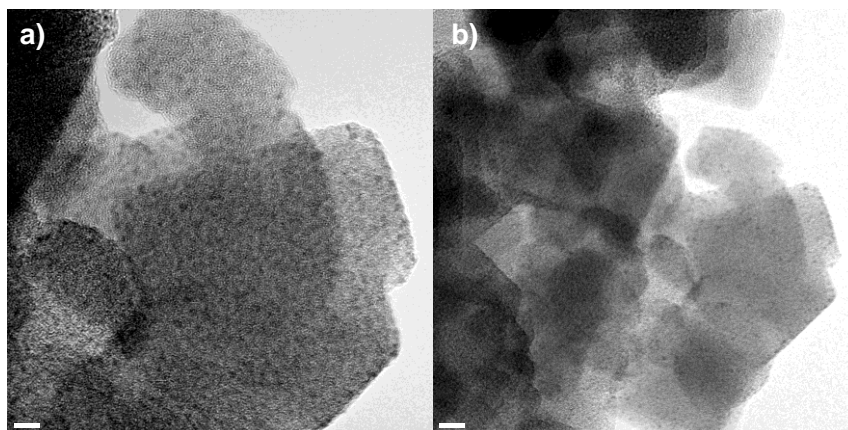


**Figure 2.** TEM images of 2.0 wt.% Pt@UiO-66-NH<sub>2</sub> at (a) high and (b) low magnification..

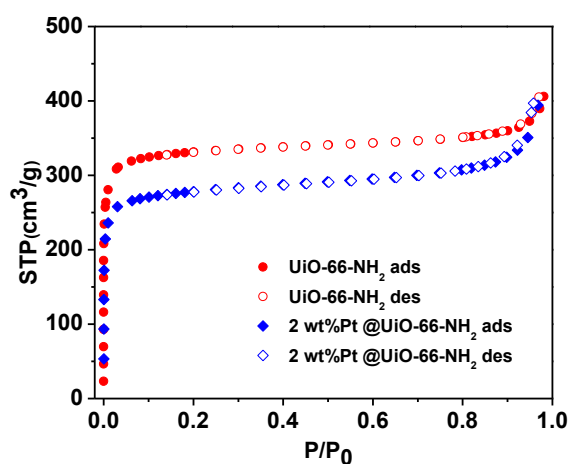
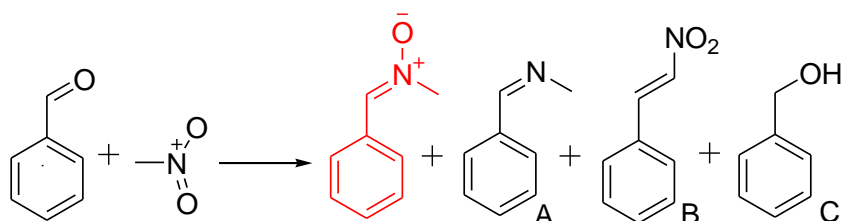


**Figure 3.** Nitrogen sorption isotherms of the as-synthesized UiO-66-NH<sub>2</sub> and 2.0 wt.% Pt@UiO-66-NH<sub>2</sub>.

Nitrogen sorption analyses show that both UiO-66-NH<sub>2</sub> and Pt@UiO-66-NH<sub>2</sub> display a Type I curve (Figure 3), suggesting the existence of micropores. The BET surface area of 2.0 wt.%Pt@UiO-66-NH<sub>2</sub> is 869 m<sup>2</sup>g<sup>-1</sup> with a micropore volume of 0.35 cm<sup>3</sup>g<sup>-1</sup>, which is lower than that of the parent UiO-66-NH<sub>2</sub> (931 m<sup>2</sup>g<sup>-1</sup> with a micropore volume of 0.38 cm<sup>3</sup>g<sup>-1</sup>). The decrease in the surface area and pore volume

of Pt@UiO-66-NH<sub>2</sub> is ascribed to the partial occupation of the cavities in UiO-66-NH<sub>2</sub> by the Pt NPs.

**Table 1.** Identification of reaction conditions by Pt@UiO-66-NH<sub>2</sub>.<sup>a</sup>



entry	Pt	H <sub>2</sub> (psi)	CH <sub>3</sub> NO <sub>2</sub>	solvent	conv. (%)	Sel. (%)			
						Nitronium	A	B	C
1	0	200	15 equiv.	Toluene	/	/	/	/	/
2	2 mol%	200	15 equiv.	Toluene	99	97	1.5	1.5	/
3	2 mol%	200	15 equiv.	Trifluorotoluene	93	94	0.5	5.5	/
4 <sup>b</sup>	2 mol%	200	15 equiv.	MeOH	98	80	1	1	/
5	2 mol%	200	15 equiv.	1,4-dioxane	90	60	18	22	/
6	2 mol%	200	15 equiv.	Cyclohexane	98	91	6	3	/
7	2 mol%	100	15 equiv.	Toluene	95	82	12	2	/
8	2 mol%	500	15 equiv.	Toluene	94	94	5.5	0.5	/
9	2 mol%	200	3 equiv.	Toluene	31	86	14	/	/

<sup>a</sup> Reaction conditions: benzaldehyde (0.1 mmol), nitromethane, solvent (1 mL), 20 °C, 12 hours, stir at 600 rpm. <sup>b</sup> Corresponding acetal was formed.

With the standard characterization techniques confirming the nature of the MOF system, we proceeded to evaluate the multifunctional catalyst Pt@UiO-66-NH<sub>2</sub>

in the tandem reactions of benzaldehyde and nitromethane at ambient temperature. As for the hydrogenation of nitromethane, the intermediate-hydroxylamine is formed. Subsequent condensation of the intermediate and benzaldehyde afford nitrone product. Bare UiO-66-NH<sub>2</sub> alone only gave negligible conversion of benzaldehyde, indicating that Pt NCs are essential in the tandem catalysis (Table 1, entry 1). Toluene is the optimum solvent over methanol, trifluorotoluene, 1,4-dioxane, cyclohexane and 1,4-dioxane (Table 1, entries 2-6). Using Pt@UiO-66-NH<sub>2</sub> as the catalyst, the reaction exhibits 99% conversion of benzaldehyde and 97% selectivity to nitrone (Table 1, entry 2). We found that the number of equivalents of nitromethane and the hydrogen pressure also impact the yield of our tandem reaction. Decreasing the pressure to 100 psi will lower the selectivity while high pressure did not improve the selectivity (Entry 7 and 8). Increasing the amount of nitromethane from 3 equivalents to 15 equivalents led to the enhanced selectivity (entry 9).

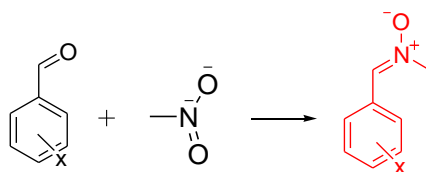
**Table 2.** Tandem nitrone synthesis by various heterogeneous catalysts.<sup>a</sup>

entry	catalyst	time (h)	H <sub>2</sub> (psi)	conv. (%)	Sel. (%)			
					Nitrone	A	B	C
1	Pt@UiO-66-NH <sub>2</sub>	12	200	99	97	1.5	1.5	/
2	Pt/carbon	12	200	98	23	24	24	/
3	Pt@UiO-66	12	200	98	28	14	3	/
4	Pt/UiO-66-NH <sub>2</sub>	12	200	3	88	12	/	/
5	Pd@UiO-66-NH <sub>2</sub>	12	200	99	/	/	/	99

<sup>a</sup> Reaction conditions: benzaldehyde (0.1 mmol), nitromethane (1.5 mmol), toluene (1 mL), metal/substrate = 2 mol%, 20 °C, stir at 600 rpm.

To elucidate the origin of excellent catalytic performance of Pt@UiO-66-NH<sub>2</sub> in this tandem reaction (Table 2, entry 1), we also tested a series of control catalysts under identical conditions. We could not achieve high selectivity over Pt/carbon (Table 2, entry 2), indicating the UiO-66-NH<sub>2</sub> plays a significant role in this selective reaction. To probe the role of -NH<sub>2</sub> in this tandem reaction, we synthesized the isorecticular UiO-66 due to the exceptional chemical flexibility of MOFs. The obtained Pt@UiO-66 shows similar Pt NCs size in TEM and identical PXRD patterns. To our surprise, the selectivity of Pt@UiO-66 is much lower than that of Pt@UiO-66-NH<sub>2</sub>, highlighting the importance of functional groups on the linkers in the design of multifunctional MOF catalysts (Table 2, entry 3).

**Table 3.** Tandem catalysis with various substituted benzaldehyde and nitromethane over Pt@UiO-66-NH<sub>2</sub>.



Entry	X	Conv.(%)	Sel. to nitronium (%)
1	2-F	99	90
2	4-Br	90	47
3	4-Cl	87	58
4	3-CN	99	88
5	4-CN	97	82

Reaction conditions: benzaldehyde (0.1 mmol), nitromethane (1.5 mmol), toluene (1 mL), metal/substrate = 2 mol%, RT, 600 rpm.

Nanoconfinement effects are of key importance in heterogeneous catalysis.<sup>22</sup> We also explored the effect of nanoconfinements rendered by the MOFs. Pt NPs deposited on the external surface of UiO-66-NH<sub>2</sub> (designed as Pt/UiO-66-NH<sub>2</sub>) was prepared for comparison. The TEM images of Pt/UiO-66-NH<sub>2</sub> show the size of Pt NPs to be ~2 nm. Pt/UiO-66-NH<sub>2</sub> showed an inferior activity and selectivity in comparison to Pt@UiO-66-NH<sub>2</sub>, highlighting the advantages of nanoconfinement effects in MOF (Table 2, entry 4). We also explored the substrate scope of the tandem reactions and various benzaldehydes have been tested (Table 3). We found that benzaldehyde with electron-withdrawing groups showed a moderate to high activity and selectivity, indicating the generality of the bifunctional catalyst.

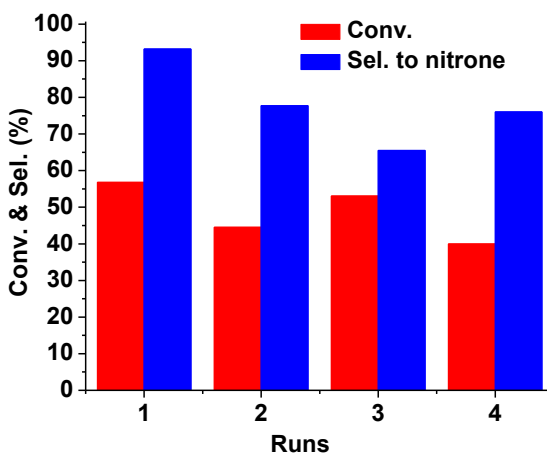


**Figure 3.** Recycling test with 2.0 wt.% Pt@UiO-66-NH<sub>2</sub> catalyst. Reaction conditions: benzaldehyde (0.1 mmol), nitromethane (1.5 mmol), toluene (1 mL), metal/substrate = 2 mol%, 20 °C, 200 psi H<sub>2</sub>, 3.5 hours, stir at 600 rpm.

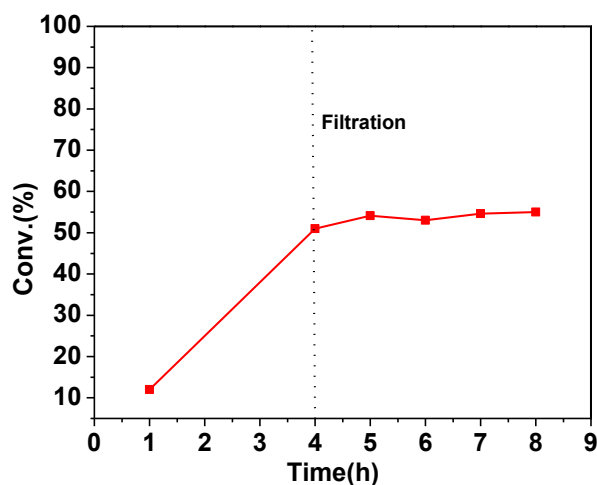


**Figure 4.** Leaching test for the tandem reaction over 2.0 wt.% Pt@UiO-66-NH<sub>2</sub>.

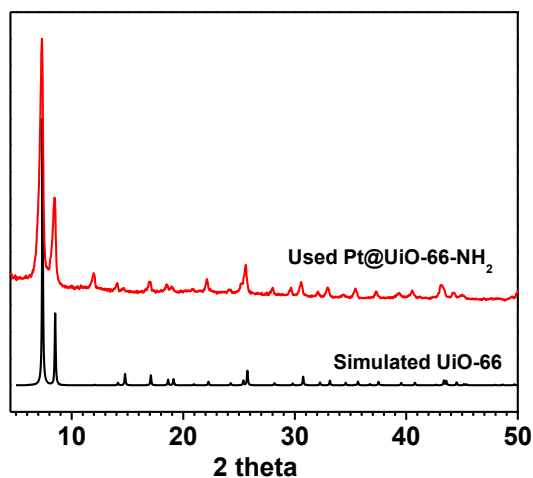


**Figure 5.** PXRD patterns of simulated UiO-66, and used 2.0 wt.% Pt@UiO-66-NH<sub>2</sub> after catalysis.

Stability and recyclability are prerequisites for practical applications. PXRD studies show that the MOFs' integrity was retained after catalysis (Figure 5). There are no obvious changes in the TEM images of the used Pt@UiO-66-NH<sub>2</sub> and used

Pt@UiO-66-NH<sub>2</sub> still possesses high BET surface areas, indicating the confinement endowed by MOFs and the robustness of catalyst during reaction. The recyclability of the catalyst was performed by isolating the MOF catalyst from the reaction media at partial conversion and reusing the catalyst in the subsequent runs. The catalyst can be recycled 4 times without significant decrease in activity and slight decrease in selectivity to nitrones. A leaching test was also utilized to confirm the heterogeneity of catalysts. Upon removal of catalyst, no further increase in either conversion of benzaldehyde was observed. Furthermore, ICP-MS analysis of the supernatant showed that there is negligible Pt leaching out in the solution. Taken together, the multifunctional catalyst Pt@UiO-66-NH<sub>2</sub> is a highly active, reusable, and robust catalyst for tandem nitron synthesis.

### Conclusion

In summary, we have prepared Pt NCs encapsulated inside the UiO-66-NH<sub>2</sub> and the multifunctional catalyst Pt@UiO-66-NH<sub>2</sub> presents excellent performance in tandem catalysis. For the first time, the tandem synthesis of nitron was realized in a heterogeneous MOFs system. Compared to Pt/carbon, Pt@UiO-66, Pt/UiO-66-NH<sub>2</sub> and Pd@UiO-66-NH<sub>2</sub>, the superior performance of Pt@UiO-66-NH<sub>2</sub> is presumably due to the synergetic cooperation from the ultrasmall Pt NCs, the amine-functionalized MOFs, and nanoconfinement effects. Furthermore, the multifunctional catalyst Pt@UiO-66-NH<sub>2</sub> is robust and can be recycled without significant loss of catalytic activity in the repetitive reuse cycles. The facile and rational design might open a new opportunity to MOF-based multifunctional catalysts, which has great

potential for broad applications in one-pot tandem reactions for the production of fine chemicals in the future.

### **Experimental section**

**Synthesis of UiO-66 and UiO-66-NH<sub>2</sub>.** Zirconium (IV) chloride (0.40g, 1.71 mmol) and corresponding organic linker acid (H<sub>2</sub>BDC or NH<sub>2</sub>-H<sub>2</sub>BDC) (1.71 mmol) were dissolved in DMF (100 mL) at room temperature. A small amount of water (0.13 mL, 6.84 mmol) was added to the solution in the synthesis of UiO-66-NH<sub>2</sub>. The obtained mixture was sealed in 480 mL Teflon PFA wide mouth jar and heated in an oven at 120 °C for 24 hours. After cooled to ambient temperature, the solid MOFs were isolated via centrifugation and washed with DMF (3 times) and methanol (3 times) every 12 hours. Afterwards, it was activated at 150 °C under vacuum (30 mTorr) for 12 hours prior to further use.

**Synthesis of 2.0 wt.% Pt NCs@UiO-66-X.** 100 mg of activated UiO-66-X was dispersed in 4 mL water and sonicated for 1 hour to achieve a homogenous dispersion. Aqueous K<sub>2</sub>PtCl<sub>4</sub> solution (4.32 mg K<sub>2</sub>PtCl<sub>4</sub> in 3 mL water) was added dropwise to the above solution under stirring (600 rpm). After 24 hours of stirring at ambient temperature, the as-prepared Pt<sup>2+</sup>-infiltrated MOF was washed three times every 12 hours with fresh water to completely remove the remaining Pt<sup>2+</sup> salts. The solid was dried under vacuum and reduced under a 50 mL/min flow of 10 % H<sub>2</sub>/Ar at 200 °C for 1 hour to afford Pt NCs@UiO-66-X.

**Characterization.** The BET surface area and pore size distribution of the catalyst were measured by nitrogen sorption isotherms at 77 K on a Micromeritics 3Flex



surface characterization analyzer. Powder X-ray diffraction patterns of the samples were recorded on a STOE Stadi P powder diffractometer using Cu K $\alpha$  radiation (40 kV, 40 mA,  $\lambda = 0.1541$  nm). The size and morphology of 2.0 wt.% Pt@UiO-66-X were investigated by using TEM and HAADF-STEM images recorded on a Tecnai G2 F20 electron microscope with an EDX analyzer (Oxford INCA EDS) operated at 200 kV. ICP-MS analysis (X Series II, Thermo Scientific) was performed to determine the actual loading of platinum in UiO-66-X. The Pt@UiO-66-X samples were dissolved in boiling aqua regia until the solid was completely dissolved.

**Tandem catalytic reaction.** The tandem reaction was carried out in a Parr 4740 High Pressure/High Temperature Pressure Vessel. Typically, 10 mg of benzaldehyde (0.1 mmol, Fisher Scientific), 1 mL of solvent, 10 mg of 2.0 wt.% Pt@UiO-66-X (2 mol% Pt) and 7 mg of mesitylene (internal GC standard, 99%, Acros Organics) were added in a vial. Then the autoclave was sealed and flushed five times with 200 psi H<sub>2</sub> (99.995%). The reaction was carried out in 200 psi H<sub>2</sub> with magnetic stirring at 600 rpm. After the reaction was finished, the products were analyzed using gas chromatograph equipped with a HP-5 capillary column (30 m  $\times$  0.32 mm  $\times$  0.25  $\mu$ m) with a flame ionization detector and Agilent 6890N/5975 GC-MS equipped with a HP-5ms capillary column (30 m  $\times$  0.32 mm  $\times$  0.25  $\mu$ m).

**Recycling of the Pt@UiO-66-NH<sub>2</sub> catalyst.** The catalyst was isolated from the reaction medium after reaction by centrifugation and the reaction solution was removed. The solid catalyst was washed with toluene for 3 times. The catalyst was reused in the second run and the catalytic activity/product selectivity of the catalyst did not show significant loss in the following run. PXRD analysis showed that the

crystal structure of the used catalyst remained intact during the catalytic cycles and catalysts remained effective within 5 cycles of the reaction.

**Leaching test of Pt@UiO-66-NH<sub>2</sub> catalyst.** The tandem reaction was stopped at partial conversion (~50%) and the MOFs catalyst was isolated via centrifugation from the solution. The reaction was continued with the filtrate in the absence of solid catalyst for additional hours. No further increase in the conversion of benzaldehyde was observed, which indicates that catalytic active sites are on the solid catalyst.

**Acknowledgment.** We thank Ames Laboratory (Royalty Account) and Iowa State University for startup funds. The Ames Laboratory is operated for the U.S. Department of Energy by Iowa State University under Contract No. DE-AC02-07CH11358. We thank Gordon J. Miller for use of PXRD in his group.

## Reference

- (1) Stanley, L. M.; Sibi, M. P. *Chem. Rev.* **2008**, *108*, 2887-2902.
- (2) Matassini, C.; Parmeggiani, C.; Cardona, F.; Goti, A. *Org. Lett.* **2015**, *17*, 4082-4085.
- (3) Gella, C.; Ferrer, E.; Alibés, R.; Busque, F.; de March, P.; Figueredo, M.; Font, J. *J. Org. Chem.* **2009**, *74*, 6365-6367.
- (4) Soldaini, G.; Cardona, F.; Goti, A. *Org. Lett.* **2007**, *9*, 473-476.
- (5) Lebel, N. A.; Balasubramanian, N. *Tetrahedron Lett.* **1985**, *26*, 4331-4334.
- (6) Maiuolo, L.; De Nino, A.; Merino, P.; Russo, B.; Stabile, G.; Nardi, M.; D'Agostino, N.; Bernardi, T. *Arabian J. Chem.* **2015**.
- (7) Katahara, S.; Kobayashi, S.; Fujita, K.; Matsumoto, T.; Sato, T.; Chida, N. *J. Am. Chem. Soc.* **2016**, *138*, 5246-5249.

- (8) Moran, J.; Pfeiffer, J. Y.; Gorelsky, S. I.; Beauchemin, A. M. *Org. Lett.* **2009**, *11*, 1895-1898.
- (9) Climent, M. J.; Corma, A.; Iborra, S.; Sabater, M. J. *ACS Catal.* **2014**, *4*, 870-891.
- (10) Meilikhov, M.; Yusenko, K.; Esken, D.; Turner, S.; Van Tendeloo, G.; Fischer, R. A. *Eur. J. Inorg. Chem.* **2010**, *2010*, 3701-3714.
- (11) Gu, X.; Lu, Z.-H.; Jiang, H.-L.; Akita, T.; Xu, Q. *J. Am. Chem. Soc.* **2011**, *133*, 11822-11825.
- (12) Choi, K. M.; Na, K.; Somorjai, G. A.; Yaghi, O. M. *J. Am. Chem. Soc.* **2015**, *137*, 7810-7816.
- (13) Chen, L.; Huang, B.; Qiu, X.; Wang, X.; Luque, R.; Li, Y. *Chem. Sci.* **2016**, *7*, 228-233.
- (14) Kuo, C.-H.; Tang, Y.; Chou, L.-Y.; Sneed, B. T.; Brodsky, C. N.; Zhao, Z.; Tsung, C.-K. *J. Am. Chem. Soc.* **2012**, *134*, 14345-14348.
- (15) Zhao, M.; Deng, K.; He, L.; Liu, Y.; Li, G.; Zhao, H.; Tang, Z. *J. Am. Chem. Soc.* **2014**, *136*, 1738-1741.
- (16) Qiu, X.; Len, C.; Luque, R.; Li, Y. *ChemSusChem* **2014**, *7*, 1684-1688.
- (17) Chen, Y.-Z.; Zhou, Y.-X.; Wang, H.; Lu, J.; Uchida, T.; Xu, Q.; Yu, S.-H.; Jiang, H.-L. *ACS Catal.* **2015**, *5*, 2062-2069.
- (18) Hinde, C. S.; Webb, W. R.; Chew, B. K. J.; Tan, H. R.; Zhang, W.-H.; Hor, T. S. A.; Raja, R. *Chem. Commun.* **2016**, *52*, 6557-6560.
- (19) Dhakshinamoorthy, A.; Garcia, H. *ChemSusChem* **2014**, *7*, 2392-2410.
- (20) Li, Y.-A.; Yang, S.; Liu, Q.-K.; Chen, G.-J.; Ma, J.-P.; Dong, Y.-B. *Chem. Commun.* **2016**, *52*, 6517-6520.
- (21) Guo, Z.; Xiao, C.; Maligal-Ganesh, R. V.; Zhou, L.; Goh, T. W.; Li, X.; Tesfagaber, D.; Thiel, A.; Huang, W. *ACS Catal.* **2014**, *4*, 1340-1348.
- (22) Xiao, J. D.; Shang, Q.; Xiong, Y.; Zhang, Q.; Luo, Y.; Yu, S. H.; Jiang, H. L. *Angewandte Chemie* **2016**.

## CHAPTER 7

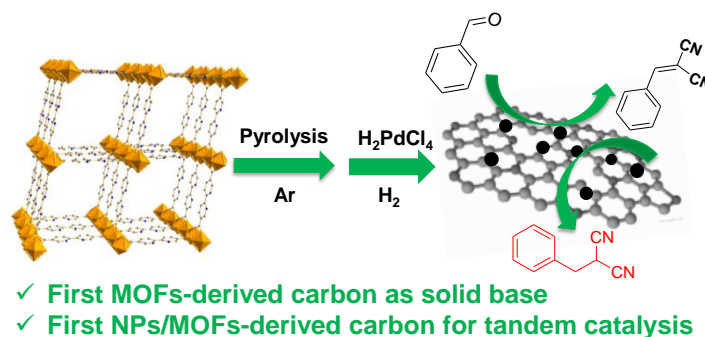
**METAL-ORGANIC FRAMEWORK DERIVED CARBONS AS SOLID BASE CATALYST AND POTENTIAL APPLICATION IN TANDEM CATALYSIS**

Submitted to *Chemical Communication*

Xinle Li, Yuhui Fang, Shuyan Qi, Weijun Sun and Wenyu Huang

**Abstract**

A facile pyrolysis of a bipyridyl metal–organic frameworks, MOF-253, produces N-doped porous carbons (Cz-MOF-253), which exhibit excellent catalytic activity in Knoevenagel condensation reaction. More importantly, by virtue of high Lewis basicity and porous nature, Cz-MOF-253 supported Pd NPs (Pd/Cz-MOF-253) presents excellent performance in a one-pot sequential Knoevenagel condensation-hydrogenation reaction. To our knowledge, this work represents the first example of MOFs-derived carbons as solid base catalyst and its potential as bifunctional catalyst in tandem catalysis.



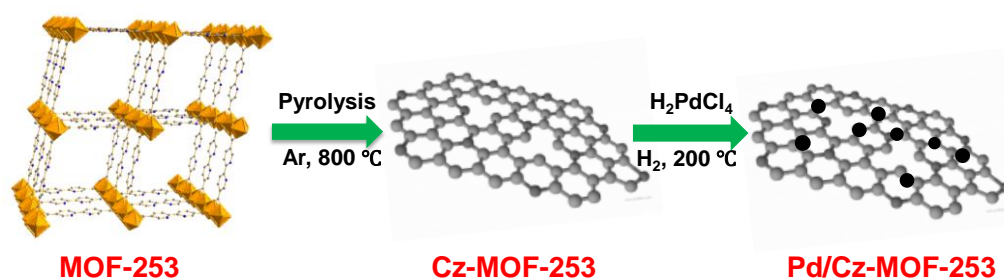
## Introduction

Porous carbon materials derived from MOFs have gained rising attention due to their tailorable structure and porosity, high surface area, enhanced stability, and homogeneous heteroatom doping, as well as widespread applications in areas of gas storage,<sup>1-3</sup> absorbents,<sup>4</sup> and supercapacitors.<sup>5</sup> Recently, the MOF-derived porous carbon holds great promise in catalysis such as metal-free electro-catalytic oxygen reduction,<sup>6,7</sup> and catalytic oxidation.<sup>8</sup> MOF-derived carbons are still capable of retaining the morphology and porosity of the MOFs precursor upon pyrolysis.<sup>9</sup> However, whether MOF-derived carbons can preserve/inherit active sites of MOFs precursor remains unexplored. It not only expands the use of MOF-derived carbons in catalysis, but also allows the flexible design of bifunctional catalysts. Inspired by this, MOF-253, which is built up from 2,2'-bipyridine-5,5'-dicarboxylic acid and Al clusters, was judiciously selected as the carbon precursor. Zhao et al. demonstrated that MOF-253 derived carbons (designed as Cz-MOF-253) possess high contents of pyridinic-N groups after pyrolysis and afford enhanced CO<sub>2</sub>/N<sub>2</sub> selectivity.<sup>10</sup> We envision that the nitrogen groups in Cz-MOF-253 serve several functions. (1) such heteroatoms dopant can affect the electronic properties of carbons, thus improving the catalytic performance in electro-catalysis;<sup>11</sup> (2) it facilitates the Pd loading and stabilizes the Pd NPs;<sup>12,13</sup> (3) it can function as catalytically Lewis basic sites and find potential (e.g., tandem catalysis) in heterogeneous catalysis. To our knowledge, there have no reports on MOF-derived carbons as solid base catalyst by far.

On the other hand, Knoevenagel condensation reactions are valued reactions for the production of  $\alpha,\beta$ -unsaturated carbonyl compounds which are widely used in

pharmaceutical, cosmetic and agrochemical industries.<sup>14</sup> Conventionally, Knoevenagel condensation reactions proceed homogeneously in the presence of basic catalysts, which are typically hindered by limited recyclability. Therefore, it is highly desirable to develop new heterogeneous catalysts that realize those reactions from the viewpoints of economy and green chemistry. To achieve more economic and environmental benefits, tandem catalysis, which enables a series of reactions to take place in one pot, have attracted tremendous attention since it avoids the need for isolation of intermediates and reduce the production of wastes.<sup>15</sup> Although metal NPs encapsulated inside MOFs for tandem catalysis have been reported recently,<sup>16-20</sup> and NPs stabilized in MOFs-derived carbons demonstrated potential in catalysis,<sup>21-23</sup> there have been minimal studies on metal NPs stabilized within MOF-derived carbons for heterogeneous tandem catalysis.

In this context, we develop a novel solid base catalyst-Cz-MOF-253 by a facile pyrolysis of bipyridyl MOFs and subsequent acid treatment (Scheme 1). The nitrogen groups serve as Lewis basic sites for Knoevenagel condensation reaction and exhibit high catalytic efficiency in comparison to other nitrogen-containing MOFs-derived carbons. Furthermore, recycling and leaching tests show that Cz-MOF-253 is a true heterogeneous catalyst. More importantly, Pd NPs stabilized within Cz-MOF-253 (Pd/Cz-MOF-253) was evaluated in a one-pot step-wise tandem reaction in which Knoevenagel condensation and subsequent hydrogenation was combined to demonstrate its integrated catalytic properties and high catalytic efficiency. To the best of our knowledge, this represents the first work that demonstrates nitrogen doped MOF-derived carbons as solid base catalysts and its potential in tandem catalysis.



**Scheme 1.** Schematic illustration of the synthesis of MOFs derived carbons and Pd NPs stabilized within MOF derived carbons for tandem catalysis.

## Results and Discussion

MOF-253 is synthesized from a solvothermal reaction of 2,2'-bipyridine-5,5'-dicarboxylic acid and  $\text{AlCl}_3 \cdot 6\text{H}_2\text{O}$ .<sup>24</sup> PXRD profiles of the as-synthesized sample matches well with simulated pattern. The MOF-253 exhibits a microporous character with BET surface area of  $1940 \text{ m}^2/\text{g}$ . To investigate the effect of carbonization temperature on the formation of carbons, MOF-253 was carbonized at 700, 800, 900 and  $1000 \text{ }^\circ\text{C}$  under argon atmosphere, giving rise to MOF-derived carbons (denoted as Cz-MOF-253-n, n refers to pyrolysis temperature).

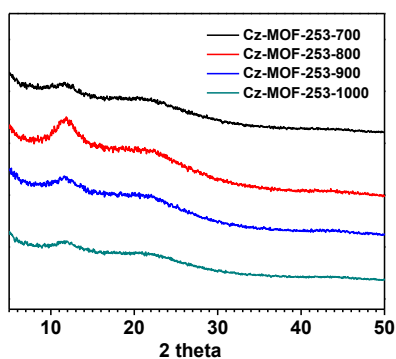


**Figure 1.** PXRD patterns of the Cz-MOF-253 derived from pyrolysis of MOF-253.

**Table 1.** Weight loss of MOF-253 in different pyrolysis temperature.

Entry	Pyrolysis temperature	Atmosphere	Weight loss percent <sup>a</sup>
1	700 °C	Ar	49.9% ± 1.0%
2	800 °C	Ar	52.1% ± 1.2%
3	900 °C	Ar	55.9% ± 1.0%
4	1000 °C	Ar	58.3% ± 0.9%
<sup>a</sup> The average weight loss and deviation is from three independent experiments.			

It is noted that higher carbonization temperature leads to more weight loss (Table 1). To remove Al<sub>2</sub>O<sub>3</sub>, the Cz-MOF-253 was treated with 20% HF and was washed with deionized water. PXRD patterns of Cz-MOF-253 carbons exhibit broad and weak peaks around 24° and 44° (Figure 1), which can be assigned to the peaks of (002) and (101) of graphitic carbon.<sup>21</sup> The peak around 12° presumably corresponds to the peak of (001) of graphene oxide. The XPS analysis for N 1s (Figure 2) reveals that there are four types of nitrogen species: pyridinic-N (398.5 ± 0.2 eV), pyrrolic-N (400.5 ± 0.3 eV), graphitic-N (401.1 ± 0.3 eV), and oxidized nitrogen N<sup>+</sup>-O<sup>-</sup> (403.4 ± 0.1 eV) in all N-involved samples. For all Cz-MOF-253 samples, pyrrolic-N (33-45%) and pyridinic-N (35-38%) are the main constituents of N contents, while the graphitic-N (12-25%) and N-oxide (4-7%) content is relatively small. With the increase of pyrolysis temperature, pyrrolic-N and pyridinic-N were partially converted into graphitic-N and N-oxide (Figure 3).



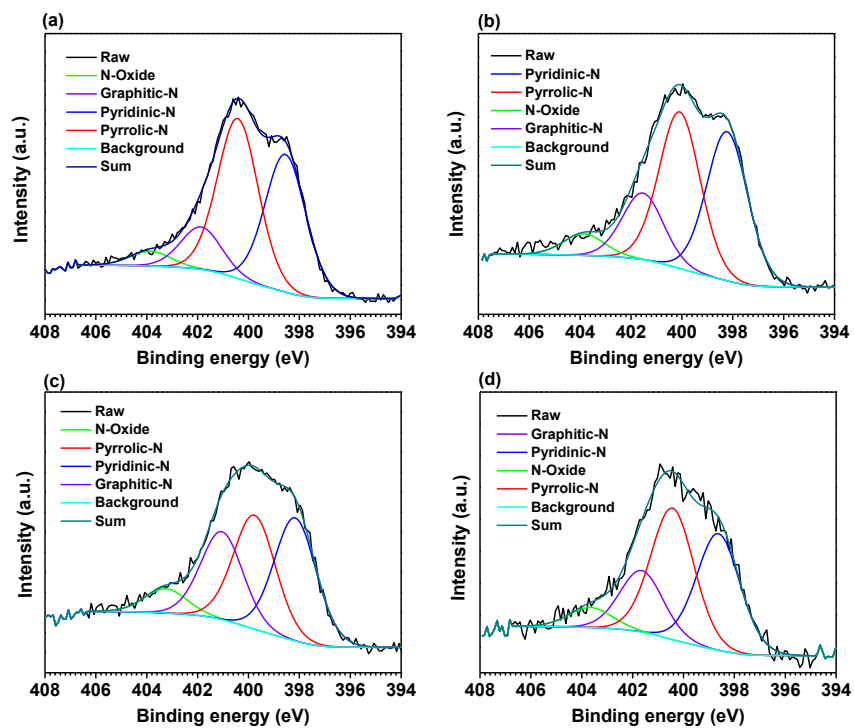


**Figure 2.** XPS spectrum of the N 1s in (a) Cz-MOF-253-700 ; (b) Cz-MOF-253-800 ; (c) Cz-MOF-253-900 ; (d) Cz-MOF-253-1000.

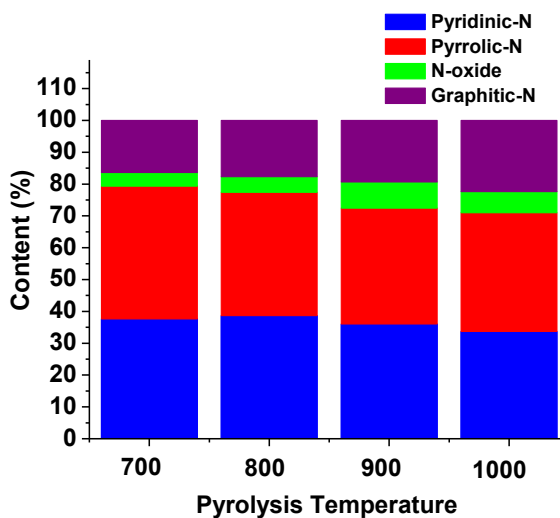


**Figure 3.** The content of various types of N for Cz-MOFs carbonized at different temperatures.

It is noteworthy that the pyrolysis temperature significantly affects the BET surface area and pore character of the resultant carbons. BET surface areas of for Cz-MOF-253-700, Cz-MOF-253-800, Cz-MOF-253-900, Cz-MOF-253-1000 are 1090, 1490, 640 and 630  $\text{m}^2/\text{g}$ , respectively.  $\text{N}_2$  sorption isotherms displayed a type-IV curve for these MOF-derived porous carbons (Figure 4). These results clearly indicate the presence of mesopores, which is further verified with the pore size distribution analysis (Figure 5).

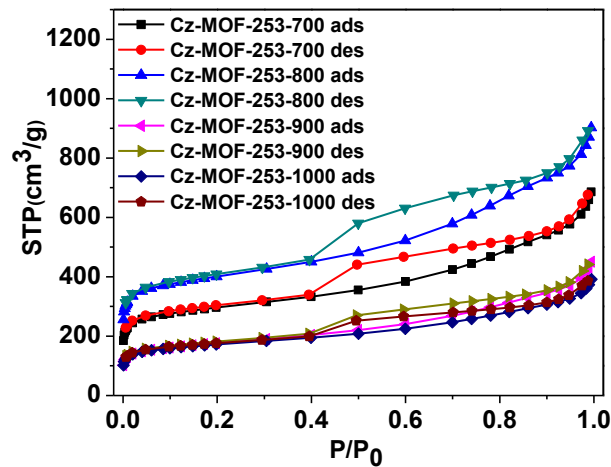


**Figure 4.**  $\text{N}_2$  sorption isotherms of the Cz-MOF-253 from different temperature.

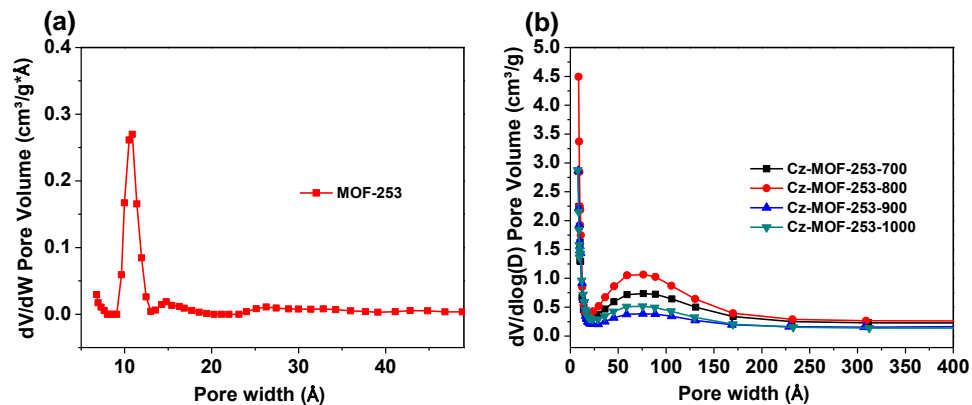


**Figure 5.** Pore size distributions of (a) MOF-253 using NLDFT method and (B) Cz-MOF-253 using BJH method.

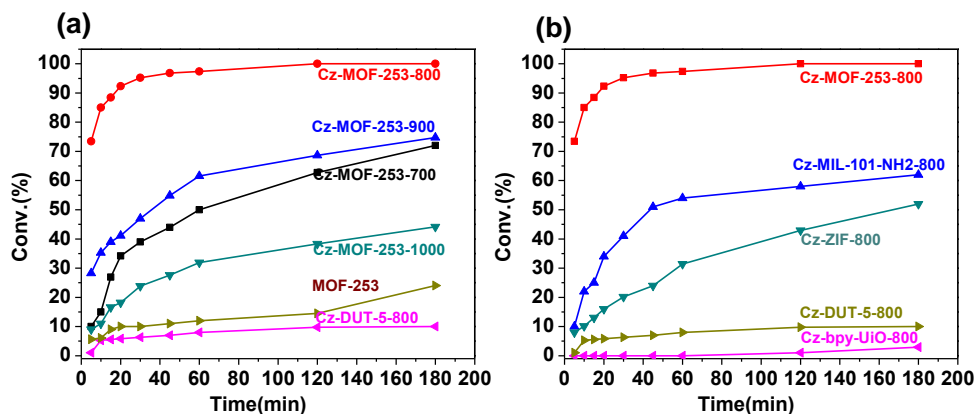


**Figure 6.** (a) Time dependent analysis of the Knoevenagel condensation reaction by Cz-Al-MOFs at different pyrolysis temperature and pristine MOF catalysts; (b) Time dependent analysis of the Knoevenagel condensation reaction by control catalysts; Reaction condition: 0.1 mmol of benzaldehyde, 0.3 mmol of malononitrile, 2 mL of toluene, and 10 mg of Cz-MOF, stir 600 rpm, 90 °C.

To evaluate the Lewis basicity of Cz-MOF-253, we run Knoevenagel condensation catalyzed by Cz-MOF-253. It is noteworthy that pyrolysis temperature leads to different activity. As shown in Figure 6a, Cz-MOF-253-800 gave the highest activity among the catalysts from pyrolysis temperature at 700, 900 and 1000 °C. To further confirm the origin of Lewis basicity, we used the carbons materials (designed as Cz-DUT-5) derived from the pyrolysis and acid treatment of DUT-5, which is isorecticular to MOF-253 but possesses no nitrogen. As expected, Cz-DUT-5 showed much lower activity under the same condition, revealing that the nitrogen serves as Lewis basic sites in Knoevenagel condensation. This data is also consistent with the fact that Cz-DUT-5-800 showed very weak desorption in its CO<sub>2</sub>-TPD profiles (Figure 7). For comparison, other nitrogen-containing porotype MOFs (i.e., ZIF-8,<sup>25</sup>

and Al-MIL-101-NH<sub>2</sub>,<sup>26</sup> with different types of nitrogen species) were selected as precursor under the same pyrolysis temperature and post-acid treatment. As shown in Figure 6b, both Cz-ZIF-8 and Cz-MIL-101-NH<sub>2</sub> exhibited inferior performance in Knoevenagel condensation, highlighting the superiority of using MOF-253 as carbon precursor. Remarkably, Cz-MOF-253-800 exhibited much higher activity than pristine MOFs, which is consistent with the CO<sub>2</sub>-TPD analysis that the density of the basic sites in the Cz-MOF-253 was significantly enhanced in comparison to pristine MOF-253 (Figure 7). This enhancement is presumably due to the higher population of basic sites and larger pores after pyrolysis, which is beneficial to the diffusion/transportation of reactants to access the active basic sites.

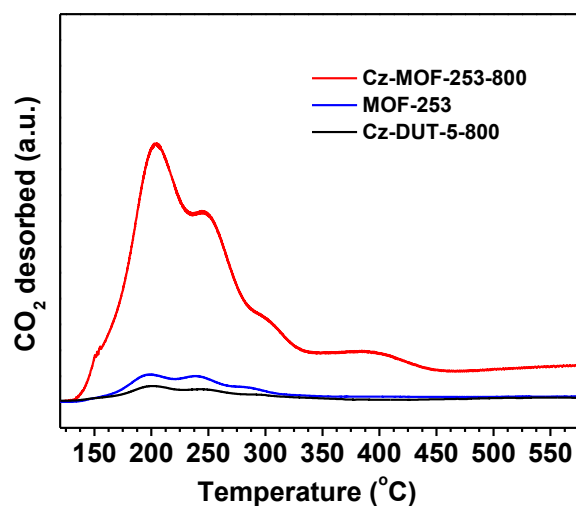
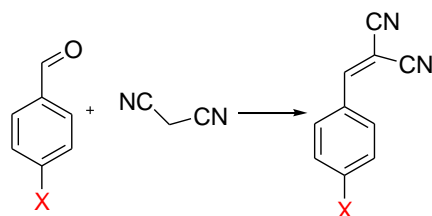


**Figure 7.** CO<sub>2</sub>-TPD profiles of Cz-MOFs and pristine MOF-253.

To demonstrate the general applicability of Cz-MOF-253-800 catalyst in Knoevenagel condensation reaction, the scope of the Cz-MOF-253-800 catalyst was investigated by conducting the Knoevenagel condensation with a variety of substituted benzaldehyde. As illustrated in Table 2, different substituted

benzaldehyde was converted to corresponding benzylidenemalononitriles with high yield. The benzaldehyde involving electron-rich groups (e.g., 2-methoxy, 4-methoxy, 4-hydroxyl), electron-withdrawing substituents (such as 4-nitro) and halide groups (e.g., 4-Br, and 4-Cl) were converted to the desired products in an efficient fashion. These results demonstrate the Cz-MOF-253-800 is highly efficient solid base catalyst for Knoevenagel condensation reaction.

**Table 2.** Knoevenagel condensation reaction of various substituted benzaldehyde and malononitrile over Cz-MOF-253-800.



Entry	X	t (h)	Conv.(%)	Sel. (%)
1	4-Br	1	99%	99%
2	4-Cl	1	99%	99%
3	4-NO <sub>2</sub>	2	99%	99%
4	4-OH	3	99%	99%
5	2-OMe	3	99%	99%
6	4-OMe	5	99%	99%

Reaction conditions: 0.1 mmol of substituted benzaldehyde, 0.3 mmol of malononitrile, 2 mL solvent, and 5 mg Cz-MOF-253-800, 90 °C, stir at 600 rpm.

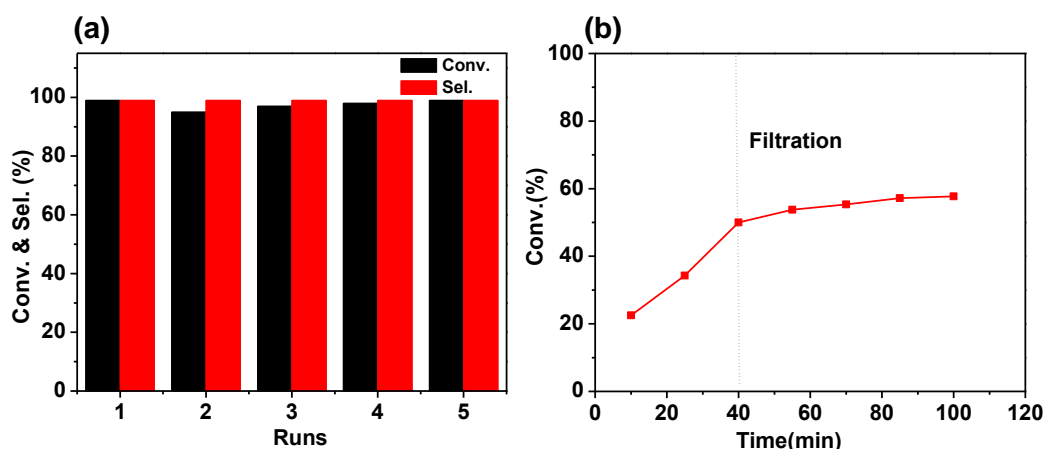


**Figure 8.** Recycle test (a) and leaching test (b) of Cz-MOF-253-800 in Knoevenagel condensation reaction. 0.1 mmol of benzaldehyde, 0.3 mmol of malononitrile, 2 mL of toluene, and 10 mg of Cz-MOF-253-800, stir 600 rpm, 90 °C, Ar, 3 hours for recycling.

The heterogeneous catalyst-Cz-MOF-253 can be reused in the Knoevenagel condensation reaction. After five reaction cycles, there was no loss in the yield of 2-benzylidenemalononitrile (Figure 8a). A filtration test was employed to further confirm the heterogeneity of the Cz-MOF-253-800 (Figure 8b). The catalyst was isolated by centrifugation when the conversion reached ca. 50% in 40 mins. Only slight increase in conversion of benzaldehyde was observed on exposing the isolated liquid to the reaction conditions upon removal of the catalyst, presumably due to the blank test. In addition, no obvious changes were observed according to the PXRD patterns of used catalysts, highlighting the robust nature of Cz-MOF-253-800 catalyst.

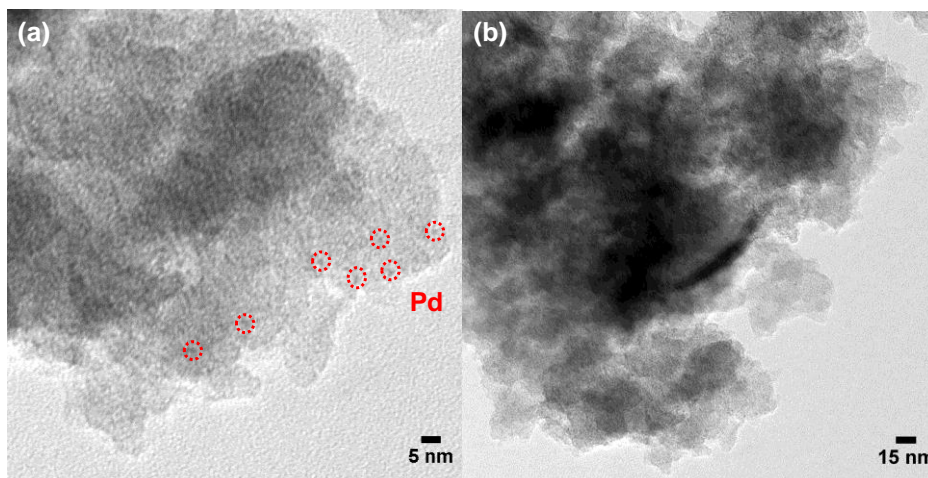


**Figure 9.** TEM images of Pd NPs stabilized in Cz-MOF-253-800 in (a) high and (b) low magnification.

Given the highly porous nature and Lewis basicity, Cz-MOF-253-800 might be suitable host for stabilizing small Pd NPs, allowing the flexible design of bifunctional catalyst for tandem catalysis. As far as we know, there are minimal studies on the bifunctional MOFs-derived carbon in tandem catalysis. Bearing these in mind, we proceeded to explore the potential of MOF-derived carbons in tandem catalysis. The obtained carbon materials were utilized as hosts to load Pd NPs by a simple incipient-wetness impregnation method (designed as Pd/Cz-MOF-253-800).<sup>25</sup> TEM images show the presence of highly dispersed and ultrasmall Pd NPs with sizes of ~1 nm (Figure 9). To examine the bifunctional nature of Pd/Cz-MOF-253-800, a successive Knoevenagel reaction-hydrogenation reaction was utilized for a proof-of-concept. As indicated in Table 3, Pd/Cz-MOF-253-800 was effective in facilitating condensation-hydrogenation reactions to afford corresponding benzylmalonitrile based on various substituted benzaldehyde in a stepwise way. To our knowledge, this

is the first example of applying metal NPs/MOF-based carbons as bifunctional catalysts in tandem reaction.

**Table 3.** Knoevenagel condensation-hydrogenation of substituted benzaldehyde with malononitrile catalyzed by Pd/Cz-MOF-253-800.

Entry	Product	Time (h)	Conv.(%)	Sel. (%)
1		17	99	99
2		17	99	99
3		17	99	99

Reaction conditions: first step, 0.1 mmol of benzaldehyde , 0.3 mmol of malononitrile, 2 mL toluene, and 5 mg Pd/Cz-MOF-253-800, 80 °C, 5 h, stir at 600 rpm; Second step, 150 psi H<sub>2</sub>, 80 °C, 12 hours, stir at 600 rpm.

## Conclusion

In conclusion, we have for the first time developed a novel solid base catalyst, N-doped MOF-253 derived porous carbons (Cz-MOF-253). Cz-MOF-253 is highly porous and exhibit high efficiency in Knoevenagel condensation reaction. Furthermore, Cz-MOF-253 is robust and can be reused up to five times. In comparison, the analogous nitrogen-free catalyst-Cz-DUT-5, and other nitrogen-MOFs derived carbon showed an inferior performance. Moreover, the high basicity



and porous nature enable the design of bifunctional catalyst and facilitate tandem condensation-hydrogenation reactions. This work delineates the first attempt that demonstrates MOF-derived carbons as solid base catalyst and its potential application in tandem catalysis. Future work on exploring new catalytic reactions based on such porous Lewis basic MOF-derived carbons is currently underway.

### Experimental section

**Characterization.** Surface analysis of the catalysts was performed by nitrogen sorption isotherms at 77 K using Micromeritics 3Flex surface characterization analyzer. Cz-MOFs samples (ca. 50 mg) were degassed under vacuum ( $\sim 5 \times 10^{-5}$  torr) at 200 °C for 4 h prior to analysis. XPS measurements were performed using a PHI 5500 Multi-technique system (Physical Electronics, Chanhassen, MN) with a monochromatized Al  $K_{\alpha}$  X-ray source ( $h\nu = 1486.6$  eV). PXRD patterns of the MOFs were obtained by a STOE Stadi P powder diffractometer using Cu  $K_{\alpha}$  radiation (40 kV, 40 mA,  $\lambda = 0.1541$  nm). CO<sub>2</sub> Temperature Programmed Desorption (TPD) experiments were carried out on a Micromeritics 3Flex instrument equipped with a mass spec detector. Typically, the sample (ca.80 mg) was pretreated under a flow of Helium (50 mL/min) at 700 °C for 1 hour. Then the sample was cooled to 100 °C under a flow of Helium and adsorbed CO<sub>2</sub> for 2 hours. Then the sample was purged with Helium (50 mL/min) at 100 °C for 30 min. The TPD data were collected from 100 °C to 600 °C at a heating rate of 20 °C/min in a flow of Helium. ICP-MS (X Series II, Thermo Scientific) analysis was performed to determine the actual

palladium content in Pd/Cz-MOFs. The samples were dissolved in perchloric acid under boiling until the solid was completely dissolved.

**Synthesis of MOF-253.**  $\text{AlCl}_3 \cdot 6\text{H}_2\text{O}$  (151 mg, 0.625 mmol) and 2,2'-bipyridine-5,5'-dicarboxylic acid (153 mg, 0.625 mmol) were dissolved in 10 mL of DMF in a 20 mL scintillation vial. The vial was heated at 130 °C for 24 hours. After cooling to ambient temperature, the white MOFs were collected via centrifugation and thoroughly washed with DMF (3 times) and methanol (3 times) every 12 hours. Finally, the MOFs were activated at 150 °C under vacuum (30 mTorr) for 12 hours prior to experimental use.

**Synthesis of DUT-5.** 4,4'-biphenyldicarboxylic acid (130 mg, 0.535 mmol) was dissolved in 15 mL of DMF in a 20 mL scintillation vial.  $\text{Al}(\text{NO}_3)_3 \cdot 9\text{H}_2\text{O}$  (260 mg, 0.7 mmol) was added and the mixture was heated to 120 °C for 24 hours. After cooling to ambient temperature, the product MOFs were collected by centrifugation and washed with DMF (3 times) and methanol (3 times) every 12 hours. Finally, the MOFs were activated at 150 °C under vacuum (30 mTorr) for 12 hours prior to experimental use.

**Synthesis of ZIF-8.** Typically, 1.68 g of  $\text{Zn}(\text{NO}_3)_2 \cdot 6\text{H}_2\text{O}$  was dissolved in 80 mL of methanol. A methanolic solution (3.70 g of 2-methylimidazole in 80 mL methanol) was added in the above solution with vigorous stirring (800 rpm) for 24 hours at ambient temperature. The product was separated by centrifugation and washed with methanol for three times, and finally dried at 150 °C under vacuum (30 mTorr) for 12 hours prior to experimental use.

**Synthesis of Al-MIL-101-NH<sub>2</sub>.** AlCl<sub>3</sub>·6H<sub>2</sub>O (0.51 g, 2.12 mmol) and 2-amino terephthalic acid (0.56 g, 3.09 mmol) were dissolved in 30 mL of DMF in a 480 mL Teflon PFA wide mouth jars. The jar was heated at 120 °C for 3 days under static conditions. After cooling to ambient temperature, the white MOFs were collected via centrifugation and thoroughly washed with DMF (3 times) and acetone (3 times). Finally, the MOFs were activated at 150 °C under vacuum (30 mTorr) for 12 hours prior to experimental use.

**Preparation of Cz-MOF-253 via pyrolysis.** MOF-253 (100 mg) was spread in a quartz boat which was placed in a temperature-programmed tube furnace. The heating rate was 2 °C/min, and the samples were carbonized at the setting temperature for 4 hours. After cooling to ambient temperature, the obtained black powder was treated with HF (20 wt.%) at 60 °C for 12 hours and was washed with deionized water. The washed Cz-MOFs samples were dried at 120 °C under vacuum (30 mTorr) for 12 hours. The same procedure was applied to other MOFs samples.

**Acknowledgment.** We thank Ames Laboratory (Royalty Account) and Iowa State University for startup funds. The Ames Laboratory is operated for the U.S. Department of Energy by Iowa State University under Contract No. DE-AC02-07CH11358. We thank Gordon J. Miller for use of PXRD instrument in his group.

## References

- (1) Pei, X.; Chen, Y.; Li, S.; Zhang, S.; Feng, X.; Zhou, J.; Wang, B. *Chin. J. Chem.* **2016**, *34*, 157-174.
- (2) Yang, S. J.; Kim, T.; Im, J. H.; Kim, Y. S.; Lee, K.; Jung, H.; Park, C. R. *Chem. Mater.* **2012**, *24*, 464-470.

- (3) Aijaz, A.; Fujiwara, N.; Xu, Q. *J. Am. Chem. Soc.* **2014**, *136*, 6790-6793.
- (4) Zhong, S.; Wang, Q.; Cao, D. *Scientific reports* **2016**, *6*.
- (5) Xia, W.; Qiu, B.; Xia, D.; Zou, R. *Sci. Rep.* **2013**, *3*.
- (6) Zhang, L.; Su, Z.; Jiang, F.; Yang, L.; Qian, J.; Zhou, Y.; Li, W.; Hong, M. *Nanoscale* **2014**, *6*, 6590-6602.
- (7) Chen, Y. Z.; Wang, C.; Wu, Z. Y.; Xiong, Y.; Xu, Q.; Yu, S. H.; Jiang, H. L. *Adv. Mater.* **2015**, *27*, 5010-5016.
- (8) Wang, X.; Li, Y. *J. Mater. Chem. A* **2016**, *4*, 5247-5257.
- (9) Tang, J.; Yamauchi, Y. *Nature Chem.* **2016**, *8*, 638-639.
- (10) Li, L.; Wang, Y.; Gu, X.; Yang, Q.; Zhao, X. *Chem.–An Asian J.* **2016**.
- (11) Yang, Q.; Xu, Q.; Yu, S. H.; Jiang, H. L. *Angew. Chem.* **2016**, *128*, 3749-3753.
- (12) Li, X.; Guo, Z.; Xiao, C.; Goh, T. W.; Tesfagaber, D.; Huang, W. *ACS Catal.* **2014**, *4*, 3490-3497.
- (13) Van Zeeland, R.; Li, X.; Huang, W.; Stanley, L. M. *RSC Adv.* **2016**, *6*, 56330-56334.
- (14) Ono, Y. *Journal of Catalysis* **2003**, *216*, 406-415.
- (15) Climent, M. J.; Corma, A.; Iborra, S.; Sabater, M. J. *ACS Catal.* **2014**, *4*, 870-891.
- (16) Chen, Y.-Z.; Zhou, Y.-X.; Wang, H.; Lu, J.; Uchida, T.; Xu, Q.; Yu, S.-H.; Jiang, H.-L. *ACS Catal.* **2015**, *5*, 2062-2069.
- (17) Zhao, M.; Deng, K.; He, L.; Liu, Y.; Li, G.; Zhao, H.; Tang, Z. *J. Am. Chem. Soc.* **2014**, *136*, 1738-1741.
- (18) Yang, Q.; Chen, Y.-Z.; Wang, Z. U.; Xu, Q.; Jiang, H.-L. *Chem. Commun.* **2015**, *51*, 10419-10422.
- (19) Li, Y.-A.; Yang, S.; Liu, Q.-K.; Chen, G.-J.; Ma, J.-P.; Dong, Y.-B. *Chem. Commun.* **2016**, *52*, 6517-6520.
- (20) Qi, Y.; Luan, Y.; Peng, X.; Yang, M.; Hou, J.; Wang, G. *Eur. J. Inorg. Chem.* **2015**, *2015*, 5099-5105.

- (21) Li, J.; Zhu, Q.-L.; Xu, Q. *Chem. Commun.* **2015**, *51*, 10827-10830.
- (22) Chen, Y.-Z.; Cai, G.; Wang, Y.; Xu, Q.; Yu, S.-H.; Jiang, H.-L. *Green Chem.* **2016**, *18*, 1212-1217.
- (23) Bao, C.; Zhou, L.; Shao, Y.; Wu, Q.; Ma, J.; Zhang, H. *RSC Adv.* **2015**, *5*, 82666-82675.
- (24) Qiu, X.; Len, C.; Luque, R.; Li, Y. *ChemSusChem* **2014**, *7*, 1684-1688.
- (25) Chen, Y.-Z.; Cai, G.; Wang, Y.; Xu, Q.; Yu, S.-H.; Jiang, H.-L. *Green Chem.* **2016**, *18*, 1212-1217.
- (26) Serra-Crespo, P.; Ramos-Fernandez, E. V.; Gascon, J.; Kapteijn, F. *Chem. Mater.* **2011**, *23*, 2565-2572.